UNIVERSITAT DE BARCELONA

Exploración y modelización de patrones socioecológicos y tecnoculturales en sociedades preindustriales de zonas áridas afro-eurasiáticas

Una aproximación multidisciplinar desde métodos cuantitativos

Andreas Angourakis

Aquesta tesi doctoral està subjecta a la llicència ***Reconeixement- NoComercial 4.0. Espanya de Creative Commons***.

Esta tesis doctoral está sujeta a la licencia ***Reconocimiento - NoComercial 4.0. España de Creative* Commons**.

This doctoral thesis is licensed under the ***Creative Commons Attribution-NonCommercial 4.0. Spain License***.

3. Análisis de datos arqueométricos de cerámicas

Resumen de capítulo • Este capítulo recoge los tres artículos a los cuales el candidato contribuyó en la línea de análisis de datos arqueométricos de cerámicas arqueológicas. La primera sección hace una breve introducción al capítulo, comentando la particularidad de las evidencias de producciones cerámicas de la región del Surkhan Daria, caso que inspira y motiva el trabajo metodológico realizado en esta línea (sección 3.1). El primer artículo trata la caracterización de un conjunto de muestras cerámicas de Kurganzol, una fortaleza ocupada durante la primera etapa del período helenístico, fundada por el ejército de Alejandro Magno (sección 3.2). Liderado por V. Martínez Ferreras, este artículo cuenta con la aportación del candidato en el análisis y presentación de datos geoquímicos (FRX), además de su colaboración en la redacción y revisión del manuscrito. El segundo artículo realiza un estudio de caracterización arqueométrica y comparación de producciones cerámicas de la antigua Termez del período helenístico (ciudadela) y yuezhi (Tchingiz Tepe y llanura aluvial), buscando elementos de continuidad y cambio tecnológico (sección 3.3). La publicación del artículo, prevista para antes de finales de 2018, sufrió retrasos en el proceso de revisión por pares y en la actualidad se cuenta con la aceptación de los editores, pero aún no disponemos de la versión maquetada. En este sentido, la aportación del doctorando coincide con la del artículo anterior: complementando el análisis estadístico de datos geoquímicos (FRX) y colaborando en la redacción y revisión del manuscrito. Por último, se incluye el artículo liderado por el doctorando que presenta los cuatro protocolos de análisis de datos de cerámicas en sus versiones consolidadas y reproducibles (sección 3.4). Este trabajo utilizó un conjunto de datos geoquímicos, mineralógicos y petrográficos de ánforas vinarias de Hispania Citerior-Tarraconensis, disponible desde la investigación previa de V. Martínez Ferreras y colaboradores, a modo de validación y demostración del desempeño de cada protocolo.

Resum de capítol • Aquest capítol recull els tres articles als quals el candidat va contribuir en la línia d'anàlisi de dades arqueomètriques de ceràmiques arqueològiques. La primera secció fa una breu introducció al capítol, comentant la particularitat de les evidències de produccions ceràmiques de la regió del Surkhan Daria, cas que inspira i motiva el treball metodològic realitzat en aquesta línia (sección 3.1). El primer article tracta la caracterització d'un conjunt de mostres ceràmiques de Kurganzol, una fortalesa ocupada durant la primera etapa del període hel · lenístic, fundada per l'exèrcit d'Alexandre el Gran (sección 3.2). Liderat per V. Martínez Ferreras, aquest article compta amb l'aportació del candidat en l'anàlisi i presentació de dades geoquímiques (FRX), a més de la seva col · laboració en la redacció i revisió del manuscrit. El segon article documenta un estudi de caracterització arqueomètrica i comparació de produccions ceràmiques de l'antiga Termez del període hel · lenístic (ciutadella) i yuezhi (Tchingiz Tepe i plana al · luvial), buscant elements de continuïtat i canvi tecnològic (sección 3.3). La publicació de l'article, prevista per abans de finals de 2018, va patir retards en el procés de revisió per parells i en l'actualitat comptem amb l'acceptació dels editors, però encara no disposem de la versió maquetada. En aquest sentit, l'aportació del doctorand coincideix amb la de l'article anterior: complementant l'anàlisi estadística de dades geoquímiques (FRX) i col · laborant en la redacció i revisió del manuscrit. Finalment, s'inclou l'article liderat pel doctorand que presenta els quatre protocols d'anàlisi de dades de ceràmiques en les seves versions consolidades i reproduïbles (sección 3.4). Aquest treball va utilitzar un conjunt de dades geoquímiques, mineralògiques i petrogràfiques d'àmfores vinàries d'Hispania Citerior-Tarraconensis, disponible des de la investigació prèvia de V. Martínez Ferreras i col · laboradors, a manera de validació i demostració de l'acompliment de cada protocol.

Chapter summary • This chapter includes the three articles to which the candidate contributed in the line of archaeometric data analysis of archaeological ceramics. The first section gives a brief introduction to the chapter, commenting on the particularity of the ceramic production evidences of the Surkhan Daria region, a case that inspires and motivates the methodological work carried out in this line (sección 3.1). The first article deals with the characterization of a set of ceramic samples of Kurganzol, a fortress occupied during the first stage of the Hellenistic period, founded by the army of Alexander the Great (sección 3.2). Led by V. Martínez Ferreras, this article integrates the contribution of the candidate in the analysis and presentation of geochemical data (FRX), in addition to his collaboration in the drafting and revision of the manuscript. The second article makes a study of archaeometric characterization and comparison of ceramic productions of the ancient Termez of the Hellenistic period (citadel) and Yuezhi (Tchingiz Tepe and alluvial plain), looking for elements of continuity and change (sección 3.3). The publication of the article, scheduled for before the end of 2018, suffered delays in the peer review process and currently is accepted by the editors, but still has not been published. In this sense, the contribution of the doctoral student coincides with that of the previous article: complementing the statistical analysis of geochemical data (FRX) and collaborating in the drafting and revision of the manuscript. Finally, we include the article led by the doctoral student who presents the four protocols for the analysis of ceramics in their consolidated and reproducible versions (sección 3.4). This work used a data set with geochemical, mineralogical, and petrographic variables concerning Roman wine amphorae from Hispania Citerior-Tarraconensis, available from the previous research of V. Martínez Ferreras and collaborators, as a way of validation and demonstration of the performance of each protocol.

3.1. Introducción

Esta línea se ha centrado en el análisis de los patrones de continuidad y cambio tecnológico en la fabricación y uso de cerámicas arqueológicas. El estudio multidisciplinario de las cerámicas arqueológicas proporciona información (*i.e.* "proxy") sobre los patrones productivos, económicos, sociales y tecnoculturales de las sociedades que las fabricaron y utilizaron (figura 3.1). En acuerdo con el contexto del proyecto CAMOTECCER, el cual ha enmarcado esta línea de la tesis (ver sección 1.1.3), el objetivo final ha sido facilitar la caracterización de cerámicas de diversa categoría (cocina, contenedores, vajilla, etc.) provenientes de los yacimientos trabajados por el ERAAUB en la región del Surkhan Daria.

La arqueología de la región de Surkhan Daria muestra la producción y consumo constantes de cerámicas, desde la Edad del Bronce hasta la actualidad. No obstante, también se documenta una fuerte discontinuidad entre ciertos períodos. En estas discontinuidades, se reflejan diversas realidades socioeconómicas (*e.g.*, comunidades de pastores y agricultores sedentarios) y entidades histórico-culturales compartidas con otras regiones de Asia Central (*e.g.*, BMAC, aqueménida, helenística, kushán).

Los pueblos establecidos en torno al Amu Daria durante el Bronce Medio (BMAC, ver sección 2.2.4, Luneau 2010) fueron productores de cerámicas a torno de alta calidad. Su producción cerámica ciertamente corrobora otras evidencias materiales de que se trataba de una sociedad "urbana", donde cabía la especialización y estandarización artesanal. Durante la Edad del Hierro cambian tanto el repertorio morfológico como la tecnología cerámica en general. Por todo el área donde antes se extendía el BMAC, las producciones cerámicas se muestran más diversas y locales, tanto en términos de estilo como de técnicas de fabricación (Lhuillier 2013).

La influencia irania se percibe de manera clara en la segunda mitad del siglo VI a.C., a partir del dominio aqueménida. Tras la conquista de Alejandro Magno a finales del siglo IV a.C., las influencias culturales helenísticas se extendieron por toda la región, siendo éstas evidentes en los aspectos morfológicos, decorativos y tecnológicos de las cerámicas (Bolelov 2001, 2011 ; Houal 2016; Martínez Ferreras, Gurt Esparraguera, Josep Maria, et al. 2016).

El final del Reino grecobactriano a mediados del siglo II a. trae nuevos cambios morfológicos y tecnológicos. Las producciones cerámicas conocidas muestran la sustitución,

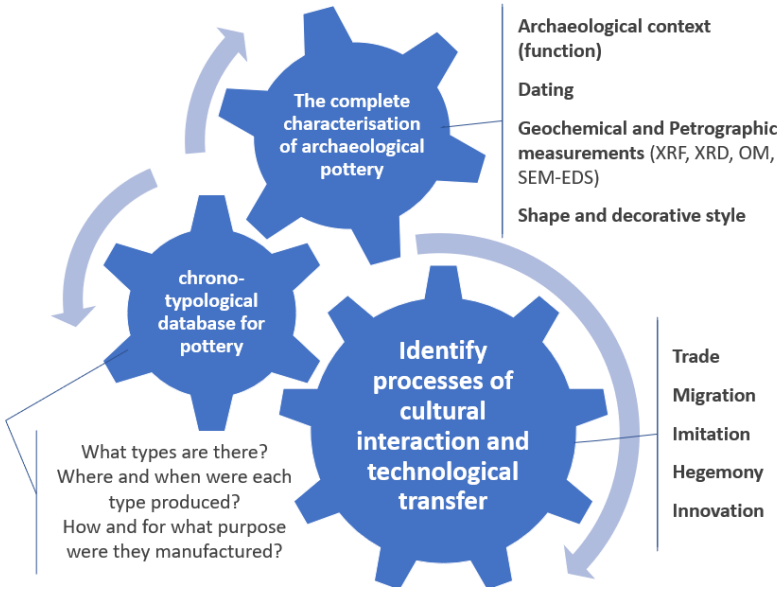

Figura 3.1: Mecanismos considerados para exploración en el caso de estudio 5 del proyecto SimulPast. Se destacan aquellos que efectivamente se incluyen en los dos modelos publicados.

en toda la región, de prácticas de tradición griega por nuevas costumbres y hábitos, sobre todo en lo referente a la cerámica fina. De manera destacada, las prácticas comensales de élite yuezhi incluyen el uso de copas cónicas y cuencos individuales, especialmente característicos, que contrastan con la variedad de cerámicas de mesa de tradición helenística.

El largo período de gobierno de la confederación yuezhi y el subsiguiente Imperio kushán se caracteriza por la introducción del budismo y la intensificación de las relaciones comerciales con la India, el Próximo Oriente, el mar Caspio y la China en el marco de la Ruta de la Seda (ver sección 2.2.4).

El repertorio cerámico característico de estas sociedades sedentarias difiere a nivel formal y tecnológico respecto al anterior y se mantiene bastante uniforme, incluso después del sometimiento de la dinastía kushán al Imperio sasánida. La emergencia del Imperio heftalita y las primeras migraciones turcas parece haber tenido un impacto degradador en esta tradición, acompañando una tendencia general al decrecimiento de las actividades urbanas (Kurbanov 2010, p. 206). La llegada de la cultura islámica a finales del siglo VII d.C. devuelve el volumen y estandarización técnica de la producción cerámica, trayendo además nuevas tecnologías, como el vidriado, que requería de materias primas

y conocimientos específicos que circulaban en la ecúmene islámica (Siméon 2012).

El primer paso en esta línea fue el diseño de una ***base de datos*** que integrase todos los datos sobre muestras cerámicas de diversa cronología desde la Edad del Bronce a época islámica, procedentes de diversos yacimientos de la región del Surkhan Daria. Los datos seleccionados son relativos al contexto histórico-arqueológico y la caracterización arqueométrica. La base de datos, implementada en Microsoft Access, contiene 15 tablas, todas con referencias directas o indirectas a las entradas de la tabla central, IndividualT, cuyas entradas corresponden a una pieza cerámica individual (figura 3.2). Posee una ontología flexible que permite la definición de períodos y localidades en la región del Surkhan Daria y más allá. Hasta la fecha, sobre todo gracias al esfuerzo de V. Martínez Ferreras, la base de datos cuenta con más de 700 individuos cerámicos de 41 yacimientos.

Después de un período de aprendizaje y experimentación con otras vías, se ha consolidado cuatro conjuntos de métodos de análisis estadístico multivariante (*protocolos*) que ayudan a identificar centros de producción (*proveniencia*) y etapas tecnoculturales en un mismo centro, a partir de datos sobre la contextualización arqueológica y la caracterización arqueométrica. Concretamente, se ha trabajado con datos de *composición geoquímica* (Fluorescencia de Rayos X o FRX) y la caracterización *mineralógica* (Difracción de rayos X o DRX) y *petrográfica*, desde la observación de láminas delgadas con microscopio óptico polarizante (OM). Los protocolos aportan—entre otras funciones—la posibilidad de tratar conjuntamente una multiplicidad de variables de naturaleza diferente (*i.e.* numéricas versus categóricas). La utilidad de los protocolos se ha comprobado gracias a su aplicación a cerámicas de diferente origen, datación y contexto (vasijas diversas de Uzbekistán y ánforas romanas de Cataluña), estudiadas previamente por la V. Martínez Ferreras.

Dada la larga etapa de desarrollo de los protocolos, dos de los trabajos incluidos en este capítulo presentan sólo el tratamiento estadístico de datos geoquímicos, equivalente a los procedimientos incluidos en el protocolo 1. Estos trabajos han tenido como objetivo la caracterización de producciones de Kurganzol (período helenístico, Martínez Ferreras, Angourakis, et al. 2016, sección 3.2) y Termez (período helenístico a yuezhi/kushán, Martínez Ferreras et al. [sin fecha], sección 3.3). Aunque el planteamiento del proyecto CAMOTECCER incluía analizar cerámicas de otros yacimientos y períodos, no ha sido posible alcanzar durante la preparación de la tesis el volumen y amplitud suficiente para emitir nuevos resultados sobre las producciones cerámicas en el Surkhan Daria. No

obstante, se han realizado múltiples pruebas sobre los datos disponibles, que repercutirán en un futuro en un artículo adicional (figura 3.3).

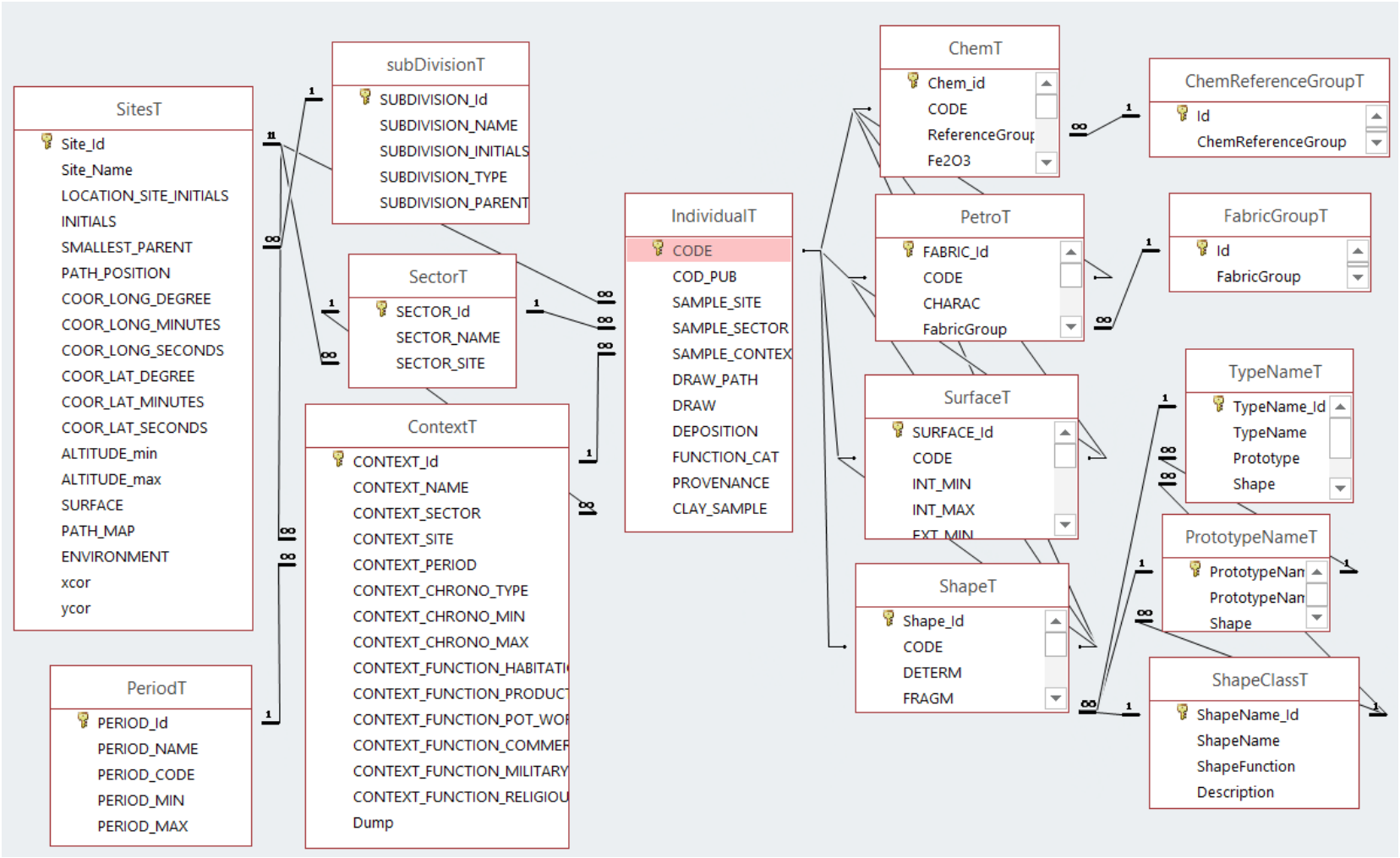

Figura 3.2: Las tablas (cuadros) y relaciones (enlaces) de la base de datos creada para el proyecto CAMOTECCER, aún en uso y desarrollo en el proyecto CERAC. La base de datos fue implementada en Microsoft Access.

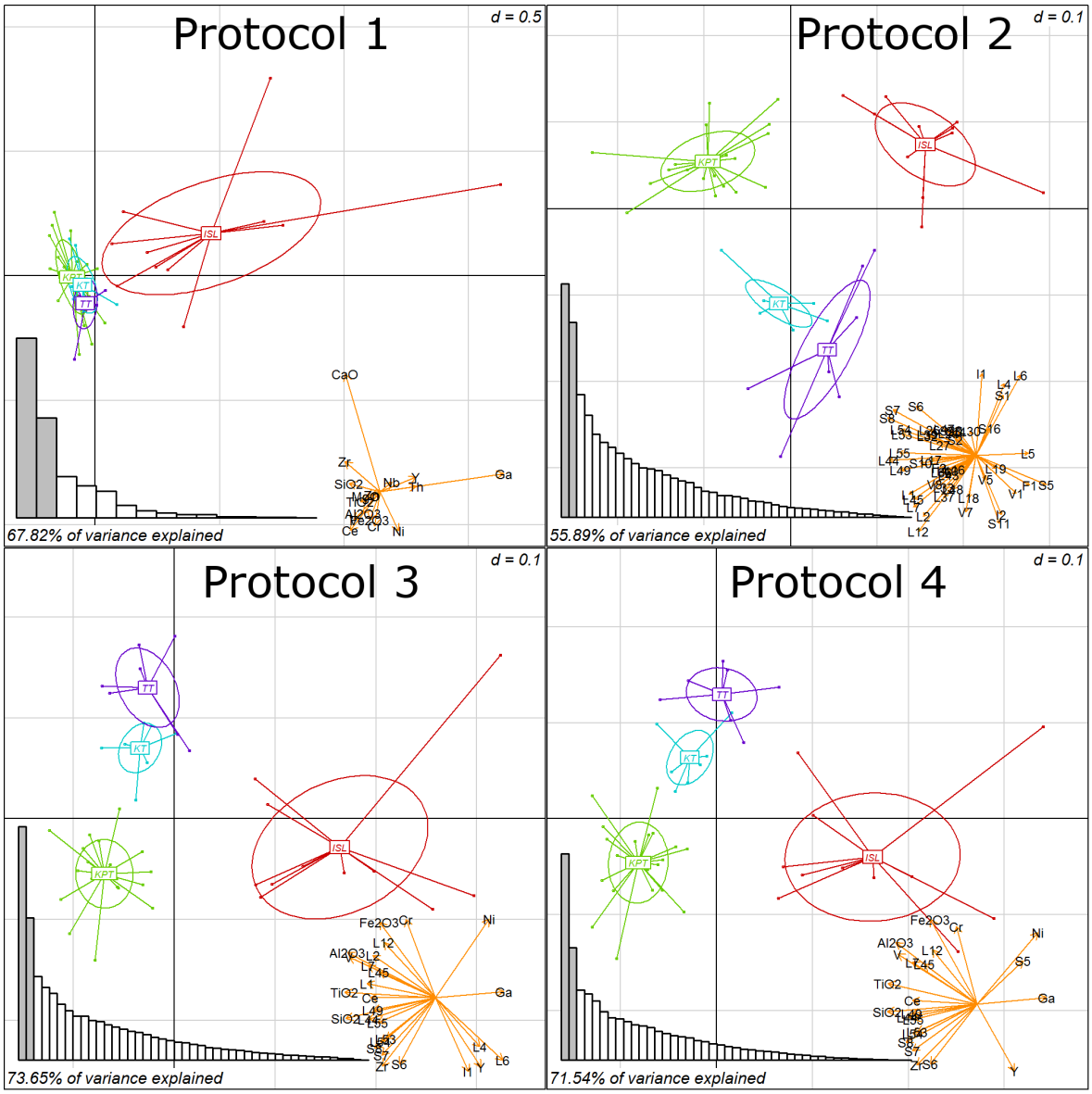

Figura 3.3: Proyección de los resultados de los cuatro protocolos, aplicados a un conjunto de muestras de cerámica fina de Termez.

Para comprobar la generalidad del método y evaluar sus resultados, se ha utilizado un conjunto de datos sobre ánforas vinarias romanas (siglos I a. C. y I d. C.), analizadas previamente por V. Martínez. Estos datos se integraron al formato de la base de datos del proyecto y se ofrecen dentro del paquete *cerUB*, con el objetivo de facilitar el aprendizaje y reproducción de los protocolos por parte de otros investigadores. Los protocolos y su aplicación sobre este conjunto de datos se presentan en el artículo publicado en *Journal of Archaeological Science* (Angourakis y Martínez Ferreras 2018, sección 3.4).

3.2. Pottery in Hellenistic tradition from ancient Bactria: The Kurganzol fortress (Uzbekistan, Central Asia)

Esta sección corresponde al siguiente artículo:

Martínez Ferreras, V. M., **Angourakis, A.**, Hein, A., Gurt Esparraguera, J. M., Sverchkov, L. M., del Corral, A. S. (2016). Pottery in Hellenistic tradition from ancient Bactria: The Kurganzol fortress (Uzbekistan, Central Asia). *Journal of Archaeological Science: Reports*. https://doi.org/10.1016/j.jasrep.2016.11.049.

Resumen Kurganzol es una de las fortalezas fundadas en la antigua Bactria durante la conquista de Alejandro Magno. Se llevó a cabo la caracterización arqueométrica de 20 fragmentos de cerámica recuperados en el asentamiento más antiguo de finales del siglo cuarto a. C. El objetivo es examinar tanto la composición como la variación de las materias primas utilizadas y la tecnología de producción involucrada en la fabricación alfera. La muestra incluía platos, tazas/tazones, cuencos, tarros, recipientes, un colador, una botella o matraz y una olla para cocinar. El programa analítico incluía Fluorescencia de rayos X, difracción de rayos X y análisis de sección delgada, así como el estudio del entorno geológico. El análisis del tratamiento superficial se realizó en tres fragmentos mediante microscopía electrónica de barrido acoplada con espectroscopia de rayos X dispersiva de energía (SEM-EDS). Los resultados se compararon con una base de datos analítica que incluye piezas de la tradición helenística de sitios coetáneos en la región (es decir, Kampyr Tepe y Termez). El análisis reveló que la mayoría de las vajillas y cerámicas comunes analizadas corresponden a una única producción local de cerámica que consiste en un material calcáreo muy fino. La composición y las características morfológicas de estas piezas permiten distinguirlas de otras producciones contemporáneas de cerámica. Sin embargo, se asignó un origen regional para algunas mercancías que confirmaban contactos entre diferentes sitios. La única olla de cocción examinada consistía en un material calcáreo con conchas como desgrasante que es compatible con una tradición tecnológica regional.

Resum Kurganzol és una de les fortaleses fundades en l'antiga Bactria

durant la conquesta d'Alexandre el Gran. Es va dur a terme la caracterització arqueomètrica de 20 fragments de ceràmica recuperats en l'assentament més antic de finals del segle quart a. C. L'objectiu és examinar tant la composició com la variació de les matèries primeres utilitzades i la tecnologia de producció involucrada en la fabricació terrissaire. La mostra incloïa plats, tasses/bols, conques, pots, recipients, un colador, una ampolla o matràs i una olla per cuinar. El programa analític incloïa Fluorescència de raigs X, difracció de raigs X i anàlisi de secció prima, així com l'estudi de l'entorn geològic. L'anàlisi del tractament superficial es va realitzar en tres fragments mitjançant microscòpia electrònica de rastreig acoblada amb espectroscòpia de raigs X dispersiva d'energia (SEM-EDS). Els resultats es van comparar amb una base de dades analítica que inclou peces de la tradició hel · lenística de llocs coetanis a la regió (és a dir, Kampyr Tepe i Termez). L'anàlisi va revelar que la majoria de les vaixelles i ceràmiques comunes analitzades corresponen a una única producció local de ceràmica que consisteix en un material calcari molt fi. La composició i les característiques morfològiques d'aquestes peces permeten distingir-les d'altres produccions contemporànies de ceràmica. No obstant això, es va assignar un origen regional per a algunes mercaderies que confirmaven contactes entre diferents llocs. L'única olla de cocció examinada consistia en un material calcari amb petxines com desgreixant que és compatible amb una tradició tecnològica regional.

ARTICLE IN PRESS
JASREP-00729; No of Pages 11
Journal of Archaeological Science: Reports xxx (2016) xxx–xxx
Contents lists available at ScienceDirect
Journal of Archaeological Science: Reports
journal homepage: www.elsevier.com/locate/jasrep

Pottery in Hellenistic tradition from ancient Bactria: The Kurganzol fortress (Uzbekistan, Central Asia)

V. Martínez Ferreras [a,*], A. Angourakis [a], A. Hein [b], J.M. Gurt Esparraguera [a], L.M. Sverchkov [c], A. Sánchez del Corral [d]

[a] ERAAUB, Department of Ancient History and Archaeology, University of Barcelona, Carrer de Montalegre, 6-8, 08001 Barcelona, Spain
[b] Institute of Nanoscience and Nanotechnology N.C.S.R. Demokritos 153 10 Aghia Paraskevi, Athens, Greece
[c] Institute of Fine Arts, Academy of Sciences of Uzbekistan, 2, Independence sq, 100029 Tashkent, Uzbekistan
[d] Department of Geography, University of Salamanca, Salamanca, Spain

ARTICLE INFO

Article history:
Received 17 June 2016
Received in revised form 14 November 2016
Accepted 29 November 2016
Available online xxxx

Keywords:
Pottery
Hellenistic influences
Ancient Bactria
Provenance
Technology
Surface treatments
Chemical analysis
Mineralogical analysis
Petrographic analysis

ABSTRACT

Kurganzol is one of the fortresses founded in ancient Bactria during the conquest of Alexander the Great. An archaeometric characterisation was conducted on 20 pottery sherds recovered in the earliest settlement dated to the late-4th BC. The aim is to examine both the composition and variation of the raw materials used and the production technology involved in pottery manufacture. The sampling included plates, cup/bowls, basins, jars, containers, a colander, a bottle or flask and a cooking pot. The analytical program comprised X-ray Fluorescence, X-ray Diffraction, and thin section analysis as well as the study of the geological environment. The analysis of the surface treatment was performed on three sherds through scanning electron microscopy coupled with energy dispersive X-ray spectroscopy (SEM-EDS). The results were compared with an analytical database that includes wares in Hellenistic tradition from coeval sites in the region (i.e. Kampyr Tepe and Termez). The analysis revealed that most of the tableware and common wares analysed correspond to a single local pottery production consisting of a very fine calcareous fabric. Composition and morphological characteristics of these wares enable distinguishing this fabric from other contemporary pottery productions. A regional origin was however assigned for a few wares confirming contacts among different sites. The only cooking pot examined consisted of a calcareous shelltempered fabric which is consistent with a regional technological tradition.
© 2016 Elsevier Ltd. All rights reserved.

1. Introduction

Pottery recalling the tableware from the Hellenistic tradition has often been recovered in most of the settlements founded in ancient Bactria (Central Asia) after Alexander the Great's conquest in the late 4th century BC. This historical region covered the nowadays territories of south Uzbekistan and Tajikistan and north Afghanistan; it was ruled by the Seleucids (Macedonian) kings, successors of Alexander, who controlled the territory comprised from the Mediterranean to north India. In Bactria, they set up a number of citadels and urban centres in the alluvial plains of the Amu Darya (the ancient Oxus river) and its tributaries, such as Ai-Khanoum and Dzhiga Tepe in northern Afghanistan, and Dalverzin Tepe, Kampyr Tepe, and Termez in southern Uzbekistan (Fig. 1). Besides their military function, these centres were trading posts on the route linking India with Bactria and Sogdia and onwards to the Caspian Sea, as well as a source of transmission of the Hellenistic culture in Central Asia (Leriche, 2007). Greek traditions persisted in most of these sites when the region became the independent Greco-Bactrian kingdom towards the mid-3rd century BC and remained until the invasion of a set of nomadic clans migrating from the North and East at mid-2nd century BC (Bernard, 1994).

A particular Hellenistic fortress in ancient Bactria is Kurganzol which, unlike the already mentioned centres, is located at the southern end of a fluvial terrace of the Uchkul River (altitude 924 m), in one of the southern foothills of the Baysuntau (Fig. 1), the south-western spurs of the Hissar Range (Uzbekistan). The area belongs to the Sherabad basin, one of the major tributaries of the Surkhan Darya that is, in turn, an affluent of the Amu Darya. The site had a diameter of 35 m and it consisted of a circular defensive wall (2.6 m thick) made of mud bricks, with the entrance at the north and six semi-circular towers attached to the north-eastern side, the most vulnerable flank (Fig. 2). Buildings of different size and layout were arranged around the edge of the defensive wall and surrounding a central courtyard provided by a water deposit in the centre. Radiocarbon dating has proved that the fortress was

* Corresponding author.
E-mail addresses: vmartinez@ub.edu (V. Martínez Ferreras), andreas.angourakis@ub.edu (A. Angourakis), a.hein@inn.demokritos.gr (A. Hein), jmgurt@ub.edu (J.M. Gurt Esparraguera), lsverchkov@mail.ru (L.M. Sverchkov), jana@usal.es (A. Sánchez del Corral).

http://dx.doi.org/10.1016/j.jasrep.2016.11.049
2352-409X/© 2016 Elsevier Ltd. All rights reserved.

Please cite this article as: Martínez Ferreras, V., et al., Pottery in Hellenistic tradition from ancient Bactria: The Kurganzol fortress (Uzbekistan, Central Asia), Journal of Archaeological Science: Reports (2016), http://dx.doi.org/10.1016/j.jasrep.2016.11.049

ARTICLE IN PRESS

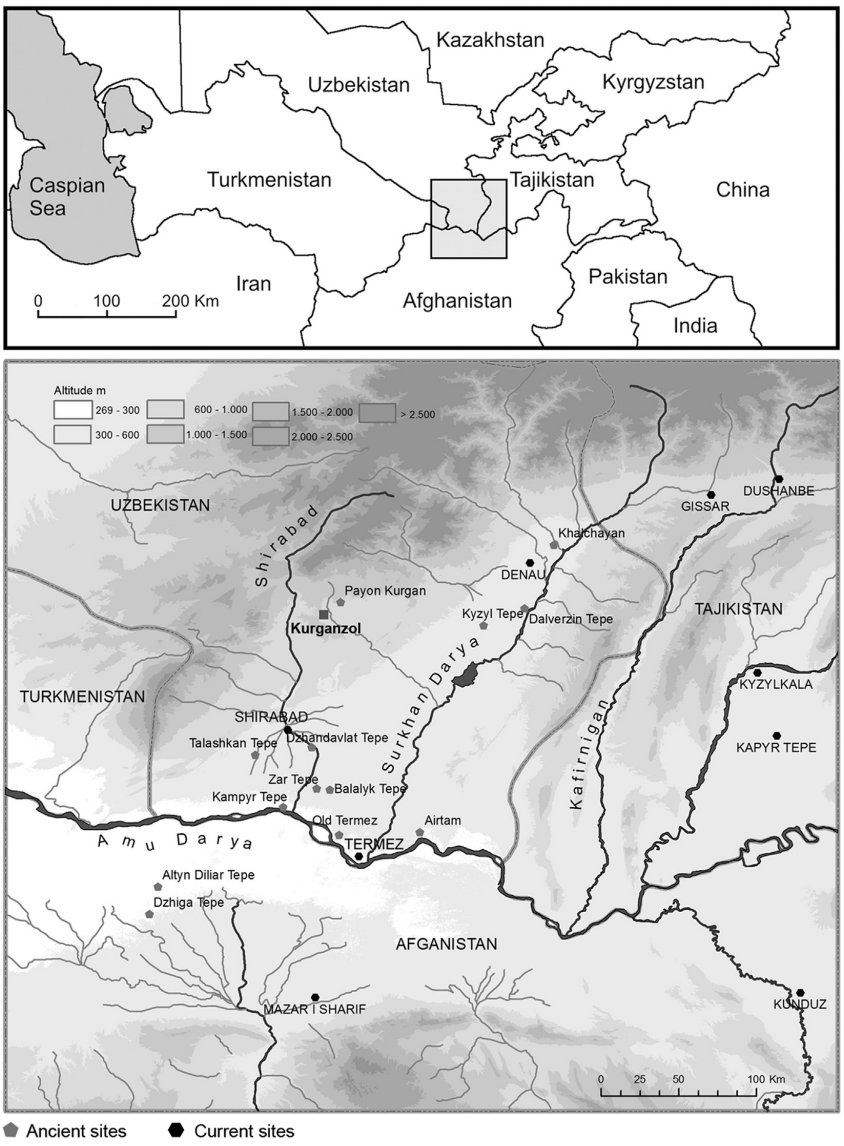

Fig. 1. Map of ancient Bactria with the location of Kurganzol and the main settlements cited in the text.
(Drawing by A. Sánchez del Corral; cartographic base: *Aster* Global Digital Elevation Map NASA, http://www.gdem.aster.ersdac.or.jp).

founded in the late 4th century BC and abandoned in the early 3rd century BC. During this period, Kurganzol endured two warlike events as suggested by traces of fire and destruction in most of the areas. The historical and archaeological data support the idea that it was one of the six citadels founded by Alexander the Great in strategic positions at checkpoints between the Amu Darya plain and Sogdia (Sverchkov, 2008, 2013).

As far as pottery is concerned, the shapes and the surface treatments of the tableware produced and used in ancient Bactria from the late 4th to mid-2nd centuries BC evoke clear Hellenistic-Mediterranean influences (i.e. red and black slips, stamped palms, incised concentric lines and applied ornaments), as several scholars have noted (Gardin, 1973; Houal, 2013; Martínez Ferreras et al., 2016). Pottery found in the earliest levels of the Kurganzol fortress comprises semi-spherical cups, bowls with rims curved inwards, plates with T-shaped or L-shaped profiles and 'fish plates', kraters used for mixing wine, and a wide range of narrow-necked and wide-necked jugs, storage jars or containers and cooking pots. These vessels were fired in both oxidising and reducing atmospheres and were mainly non-slipped although a few sherds present red or black slips. They primarily exhibit flat bases

Please cite this article as: Martínez Ferreras, V., et al., Pottery in Hellenistic tradition from ancient Bactria: The Kurganzol fortress (Uzbekistan, Central Asia), Journal of Archaeological Science: Reports (2016), http://dx.doi.org/10.1016/j.jasrep.2016.11.049

ARTICLE IN PRESS

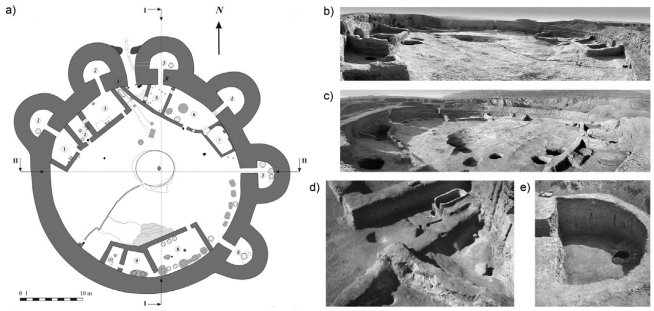

Fig. 2. a) General plan of Kurganzol; b/c) general photographs of the archaeological site; d) Room 4 containing a ceramic bathtub; e) one of the towers of the fortification. (From Sverchkov, 2013).

although a few of them are disk-shaped or slightly concaves (Sverchkov, 2008, 2013).

As part of an ongoing research project focused on the study of pottery in Hellenistic tradition from ancient Bactria, we present the archaeometric characterisation of 20 pottery sherds from the earliest levels of the Kurganzol fortress including tableware, common wares, and a cooking pot (Fig. 3). The geo-chemical composition of the pottery pastes has been identified by using X-ray Fluorescence (XRF-WD), X-ray Diffraction (XRD) and thin section optical microscopy (OM). Surface coatings were investigated on three selected samples through the scanning electron microscopy equipped with an energy dispersive X-ray spectrometer (SEM-EDS). The aim is to shed light on the composition and technological characteristics of the pottery used at the fortress during the Seleucid period. Since no pottery kiln has been recovered at the site, the geochemical composition of the pottery from Kurganzol has been compared with the data available of coeval tableware previously characterised from two Hellenistic sites located on the north bank of the Amu Darya: Kampyr Tepe (KPT), where two pottery centres with several kilns have been found (Martínez Ferreras et al., 2016), and the Citadel of Termez (TC) (Martínez Ferreras et al., submitted). The final aim is to explore possible relationships of provenance between the wares found at Kurganzol and those from two centres in the alluvial plane, as well as to investigate the degree of technological standardisation in pottery manufacture at a regional level.

2. Materials and methods

Sampling was restricted to 20 vessels from a pottery assemblage recovered in the excavations conducted in 2008 at the site. The selected sherds cover all functional categories, including both the more representative types as well as a few singular vases. They consists of six plates related to types P-2, P-6, P-7 (K1 to K4, K6, K7), a hand-made plate (K8), two bowls of types B-1 and B-6 (K5, K10), one platter (K9), one colander (K11), two storage jars (K12 and K13), one basin (K14), three containers or storage vessels (K15, K16 and K19), one krater or storage jar (K17), one bottle or flask (K18) and a cooking pot (K20) (Fig. 3, Table 1). The pottery assemblage from Kampyr Tepe and Termez includes plates, bowls, cups, platters, jars, containers or storage jars, and kraters of various prototypes (Martínez Ferreras et al., 2016, submitted).

The geochemical analysis was carried out at the CCiT-UB Laboratory of the University of Barcelona. XRF-WD was performed by using a PANalytical Axios-Max advanced spectrometer with a Rh excitation source while pottery samples from Kampyr Tepe and Termez were analysed by using a Philips PW 2400 spectrometer with an Rh excitation source. The surfaces of the sherds were first removed and then the samples were grinded in a mill. In all cases, major and minor elements were determined by preparing duplicates of glassy pills using 0.3 g of powdered specimens in an alkaline fusion with lithium tetraborate at 1/20 dilution and firing it at a temperature of 1150 °C using a high frequency induction furnace Perl'X-2. Trace elements and Na_2O were determined by powdered pills made from 6 g of dry sample mixed with 2 ml of a solution of a synthetic resin (Elvacite 2044, 20% in acetone). The mixture was homogenized in an agate mortar and pressed within an aluminium capsule containing boric acid by using a Herzog press.

The concentrations were quantified by a calibration line performed with sixty International Geological Standards. The loss on ignition (LOI) was determined by firing 0.3 g of dried specimen at 950 °C for 3 h. XRD was performed on the same powdered specimens using a PANalytical X'Pert PRO diffractometer, working with the Cu Kα1 radiation ($\lambda = 1.5406$ Å) as the incident beam, with a working power of 45 kV and 40 mA. Primary, firing and secondary crystalline phases were evaluated using the X'Pert High Score software by PANalytical. Petrographic thin section analysis was performed using a polarising microscope Olympus BX43F. The images were obtained with an Olympus DP73-WDR digital camera connected to the microscope and to the image analysis software Stream Basic, through which measurements and evaluations were performed.

Surface coatings were investigated on samples K2, K9 and K11 at the NCSR "Demokritos" in Athens. Freshly fractured samples were examined and photographed first under the optical microscope and then carbon coated for the SEM examination. It was carried out using an FEI, Quanta Inspect D8334 scanning electron microscope, coupled with an EDS. The samples were studied both in secondary electron and in backscattering mode in order to examine microstructures of ceramic bodies and surfaces. In order to evaluate the (dis)similarity of the chemical composition of both the ceramic body and the surface of each sample, at least three areas per sample (typically c. 50×50 μm^2 in the body and c. 50×20 μm^2 in the surface) were selected to be analysed with EDS. Even though the accuracy of SEM-EDS of fractured sections is limited compared to analyses of plane and polished surfaces, multiple measurements provide a basic estimation of precision and assessment of significant compositional differences.

3. Results

3.1. Analysis of the pottery pastes

The chemical concentrations of the 20 pottery sherds determined by XRF-WD (Table 2(a)) were treated statistically in order to calculate, first, the compositional variation matrix (CVM), which provides the total variation and the variability that each element introduces in the data set (Table 2(b)) (Buxeda i Garrigós, 1999). The resulting CVM reveals a relatively high total variation (vt = 0.656), which suggests the existence of more than one pottery production. Moreover, the τ_i values (total sum of variances in column i) indicate that most of the variability is caused by P_2O_5, CaO, Pb, Sr and Na_2O. Table 2(a) shows that P_2O_5

Please cite this article as: Martínez Ferreras, V., et al., Pottery in Hellenistic tradition from ancient Bactria: The Kurganzol fortress (Uzbekistan, Central Asia), Journal of Archaeological Science: Reports (2016), http://dx.doi.org/10.1016/j.jasrep.2016.11.049

ARTICLE IN PRESS

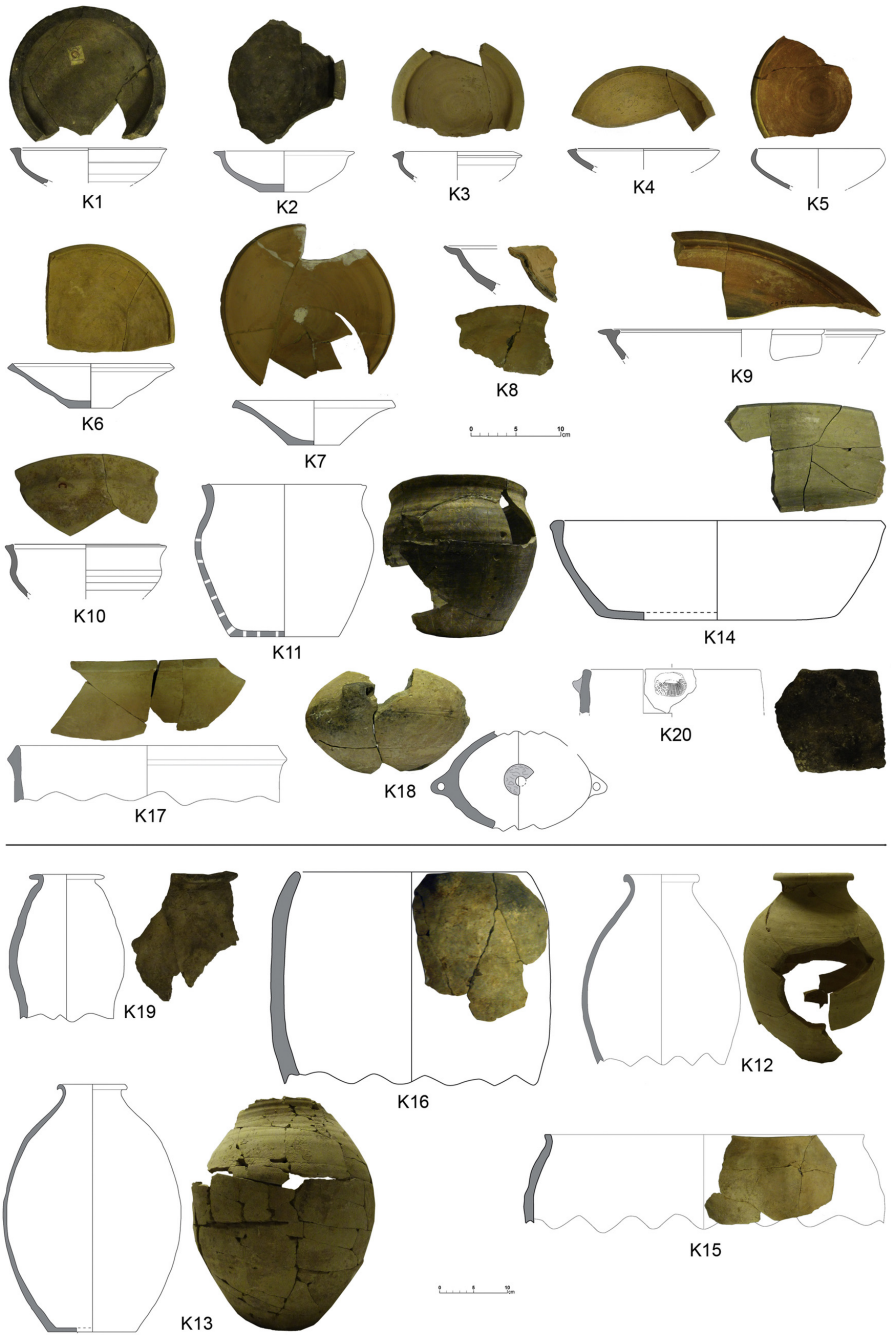

Fig. 3. Drawings and pictures of the pottery analysed from Kurganzol.

values are very high in samples K13, K15 and K16; Pb values vary from 7 ppm in K13 to 24/25 ppm in K8 and K17, while Sr concentrations oscillate between 235 and 581 ppm. P_2O_5 and Pb enrichment in specific sherds might be the consequence of post-depositional contaminations. The former appears commonly perturbed in pottery deposited in anthropised environments (Maritan and Mazzoli, 2004). The high

Please cite this article as: Martínez Ferreras, V., et al., Pottery in Hellenistic tradition from ancient Bactria: The Kurganzol fortress (Uzbekistan, Central Asia), Journal of Archaeological Science: Reports (2016), http://dx.doi.org/10.1016/j.jasrep.2016.11.049

ARTICLE IN PRESS

Table 1
Pottery analysed from Kurganzol.

Sample	Description	Prototype	Analysis
K1	Black slipped plate	P-2	XRF, XRD
K2	Black slipped plate	P-2	OM, XRF, XRD
K3	Plate	P-2	OM, XRF, XRD
K4	Plate	P-7	XRF, XRD
K5	Bowl	B-1	XRF, XRD
K6	Plate	P-6	OM, XRF, XRD
K7	Plate	P-6	OM, XRF, XRD
K8	Hand-made plate	P-2	OM, XRF, XRD
K9	orange slipped platter	–	OM, XRF, XRD
K10	Bowl/Cup	B-6	OM, XRF, XRD
K11	Black slipped colander	–	OM, XRF, XRD
K12	Storage jar	–	XRF, XRD
K13	Storage jar	–	OM, XRF, XRD
K14	Basin	–	OM, XRF, XRD
K15	Container/storage vessel	–	OM, XRF, XRD
K16	Container/storage vessel	–	OM, XRF, XRD
K17	Krater/storage jar	–	XRF, XRD
K18	Bottle/Flask	–	OM, XRF, XRD
K19	Container/storage jar	–	OM, XRF, XRD
K20	Cooking pot	–	OM, XRF, XRD

$\tau_{\cdot CaO}$ value is mainly due to the extremely high concentration of this element in the shell-tempered cooking pot K20. Nevertheless, in some cases, variability in CaO could be related to weathering processes in which other elements such as Sr and Ba may have undergone perturbations in their content (Buxeda i Garrigós, 1999). The cooking pot K20 is, together with K3 and K7, the ware with the lowest value in Na_2O while this concentration appears tripled in two common wares, K13 and K15. As observed in the petrographic examination (see below), these differences could be due to the crystallisation of secondary sodium chlorides (halite) within the pottery voids, a weathering process that is common in most of the sites of ancient Bactria (Martínez Ferreras et al., 2016; Tsantini et al., 2016).

In order to explore the compositional similarity/dissimilarity among the samples on the subcomposition Fe_2O_3, Al_2O_3, MnO, TiO_2, MgO, CaO, K_2O, SiO_2, Ba, Rb, Th, Nb, Zr, Y, Ce, Ga, V, Zn, Ni, and Cr, robust Principal Component Analysis (robust PCA) was performed following the procedure explained in Filzmoser et al. (2009). Robust PCA has proven to produce a graphical projection that is less sensible to the presence of outliers, thus better representing the main information. This procedure includes a sequence of isometric and centred log-ratio transformations that are required to cope with the special geometry of compositional data (Aitchison, 1986) while allowing the application of robust PCA. Additionally, we applied three different criteria for the detection of outliers on the matrix of Euclidean distances between samples: if the mean (MD) or the median (MdD) of distances from an individual is greater than a certain threshold; or if the score given by the Local Outlier Factor surpass a threshold (LOF with k = 2; Breuning et al., 2000). The threshold under each criterion was fixed at Md + 2MAD, where Md is the median of the corresponding value for all individuals and "MAD" is the "Median Absolute Deviation" or the absolute deviation around the median (Ramsey and Ramsey, 2007).

The first two principal components (Fig. 4a), which represent 85.85% of the original variability, place most of the samples analysed ($n = 14$) in a single group of calcareous wares (7–12 wt% CaO). The outliers detected under the three criteria mostly coincide with those visibly separated when considering the first two principal components: three calcareous vessels—the platter K9, the jar K13, and the basin K14, which is relatively close to the formers, but was not pointed out by the criteria; the plate K7 and the hand-made plate K8, which are relatively distant to the main group—the former exhibiting the highest values in Fe_2O_3, Al_2O_3, Rb, Ga, V, and Zn, and the latter a CaO percentage of 5.9 wt%, slightly lower to those of the main group; last, the shell-tempered cooking pot K20 appears clearly isolated due to a very high CaO concentration (23.5 wt%) to the detriment of the remaining elements, particularly Fe_2O_3, Al_2O_3, SiO_2 and most of the trace elements. Therefore, according to the chemical composition, most of the wares analysed from Kurganzol—except possibly K7, K8, K9, K13, K14, and K20—could be assigned to a single provenance.

To address the comparative study with the coeval tableware and common wares recovered at Kampyr Tepe (KPT) and at the Citadel of Termez (TC), the same procedures were repeated on the subcomposition Fe_2O_3, Al_2O_3, TiO_2, MgO, CaO, K_2O, SiO_2, Ba, Rb, Th, Nb, Zr, Y, Ce, Ga, V, Zn, Ni and Cr, without considering sample K20. Additionally, PERMANOVA and PERMDISP tests were executed (Anderson and Walsh, 2013) in order to identify significant location and dispersion differences between the assemblages of the three sites.

In the first two principal components (Fig. 4b), which denote 50.55% of the original variability, most of the samples from Kurganzol are joined and positioned apart from most of the wares from Termez and Kampyr Tepe. First, this distribution confirms the chemical similarity among most of the wares analysed from Kurganzol, thus supporting their attribution to the same pottery workshop or production area. Secondly, the separation between Kurganzol main group and the assemblages of Termez and Kampyr Tepe is proven to be significant (PERMANOVA's p-value is <0.01), discarding a single source of raw materials; though the higher internal diversity within each assemblage is also indicated (PERMANOVA's r-squared is low). Specifically regarding Kurganzol, and in consonance to the previous analysis (Fig. 4a), two plates (K7 and K8), a platter (K9), a jar (K13), and a basin (K14) are shown to be significantly different from Kurganzol main group. In fact, the platter K9 appears to have the most similar composition to the group of vessels from Termez and Kampyr Tepe.

The diffractograms obtained by XRD were examined to give insight in the mineralogical composition of the pottery sherds (Fig. 5). Samples clustered in group KGZ can be divided into several categories according to the mineralogical phases identified, which are related to different firing conditions. A first category corresponds to the vessels fired at a low temperature in reducing (K2, K11, K18, and K6) and oxidising (K1) atmosphere. The diffractograms exhibit only primary mineralogical phases (quartz, calcite, plagioclase, illite-muscovite and K-feldspar) while hematite has crystallised only in sample K6. Therefore, the estimated firing temperature (EFT) has been fixed around 750/800–850 °C. In the diffractograms of three storage vessels, K12, K15, and K19, the same primary phases coexist with incipient firing phases (diopside, gehlenite and hematite) suggesting an EFT around 850–900 °C. The third category includes samples fired between 900 and 950 °C (K4, K10, K16, and K17), in which calcite and illite-muscovite appear decreased, while the firing phases are notably increased. Finally, the firing temperature has been estimated high (950–1000/1050 °C) in two vessels K3 and K5, since calcite and phyllosilicates have totally disappeared, gehlenite is significantly reduced and diopside has increased. Regarding the samples not included in the chemical group KGZ, the diffractogram of the hand-made plate K8 exhibits only primary phases suggesting an EFT around 750/800–850 °C. The initial crystallisation of firing phases can be recognised in samples K7 and K9 which denotes an EFT around 850–900 °C. The firing phases observed in the diffractogram of the basin K14 are in accordance to those identified in the third category while the mineralogical composition of the storage jar K13 is equivalent to that defined in the fourth category. The mineralogical composition of the cooking pot K20 presents major differences; it is composed of primary phases (mainly calcite and also dolomite, quartz, and illite-muscovite) indicating a very low firing temperature (EFT: 700–800).

Examination of thin sections under the polarising microscope points to nine different petrographic fabrics. First, KGZ-A comprises most of the tableware linked in the main chemical group: bowls (K5, K10), plates (K1, K2, K3, K4, K6), the colander (K11), the storage jar K12 and the flask K18 (Fig. 6). It consists of a calcareous fine fabric, with abundant non-plastic inclusions in the fine fraction (≤0.125 mm grain size) and few to common in the coarse fraction (≤0.3 mm grain size), well sorted. The latter contains subangular to subrounded crystals of quartz,

Please cite this article as: Martínez Ferreras, V., et al., Pottery in Hellenistic tradition from ancient Bactria: The Kurganzol fortress (Uzbekistan, Central Asia), Journal of Archaeological Science: Reports (2016), http://dx.doi.org/10.1016/j.jasrep.2016.11.049

Table 2
a) XRF normalised data (% for major elements and ppm for trace elements) of the 20 samples analysed by XRF and the loss on ignition (LOI) (in %); b) Summary of the Compositional Variation Matrix of the samples analysed; According to Buxeda i Garrigós (1999): vt = total variation; $\tau_{.i}$ = total sum of variances in column i; $vt/\tau_{.i}$ = percentage of variance in the logratio covariance matrix using the component x_i as divisor due to the total variation; $r_{v.\tau}$ = correlation between the values τ_{ij} ($i \neq j$) and the corresponding values $\tau_{.i}$ ($j = 1, \ldots, i-1, i+1, \ldots, S$).

a)

	Fe_2O_3	Al_2O_3	MnO	P_2O_5	TiO_2	MgO	CaO	Na_2O	K_2O	SiO_2	Ba	Rb	Th	Nb	Pb	Zr	Y	Sr	Ce	Ga	V	Zn	Cu	Ni	Cr	LOI
K1	5.45	14.81	0.08	0.19	0.67	2.54	8.64	1.15	3.64	55	416	109	13	11	22	158	24	290	52	17	122	86	21	35	81	7.4
K2	5.23	14.20	0.07	0.17	0.65	2.54	9.19	1.11	3.48	53	386	98	13	10	20	148	22	239	61	18	116	83	23	32	78	10.2
K3	6.27	17.24	0.07	0.19	0.75	3.04	9.53	0.98	3.43	57	397	131	14	11	15	152	25	260	60	20	139	88	19	39	100	1.2
K4	6.09	16.85	0.07	0.20	0.73	2.88	9.12	1.01	3.60	56	411	132	14	11	21	154	26	300	60	21	143	85	19	40	97	3.2
K5	6.22	17.11	0.08	0.26	0.74	3.16	9.13	1.13	3.42	57	431	131	15	12	13	165	26	291	70	20	139	89	21	42	98	1.4
K6	6.22	16.98	0.08	0.18	0.75	2.87	7.71	1.12	3.60	57	426	131	14	12	22	156	25	266	65	21	137	99	23	39	89	3.3
K7	6.97	18.84	0.07	0.18	0.77	3.07	7.23	0.87	3.76	57	363	152	14	11	21	150	25	255	53	23	167	96	16	37	103	1.7
K8	5.29	17.91	0.07	0.17	0.76	2.41	5.91	1.01	3.69	57	410	130	15	12	25	155	26	285	66	21	120	90	26	36	75	4.9
K9	5.09	13.60	0.09	0.35	0.60	3.16	10.31	1.24	3.41	56	461	99	13	10	20	143	24	373	48	16	93	79	21	34	69	6.0
K10	5.52	15.12	0.07	0.28	0.69	2.98	9.91	1.40	3.65	56	445	114	14	11	21	153	25	409	56	18	125	83	20	35	83	4.5
K11	5.49	14.88	0.06	0.17	0.68	2.58	9.08	1.01	3.48	52	370	103	13	10	19	138	23	235	50	18	121	81	22	31	70	10.2
K12	6.10	16.24	0.08	0.23	0.73	3.06	8.23	1.28	3.49	58	446	124	14	12	21	155	25	324	64	20	135	89	16	39	92	3.2
K13	5.62	14.90	0.08	0.40	0.70	3.10	9.52	1.78	2.80	59	469	88	14	11	7	162	25	399	65	18	112	67	21	39	81	2.2
K14	5.58	14.67	0.08	0.19	0.64	3.09	11.94	1.23	3.20	55	436	116	14	10	14	153	24	581	65	18	114	80	22	38	88	4.2
K15	6.22	15.90	0.08	0.49	0.72	2.99	7.15	1.94	3.71	58	415	118	14	11	17	151	24	366	57	19	113	88	24	39	84	2.6
K16	5.51	14.88	0.08	0.58	0.70	2.70	7.87	1.49	3.44	60	522	113	14	11	12	173	26	467	60	18	114	78	19	37	82	2.7
K17	5.83	15.17	0.08	0.20	0.69	3.17	9.07	1.48	3.26	58	485	118	14	11	24	164	24	343	59	19	111	82	20	37	81	3.0
K18	5.90	15.71	0.08	0.23	0.72	2.86	8.15	1.24	3.54	57	423	118	15	11	22	157	25	297	57	19	126	82	18	37	89	4.0
K19	5.64	14.78	0.08	0.18	0.68	3.04	9.32	1.41	3.32	57	457	112	13	11	21	154	25	471	61	18	109	80	24	38	81	4.4
K20	3.60	8.72	0.04	0.28	0.41	2.86	23.50	0.64	2.34	35	171	66	10	7	11	107	17	439	31	11	125	66	11	20	103	23.3

b)

	Fe_2O_3	Al_2O_3	MnO	P_2O_5	TiO_2	MgO	CaO	Na_2O	K_2O	SiO_2	Ba	Rb	Th	Nb	Pb	Zr	Y	Sr	Ce	Ga	V	Zn	Cu	Ni	Cr
$\tau_{.i}$	0.784	0.882	0.923	4.085	0.791	0.912	3.536	1.694	0.795	0.694	1.234	1.036	0.703	0.728	3.003	0.694	0.676	2.483	0.964	0.868	1.186	0.827	1.269	0.818	1.225
$vt/\tau_{.i}$	0.837	0.744	0.711	0.161	0.830	0.720	0.186	0.387	0.826	0.945	0.532	0.633	0.934	0.901	0.219	0.946	0.970	0.264	0.681	0.756	0.553	0.793	0.517	0.802	0.536
$r_{v.\tau}$	0.988	0.972	0.958	0.423	0.981	0.903	0.359	0.757	0.968	0.992	0.917	0.955	0.999	0.989	0.956	0.998	0.999	0.319	0.983	0.974	0.891	0.955	0.955	0.984	0.821
vt	0.656																								

Please cite this article as: Martínez Ferreras, V., et al., Pottery in Hellenistic tradition from ancient Bactria: The Kurganzol fortress (Uzbekistan, Central Asia), Journal of Archaeological Science: Reports (2016), http://dx.doi.org/10.1016/j.jasrep.2016.11.049

ARTICLE IN PRESS

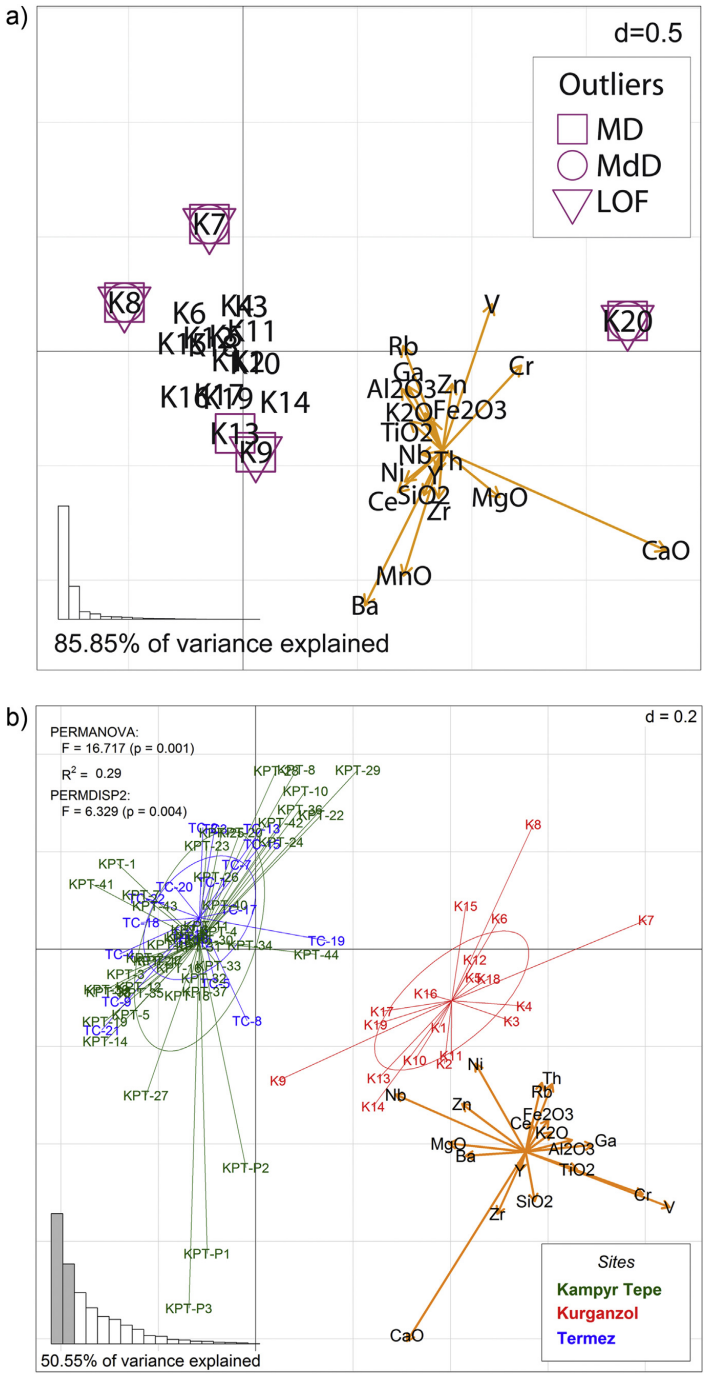

Fig. 4. Biplot of the two first principal components considering: a) the wares from Kurganzol; b) wares from Kurganzol (except K20) together with the tableware from Kampyr Tepe and Termez.

Please cite this article as: Martínez Ferreras, V., et al., Pottery in Hellenistic tradition from ancient Bactria: The Kurganzol fortress (Uzbekistan, Central Asia), Journal of Archaeological Science: Reports (2016), http://dx.doi.org/10.1016/j.jasrep.2016.11.049

ARTICLE IN PRESS

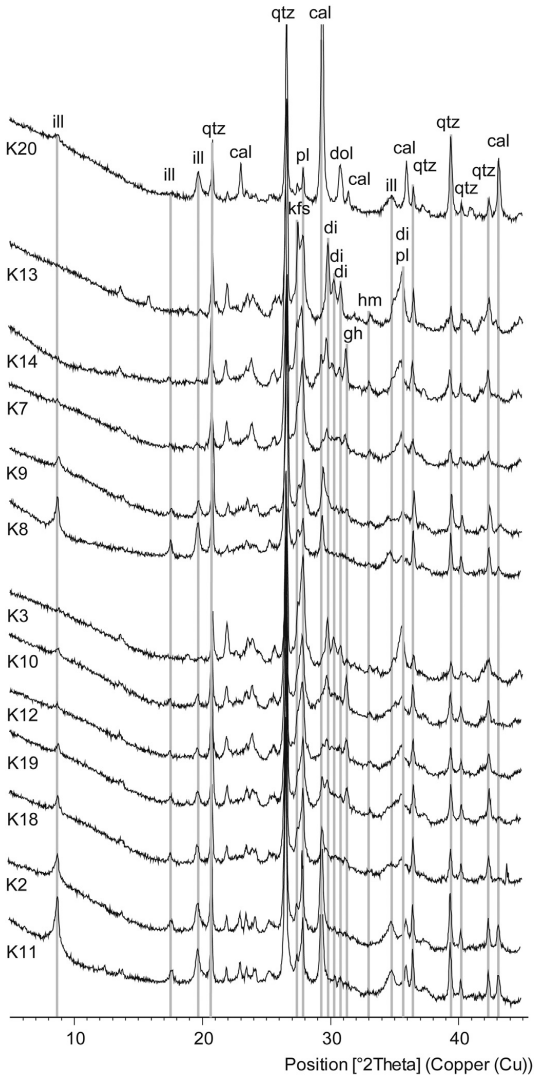

Fig. 5. X-ray diffractograms of the pottery from Kurganzol; cal: calcite; di: diopside; dol: dolomite; gh: gehlenite; hm: hematite; ill: illite-muscovite; kfs: K-feldspar; pl: plagioclase; qtz: quartz.

plagioclase, and K-feldspar as predominant inclusions; Ca-microfossils, partially or totally decomposed in micritic calcite during the firing process, are dominant; muscovite flakes and metamorphic rock fragments (schist and quartzite) are frequent; fragments of chert are common; opaque minerals and biotite are rare. A second fabric (KGZ—B) includes three common wares (K14, K16, K17) which exhibit a calcareous vitrified matrix with frequent voids (micro- to macro- vughs and vesicles). Inclusions are abundant and fine (silt to fine sand grain sized) and consist of the same lithological types including coarse nodules of calcite (limestone) partially decomposed, and fine to coarse ferruginous nodules.

The petrographic composition of the rest of the samples differs from that of the previous groups and they represent different petrographic fabrics. Two containers (K15 and K19) and the plate K8 were probably hand-made (Fig. 6). The matrix of sample K15 displays streaks of red-coloured clay (low calcareous) and ferruginous aggregates, which probably indicate clay mixing; micro- to meso- vesicles and meso- to macro-vughs are common and they usually appear filled with small crystals of halite. Its occurrence seems to be the product of weathering processes associated with the circulation of chloride-rich solutions precipitating as secondary salts inside the voids, as observed in other pottery assemblages analysed from Kampyr Tepe (Martínez Ferreras et al., 2016) and ancient Termez (Tsantini et al., 2016). The fine fraction is abundant and constituted by small flakes of phyllosilicates and crystals (probably quartz and feldspars); the coarse fraction (≤0.4 mm) is scarce and consists of quartz, feldspars, opaque minerals, muscovite, and schist fragments. K19 is very porous and exhibits abundant meso- and macro-vesicles and channels, mainly due to the total decomposition of organic material (probably straw) and the partial decomposition of Ca-fossils and calcite (micrite) (≤2 mm sized); Besides these non-plastic inclusions, coarse fraction (≤0.4 mm) comprises silty aggregates and the same rock crystals identified in the main petrographic group (KGZ-A). The groundmass is very heterogeneous in sample K8, prevalently consisting in streaks of light-coloured clay (richer in carbonates) with inclusions and frequent porosity (micro- and meso- vughs and vesicles and few channels), and thinner bands of red-coloured clay without inclusions; fine fraction (≤0.125 mm) is common to abundant while coarse fraction (≤0.4 mm) is common and is constituted by crystals of quartz and feldspars, Ca-fossils and bivalves and metamorphic rock fragments (schist).

The plate K7 is characterised by a very homogeneous Fe-rich matrix, vitrified, with common porosity (micro- and meso- vughs and vesicles) mainly due to the decomposition of carbonates; the fine fraction is almost inexistent while the coarse fraction is common to abundant, generally fine (≤0.3 mm), with a few larger grains (≤0.6 mm). Non-plastic inclusions comprise predominant plagioclase and K-feldspar grains, frequent quartz and mica flakes, common calcite (micrite), sedimentary and metamorphic rock fragments, and rare opaque minerals and biotite. The storage jar K13 presents a calcareous matrix, vitrified, with frequent voids, mainly due to the decomposition of carbonates and filled with secondary crystals of halite; the fine fraction (≤0.125 mm) is abundant and the coarse fraction (≤0.4 mm) is few to common and comprises plagioclase and K-feldspar as predominant inclusions; quartz and metamorphic rock fragments (schist and quartzite) are frequent, mica flakes are common and opaque and heavy minerals are rare. The platter K9 presents a calcareous matrix, semi-vitrified; fine fraction (≤0.125 mm) is abundant and is mainly composed of fine grains of quartz, feldspars, carbonates and mica flakes; coarse fraction (≤1 mm) is common and constituted by prevalent plagioclase, K-feldspar and quartz crystals and metamorphic rock fragments (quartzite, schist); calcite (micrite and sparite), Ca-microfossils and sedimentary rock fragments are frequent; chert fragments and mica flakes are common; clinopyroxene, amphibole, and opaque minerals are rare. The shell-tempered cooking pot K20 exhibits a calcareous matrix, poorly vitrified, with frequent voids due to the decomposition of Ca-microfossils and bivalves; inclusions are subangular to subrounded, poorly sorted, oriented parallel to the vessel margins; fine fraction (≤0.125 mm) is common to abundant and consists of small crystals (quartz and feldspars), carbonates and mica flakes; coarse fraction is abundant and mostly constituted by Ca-microfossils (≤0.5 mm) and shell fragments (generally ≤2 mm but some bivalves arise ≤4 mm).

3.2. Analysis of the surface treatments

As it could be expected from the XRD examination the degree of vitrification observed in the three samples investigated by SEM (K2, K9, and K11) was comparably low. The body of the reddish slipped platter K9 presented a significant initial vitrification while the bodies of the other two black slipped wares exhibited only marginal vitrification.

Please cite this article as: Martínez Ferreras, V., et al., Pottery in Hellenistic tradition from ancient Bactria: The Kurganzol fortress (Uzbekistan, Central Asia), Journal of Archaeological Science: Reports (2016), http://dx.doi.org/10.1016/j.jasrep.2016.11.049

ARTICLE IN PRESS

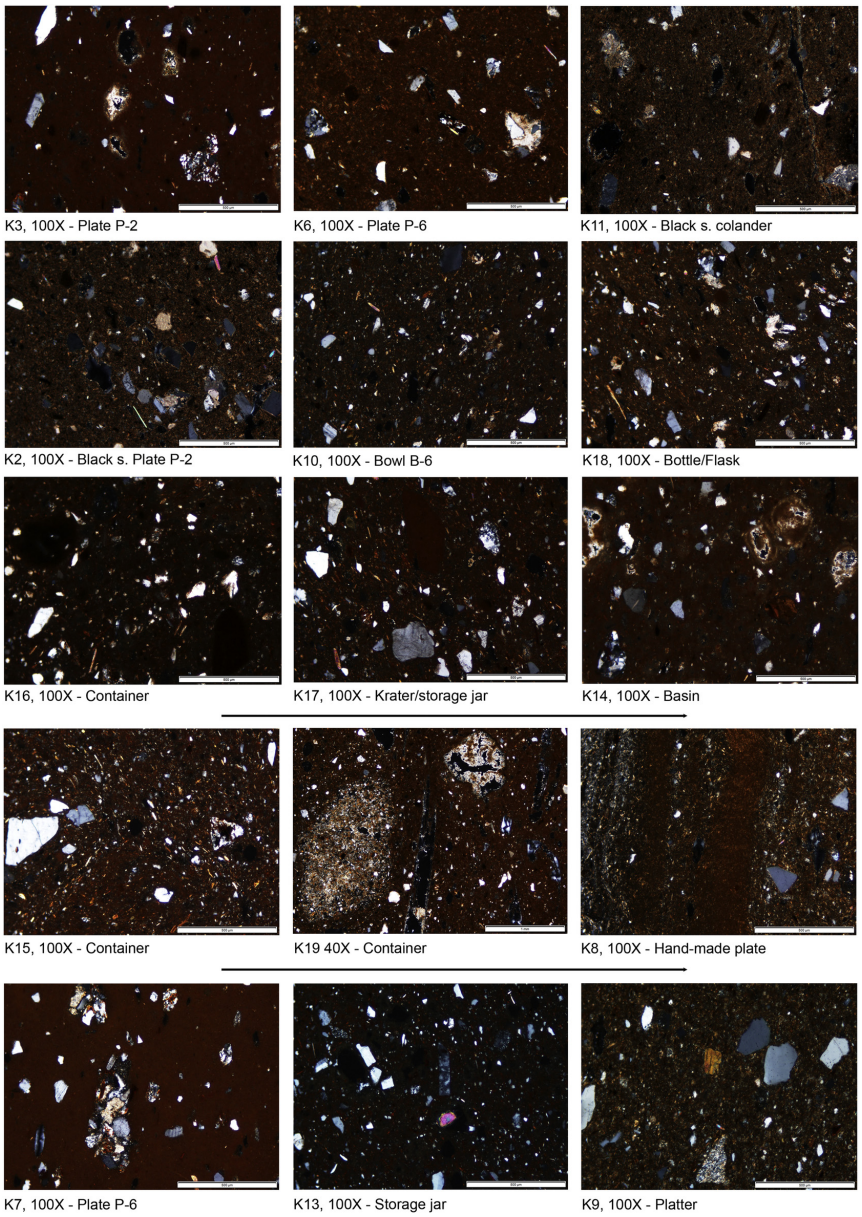

Fig. 6. Thin-section microphotographs with crossed polarised light (xp) of the pottery from Kurganzol.

Furthermore, the surface layers presented hardly a higher degree of vitrification compared with the bodies even though their paste appeared to have been refined and the surface was apparently burnished (Fig. 7). The thickness of the surface layers was typically from 20 μm up to 40 μm. At least in the case of the examined samples, a slipped surface could not be observed probably due to insufficient firing temperatures.

Table 3 presents the average elemental compositions of body and slip of each sample according to SEM-EDS of the fractured sections. Although they are based on semi-quantitative data, the examination of the results points to two tendencies. The two samples K2 and K11 both present no significant compositional differences of the paste used for the surface in comparison with the clay used for the body construction. There appears to be a small trend to higher iron concentrations in

Please cite this article as: Martínez Ferreras, V., et al., Pottery in Hellenistic tradition from ancient Bactria: The Kurganzol fortress (Uzbekistan, Central Asia), Journal of Archaeological Science: Reports (2016), http://dx.doi.org/10.1016/j.jasrep.2016.11.049

ARTICLE IN PRESS

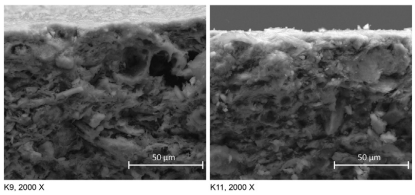

Fig. 7. SEM micrographs in secondary electron mode.

the surface layers but still within the variation estimated by the standard deviation. K2 furthermore presented a slightly reduced calcium content probably due to a basic refinement of the clay. K9 was the only sample which presented significant compositional differences of the surface layer with a clearly reduced calcium content and an increased potassium content. The calcium content determined on the surface was only half of the calcium content measured on the body. This was assumedly achieved by a more elaborate refinement of the clay paste by elutriation, removing coarse components such as carbonates. The potassium enrichment, on the other hand, could have been achieved by the addition of plant ash, indicated for example also by an enrichment of sulphur in the surface layer.

4. Discussion and conclusions

At least nine different pottery productions have been recognised among the sherds analysed. Nevertheless, most of the wares can be associated with a single clayey source and major differences are related to two specific technological processes: 1) raw materials processing to make up particular pastes (i.e. adding different tempers, mixing clays), and 2) modelling (i.e. by hand or using a wheel). Therefore, all the vessels analysed from Kurganzol can be attributed to a local/regional origin and differences are rightly correlated with the technological choices involved in the manufacture of different functional/technological pottery categories (tableware, common wares, storage vessels and cooking pots). This assumption is supported by the consistency of the main aplastic inclusions between the samples and by the low chemical variability (tv = 0.107) provided by the calculation of the compositional variation matrix when excluding the cooking pot K20.

The first production (KGZ-A) is composed of most of the tableware (plates and bowls) and some common wares (colander, flask, and a jar), which were produced using calcareous fine pastes and fired with both oxidising and reducing atmospheres. Group KGZ-B contains three common wares (K14, K17, and K16) which were manufactured by using slightly different raw materials since non-plastic inclusions include coarse Ca-fossils, limestone and ferruginous nodules. Nevertheless, the geochemical composition identified in the two fabrics is consistent with the geological environment and major differences can be explained by the procurement of raw materials in slightly different clayey deposits near the site or in the nearby area. Thus, the Baysun-Kugitang-tau mountain range comprises materials ranging from the Cretaceous —claystone, siltstone, marlstone and limestone with shells (especially frequent in the Senonian)— to the Miocene —limestone, dolomites, and gypsum— and the Pliocene —grey-brown siltstone, claystone, sandstone, and conglomerates— (Nikolaev, 2002). It must be emphasised that the slips used in samples K2 and K11 are similar to the receipt 1 identified at Kampyr Tepe which consists in no or at least no significant compositional differences between the surface and the body (Martínez Ferreras et al., 2016).

Three hand-made wares (K8, K15, and K19) were also produced by using illitic clays and the main non-plastic inclusions match with that found in the previous groups; Furthermore, a provenance from the Amu Darya basin is excluded because of the absence of crystals derived from volcanic rocks (Echallier, 1981; Sánchez del Corral and Thum, 2012; Martínez Ferreras et al., 2016, submitted; Tsantini et al., 2016) and therefore, a local/regional origin could be proposed for them. However, two different clays were mixed to produce the plate K8 and the container K15 and two specific tempers —organic (probably straw) and calcareous (micrite and Ca-fossils)— were added to the clayey sediment to produce the container K19. Diversity in raw materials procurement, processing and modelling could be intentional and probably linked to the intended function of the vessels, since they entail differences in the mechanical properties and performance characteristics. According to the geological environment, even the shell-tempered cooking pot can be attributed to a local/regional production. However, the manufacture of these pots appears to be a long-lasting regional tradition that spanned in the Amu Darya plain and the Surkhan Darya depression from the Bronze Age to the Islamic period: e.g. at Shortugaï (Afghanistan) (Echallier, 1981) and at ancient Termez (Uzbekistan) (Gurt Esparraguera et al., 2015). Samples K7, K9, and K13 exhibit major differences in their petrographic composition and, according to the chemical results, they must be considered as outliers. The platter K9 resembles the coeval pottery produced at Kampyr Tepe. The presence of crystals derived from effusive volcanic rocks confirms that this slipped platter was produced in this pottery workshop or in another centre in the Amu Darya basin. Moreover, the recipe followed to produce the slip of sample K9 has also been identified at the coeval site of Kampyr Tepe (Martínez Ferreras et al., 2016).

The study suggests that the fortress was mainly supplied by pottery produced locally. The outliers identified are imports produced elsewhere in the region or, more specifically, in the pottery workshops located in the Amu Darya (at least a platter). This evidence reveals the existence of relationships between the military garrisons established at different points of ancient Bactria. Moreover, the technological processes involved in the manufacture of the vessels found in all these sites were highly standardised in terms of pastes (calcareous fine

Table 3
Thickness of the slips and chemical composition of the slips and pottery bodies (ave: average, stdev: standard deviations).

			Na_2O	MgO	Al_2O_3	SiO_2	P_2O_5	SO_3	Cl_2O	K_2O	CaO	TiO_2	MnO	Fe_2O_3
K2	Body	*ave.*	1.0	3.0	16.8	57.7	0.2	0.2	0.2	4.1	9.4	0.9	0.2	6.3
		stdev.	0.3	0.2	0.4	1.0	0.1	0.1	0.1	0.2	0.7	0.2	0.1	0.5
	Surface	*ave.*	0.7	3.1	16.8	58.2	0.2	0.5	0.2	4.3	7.7	0.9	0.3	7.2
	(c. 30–40 µm)	*stdev.*	0.1	0.4	1.5	1.2	0.2	0.2	0.1	0.1	1.2	0.0	0.1	0.9
K9	Body	*ave.*	0.9	3.5	15.1	54.1	0.4	0.5	0.4	4.0	13.1	0.7	0.2	6.9
		stdev.	0.1	0.1	0.2	2.9	0.2	0.2	0.1	0.3	1.6	0.2	0.2	0.5
	Surface	*ave.*	1.0	3.1	14.9	59.1	0.5	1.2	0.5	4.9	6.2	0.7	0.2	7.5
	(c. 30–40 µm)	*stdev.*	0.2	0.3	1.6	1.6	0.3	0.5	0.5	0.3	1.2	0.1	0.2	1.0
K11	Body	*ave.*	0.7	2.7	16.3	54.7	0.3	0.6	0.2	4.2	11.3	0.9	0.2	7.7
		stdev.	0.1	0.3	1.0	1.1	0.1	0.2	0.1	0.2	0.9	0.4	0.0	1.5
	Surface	*ave.*	1.0	2.9	16.7	52.8	0.3	0.5	0.2	4.2	11.0	1.5	0.3	8.5
	(c. 20–30 µm)	*stdev.*	0.3	0.4	1.3	2.5	0.2	0.2	0.1	0.5	2.1	0.9	0.1	2.3

Please cite this article as: Martínez Ferreras, V., et al., Pottery in Hellenistic tradition from ancient Bactria: The Kurganzol fortress (Uzbekistan, Central Asia), Journal of Archaeological Science: Reports (2016), http://dx.doi.org/10.1016/j.jasrep.2016.11.049

ARTICLE IN PRESS

fabrics), vessels shapes and surface treatments. Given the relevance of studying ancient pottery to better understand the dynamics of the period of conquest and the development of the Hellenistic traditions in ancient Bactria, future research will be focused on the investigation of new pottery sherds from Kurganzol and other Hellenistic sites in the region.

Supplementary data to this article can be found online at http://dx.doi.org/10.1016/j.jasrep.2016.11.049.

Acknowledgements

This study was performed within the CAMOTECCER research project (HAR2012-32653), funded by the Spanish Ministry of Economy and Competitiveness (MINECO) and led by Dr. V. Martínez Ferreras in the framework of two post-doctoral research contracts (JCI-2011-10963 and RYC-2014-15789) granted by MINECO. The research was also supported by the project HAR2008-01730, funded by Spanish Ministry of Science and Innovation (MICINN) and led by Dr. J.M. Gurt. A. Angourakis worked on this paper through the FPI contract (BES-2013-062691) funded by the MINECO Spanish Ministry.We are most grateful to Dr. Sh. Pidaev, director of the Institute of Fine Arts of the Academy of Science of Uzbekistan, and to the archaeologists in charge of the excavation of Kurganzol for the samples provided. The authors thank the anonymous Referees for their helpful comments on earlier drafts of this paper.

References

Aitchison, J., 1986. The Statistical Analysis of Compositional Data. Chapman and Hall, London.

Anderson, M.J., Walsh, D.C.I., 2013. PERMANOVA, ANOSIM, and the mantel test in the face of heterogeneous dispersions: what null hypothesis are you testing? Ecol. Monogr. 83, 557–574.

Bernard, P., 1994. The Greek Kingdoms of Central Asia. In: Harmatta, J., Puri, B.N., Etemadi, G.F. (Eds.), History of Civilizations of Central Asia. Vol. II. The Development of Sedentary and Nomadic Civilizations: 700 B.Cto A.D Vol. 250. UNESCO Publishing, (Paris), pp. 99–129.

Breuning, M., Kriegel, H., Ng, R.T., Sander, J., 2000. LOF: Identifying Density-based Local Outliers, Proceedings of the ACM SIGMOD International Conference on Management of. Data, Dalles.

Buxeda i Garrigós, J., 1999. Alteration and contamination of archaeological ceramics: the perturbation problem. J. Archaeol. Sci. 26, 295–313.

Echallier, J.C., 1981. La Production des céramiques protohistoriques de Shortugaï (Afghanistan). Etude pétrographique. Paléorient 7, 115–119.

Filzmoser, P., Horn, K., Reimann, C., 2009. Principal component analysis for compositional data with outliers. Environmetrics 20, 621–632.

Gardin, J.C., 1973. Les Céramiques. In: Bernard, P. (Ed.), Fouilles d'Aï-Khanoum I (Campagnes 1965, 1966, 1967, 1968). Mémoires de la Délégation Archéologique Française en Afghanistan 21, pp. 121–188 Paris.

Gurt Esparraguera, J.M., Ariño Gil, E., Martínez Ferreras, V., Pidaev, S.R., 2015. The Buddhist occupation of Tchingiz Tepe (Termez, Uzbekistan) in the Kushan period through the ceramic contexts. Archaeol. Res. Asia 3:19–33. http://dx.doi.org/10.1016/j.ara.2015.04.003.

Houal, J.B., 2013. La céramique de Termez des époques antique et médiévale. In: Bendezu-Sarmiento, J. (Ed.), L 'Archéologie Française en Asie Centrale, Nouvelles recherches et enjeux socioculturels. Cahiers d'Asie Centrale 21/22, pp. 423–442 De Boccard, (Paris).

Leriche, P., 2007. Bactria, land of a thousand cities. In: Hermann, G., Cribb, J. (Eds.), After Alexander. Central Asia before Islam. Proceeding of the British Academy 133. Oxford University Press, Oxford, pp. 121–153.

Maritan, L., Mazzoli, C., 2004. Phosphates in archaeological finds: implications for environmental conditions of burial. Archaeometry 46, 673–683.

Martínez Ferreras, V., Gurt Esparraguera, J.M., Hein, A., Pidaev, S.R., Rtveladze, E.V., Bolelov, S.B., 2016. Tableware in the Hellenistic tradition from the city of Kampyr Tepe in ancient Bactria (Uzbekistan). Archaeometry 58 (5), 736–764.

Martínez Ferreras, V., Gurt Esparraguera, J.M., Ariño Gil, E., Sánchez del Corral, A., Hein, A., Angourakis, A., Pidaev, Sh., Assessing cultural patterns in ancient Termez (Uzbekistan) through the pottery: from the Hellenistic tradition to the nomadic influences. Geoarchaeology, (submitted).

Nikolaev, V.G., 2002. Afghan–Tajik depression, Architecture of sedimentary cover and evolution. Russ. J. Earth Sci. 4 (6), 399–421.

Ramsey, P.H., Ramsey, P.P., 2007. Optimal trimming and outlier elimination. Journal of Modern Applied Statistical Methods 6 (2) (Article 2). http://digitalcommons.wayne.edu/jmasm/vol6/iss2/2.

Sánchez del Corral, A., Thum, H., 2012. Geomorphology and Late Holocene morphogenesis of Tchinguiz Tepe hill (Old Termez, Uzbekistan, Central Asia). Quat. Int. 281, 89–104.

Sverchkov, L.M., 2008. The Kurganzol Fortress (on the History of Central Asia in the Hellenistic Era). Ancient Civilizations from Scythia to Siberia 14. Koninklijke Brill NV, Leiden, pp. 123–191.

Sverchkov, L.M., 2013. Kurganzol. Kryepost Alyeksandra na yugye Uzbyekistana. SMI-ASIA, Taskhkent.

Tsantini, E., Martínez Ferreras, V., Ariño Gil, E., Gurt Esparraguera, J.M., Pidaev, S.R., 2016. Pottery production in the Buddhist communities in Central Asia: the Kushan-Sassanian pottery workshop of Kara Tepe (Termez, Uzbekistan). Archaeometry 58 (1), 35–56.

Please cite this article as: Martínez Ferreras, V., et al., Pottery in Hellenistic tradition from ancient Bactria: The Kurganzol fortress (Uzbekistan, Central Asia), Journal of Archaeological Science: Reports (2016), http://dx.doi.org/10.1016/j.jasrep.2016.11.049

3.3. Assessing Hellenistic to nomadic cultural patterns through pottery in ancient Termez, Uzbekistan

Verònica MARTÍNEZ FERRERAS[a], Andreas ANGOURAKIS[a], Anno HEIN[b], Meritxell AULINAS JUNCÀ[c], Maite GARCIA-VALLÉS[c], Josep M. GURT ESPARRAGUERA[a], Enrique ARIÑO GIL[d], Ana SÁNCHEZ DEL CORRAL[d], Shakir R. PIDAEV[e]

[a] ERAAUB, Department of History and Archaeology, Faculty of Geography and History, University of Barcelona, Barcelona, Spain (vmartinez@ub.edu; andreas.angourakis@ub.edu; jmgurt@ub.edu).
[b] Institute of Nanoscience and Nanotechnology N.C.S.R. Demokritos, Athens, Greece (a.hein@inn.demokritos.gr).
[c] Faculty of Geology, University of Barcelona, Barcelona, Spain (meritxellaulinas@ub.edu; maitegarciavalles@ub.edu).
[d] Faculty of Geography and History, University of Salamanca, Salamanca, Spain (argil@usal.es; jana@usal.es).
[e] Institute of Fine Arts, Academy of Sciences of Uzbekistan, Tashkent, Uzbekistan (shakirdjan@mail.ru).

Esta sección corresponde al siguiente artículo:

MARTÍNEZ FERRERAS, V., ANGOURAKIS, A., HEIN, A., AULINAS JUNCÀ, M., GARCIA-VALLÈS, M., GURT ESPARRAGUERA, J.M., ARIÑO GIL, E., SANCHEZ DEL CORRAL, A. y PIDAEV, S.R., [sin fecha]. Assessing Hellenistic to nomadic cultural patterns through pottery in ancient Termez, Uzbekistan. *Geoarchaeology.*

Dado que aún no existe una versión publicada a fecha del depósito de la tesis, la paginación y la numeración de subsecciones y figuras han sido adaptadas.

Resumen Presentamos la contextualización arqueológica y la caracterización arqueométrica de cerámicas finas y comunes con y sin engobe de Termez (sur de Uzbekistán). Los objetivos son, en primer lugar, evaluar la fabricación de cerámica en la ciudad y región (antigua Bactriana) después de la conquista de Alejandro Magno a finales del siglo IV a. C. para detectar influencias de la cultura helenística mediterránea; y, segundo, investigar la evolución en la fabricación de cerámica después de la llegada de las tribus

nómadas Yuezhi a mediados del siglo II a. C. Se realizaron análisis de fluorescencia de rayos X, difracción de rayos X y secciones delgadas en los recipientes y en diversas materias primas locales para examinar la procedencia y los procesos tecnológicos involucrados en la fabricación de cerámica (adquisición y procesamiento de materias primas, conformación y cocción). Los tratamientos superficiales se analizaron usando microscopía electrónica de barrido equipada con un espectrómetro de rayos X de dispersión de energía (SEM-EDS). El estudio revela que todas las mercancías analizadas son productos locales/regionales hechos al torno, lo que sugiere un alto grado de estandarización tecnológica en la adquisición y el procesamiento de las materias primas en el período considerado. La principal diferencia entre las dos tradiciones de alfarería se refiere a la forma de los recipientes, apuntando a nuevos patrones de consumo después de la invasión nómada.

Resum Presentem la contextualització arqueològica i la caracterització arqueomètrica de ceràmiques fines i comunes amb i sense engalva de Termez (sud de l'Uzbekistan). Els objectius són, en primer lloc, avaluar la fabricació de ceràmica a la ciutat i regió (antiga Bactriana) després de la conquesta d'Alexandre el Gran a la fi del segle IV a. C. per detectar influències de la cultura hel · lenística mediterrània; i, segon, investigar l'evolució en la fabricació de ceràmica després de l'arribada de les tribus nòmades Yuezhi a mitjans del segle II a. C. Es van realitzar anàlisis de fluorescència de raigs X, difracció de raigs X i seccions primes en els recipients i en diverses matèries primeres locals per examinar la procedència i els processos tecnològics involucrats en la fabricació de ceràmica (adquisició i processament de matèries primeres, conformació i cocció). Els tractaments superficials es van analitzar utilitzant microscòpia electrònica de rastreig equipada amb un espectròmetre de raigs X de dispersió d'energia (SEM-EDS). L'estudi revela que totes les mercaderies analitzades són productes locals/regionals fets al torn, el que suggereix un alt grau d'estandardització tecnològica en l'adquisició i el processament de les matèries primeres en el període considerat. La principal diferència entre les dues tradicions de terrisseria es refereix a la forma dels recipients, apuntant a nous patrons de consum després de la invasió nòmada.

Abstract We present the archaeological contextualisation and the archaeo-

metric characterisation of slipped and non-slipped tableware and common wares from Termez (south Uzbekistan). The aims are, first, to evaluate pottery manufacture in the city and the region (ancient Bactria) after the conquest of Alexander the Great in the late 4th century B.C so as to detect influences from the Hellenistic Mediterranean culture; and, second, to investigate the evolution in pottery manufacture following the arrival of the Yuezhi nomadic tribes in the mid-2nd century B.C. X-ray fluorescence, X-ray diffraction, and thin-section analyses were performed on the vessels and on various local raw materials to examine the provenance and the technological processes involved in pottery manufacture (raw materials procurement and processing, shaping and firing). Surface treatments were analysed by using scanning electron microscopy equipped with an energy dispersive X-ray spectrometer (SEM-EDS). The study reveals that all the wares analysed are local/regional wheel-thrown products, suggesting a high degree of technological standardisation in the procurement and processing of raw materials in the period considered. The main difference between the two pottery traditions concerns the shape of the vessels, pointing to new consumption patterns after the nomadic invasion.

Keywords Ancient Bactria; Pottery; Provenance; Technology; Cultural interactions

---

3.3.1. Introduction

Hellenistic cultural influences spread from the Mediterranean to Central Asia after Alexander the Great's conquest in the late 4th century B.C (Bernard, 1994). The strongest evidence of these influences is found in Ancient Bactria, the historical region comprising both sides of the Amu Darya (ancient Oxus River), present-day territories of southern Uzbekistan and Tajikistan and northern Afghanistan (Figure 3.4). The Seleucids, successors of Alexander, took control of the region, founding many settlements at strategic points along the routes linking Bactria with India and onwards to the Caspian Sea (Leriche, 2007). In the mid-3rd century B.C, the satrap of Bactria, Diodotus, declared himself king and founded the Greco-Bactrian kingdom. However, this change in

the political situation did not bring about a significant cultural shift. For instance, the tableware produced and used from the late 4th and mid-2nd century B.C at Ai-Khanoum and Dzhiga Tepe in northern Afghanistan, Merv in Turkmenistan, and Termez, Kampyr Tepe, Dalverzin Tepe and Kurganzol in southern Uzbekistan (Gardin, 1973; Nekrasova & Pugachenkova, 1978; Pidaev, 1984, 1991a; Bolelov, 2001, 2011; Sverchkov, 2008; Houal, 2013; Lyonnet, 2013; Puschnigg, 2013; Martínez Ferreras et al., 2016, in press), presents clear resemblances with the coeval vessels from the Mediterranean Hellenistic tradition (Morel, 1981). They consist of non-slipped and reddish-orange or black slipped kraters, cups, bowls, paterae and 'fish' plates, some with stamped palms and applied ornaments. However, a few workshops producing pottery have been identified at Kampyr Tepe, Dalverzin Tepe and Ai-Khanoum.

The Hellenistic influences on the region of declined from the mid to the late 2nd century B.C. when several Iranian nomadic tribes, generically the Saka, migrated from the North and East. A few decades later, another wave of nomadic peoples, the Yuezhi or Yüeh-chih, conquered and occupied the area north of the Amu Darya (Enoki, Koshelenko & Haidary, 1994: 179-180). The tableware and common wares used in this period display a varied repertoire that diverges significantly from earlier vessels. For instance, kraters and 'fish' plates are not present in the archaeological record, and the profiles of cups, plates and jars/containers differ notably. Wares with oxidised pastes were commonly slipped while greyish pastes became predominant at most of the sites where the nomads settled, including Termez (Houal, 2013), Dalverzin Tepe (Nekrasova & Pugachenkova, 1978: 146-150), Mirzakultepe (Pidaev, 1991b) and the lower Kafirnigan valley (Mandelshtam, 1975). Little is known about the pottery workshops that operated during this period, although archaeologists believe that some of the earlier pottery centres remained operative during the nomadic occupation.

In this study, we present the archaeometric characterisation of the tableware dated to the Seleucid, Greco-Bactrian and Yuezhi periods and found at three different sites in the ancient city of Termez in northern Bactria: the Citadel, the settlement on the alluvial plain (sectors AC1 and AC2) and the Tchingiz Tepe fortress (sector RB1) (Figure 3.5). We first contextualised the vessels from reliable archaeological stratigraphy and 14C dating to establish a preliminary chrono-typological classification. We then examined the geochemical, mineralogical and petrographic composition of the vessels to shed new light on their provenance and the technological processes involved in their manufacture (the procurement and processing of raw materials, forming, surface treatment and

firing). Given there is still no evidence of ceramic workshops dating from this period in Termez, provenance was further investigated by comparing the chemical, mineralogical and petrographic composition of the sherds with clayey sediments collected at the site. Moreover, the research also included an extensive study of the geomorphology and geology of the area using topographic and geological maps. The main goals are:
1. To distinguish local from imported products and to determine the recipes and technologies used in the manufacture of the vessels;
2. To characterise the pottery technology of the Seleucid and Greco-Bactrian periods and to detect the influences of the Hellenistic Mediterranean culture;
3. To determine whether the nomadic occupation resulted in other technological changes besides variations in the vessels' morphology;
4. To assess the technological evolution in pottery manufacture during the Hellenistic and nomadic periods, including any cultural interactions between the two traditions.

3.3.2. Natural landscapes and geological background

Ancient Termez is located in the southern part of the Surkhan Darya valley and the catchment area of the Amu-Surkhan hydrological system (Figure 3.4). The valley extends NNE to SSW, and is delimited to the north by the mountains of Gissar (the western part of the Tien Shan range), to the west by those of Baysuntau-Kugitangtau which terminate on the shores of the Amu Darya, and to the east by the Babatag range, with the Kafirnigan valley beyond it. The floodplain on which ancient Termez was located has an almost flat topography (mean altitude 300 m), although its physiography includes some hills that provide evidence of the area's geology (Figure 3.5). The geomorphological units identified are organised as follows (Sánchez del Corral & Thum, 2012):
1. The recent fluvial domain of Amu Darya-Surkhan Darya, which divides into two surfaces: S1 (altitude ~ 307 m) and S2 (between 300 and 292 m). S1 comprises the remains of the northern sector together with Kara Tepe, Tchingiz Tepe and part of Rabat. S2, which might be defined as the present-day floodplain, contains the cultic complex (with significant outcrops of bedrock), together with the Citadel and the rest of the old city. The two levels are linked by an escarpment, interpreted as erosional (fluvial?), possibly with some structural control.
2. Inselbergs that crop out over the upper surface (S1) as residual structural reliefs linked to the Baysuntau-Kugitangtau range, which terminates on the shores of the Amu

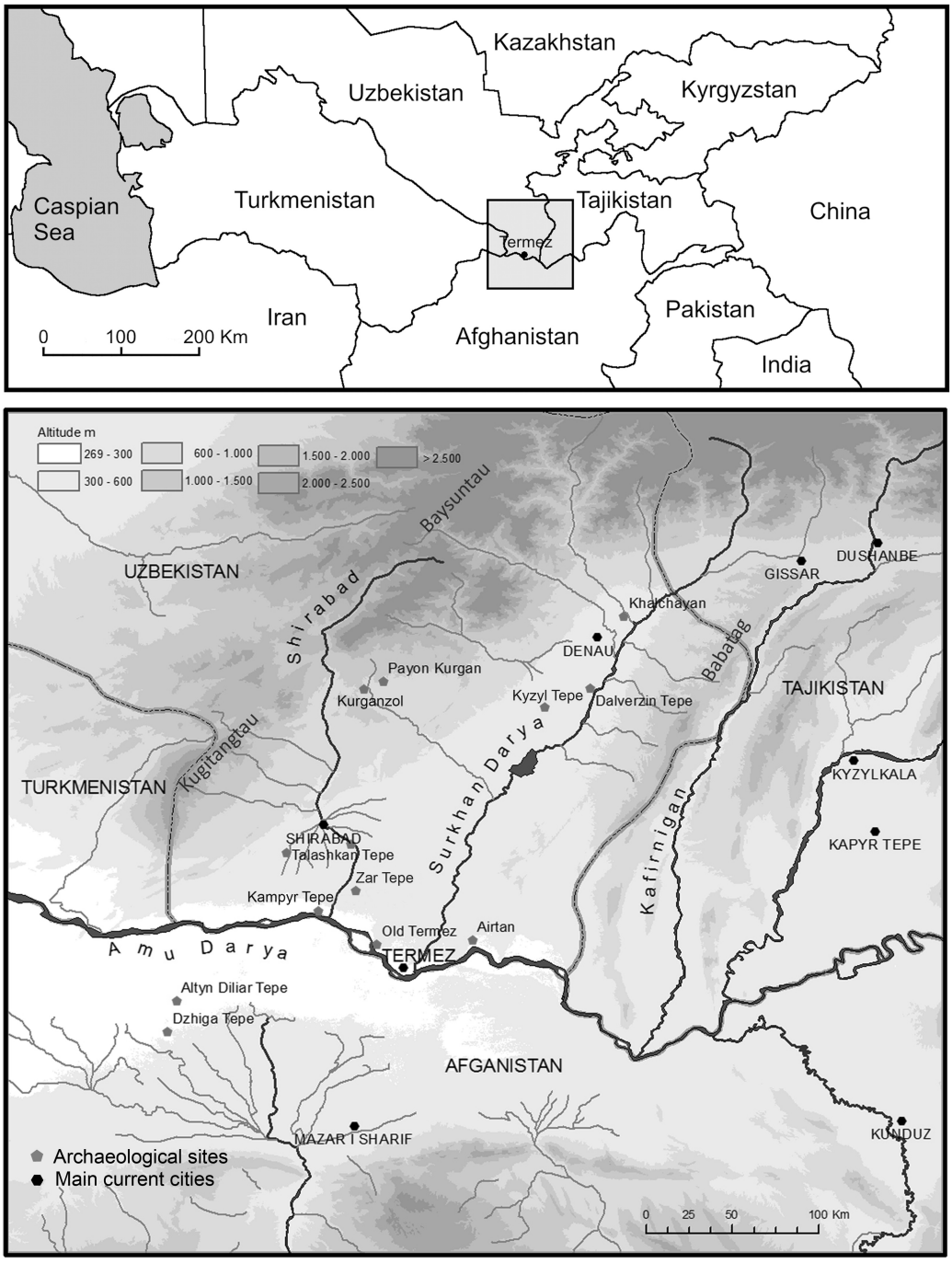

Figura 3.4: Map of ancient Bactria showing the location of Termez and the main settlements cited in the text (drawing by A. Sánchez del Corral; cartographic base: Aster Global Digital Elevation Map NASA, http://www.gdem.aster.ersdac.or.jp). , *Figure 1 in the original.*

Darya.

Geologically, the Surkhan Darya valley forms part of the Afghan-Tajik depression which spans areas located in Tajikistan, Afghanistan and Uzbekistan. The depression comprises a Hercynian basement, with Precambrian-Palaeozoic high-grade metamorphic rocks cropping out mostly in the orogenic margins, and Permian-Triassic sedimentary and volcanic rocks to the north, east and south (e.g., Leith & Alvarez, 1985; Yachminnikov & Nikolaev, 1990; Bourgeois et al., 1997; Nikolaev, 2002). The filling of the Afghan-Tajik depression includes mainly Mesozoic and Cenozoic sediments that have undergone several deformation episodes as a consequence of the indentation of the Pamir into the Asian continent when India and Asia collided (see Figure 3 in Sánchez del Corral & Thum, 2012). The Mesozoic-Cenozoic sedimentary cover comprises a lower (Pre-Molasse) assemblage deposited between the Jurassic and Eocene-Oligocene, and an upper (Molasse) assemblage belonging to the Miocene and Pliocene (Yachminnikov & Nikolaev, 1990; Nikolaev, 2002; Sánchez del Corral & Thum, 2012). According to Russian geological cartography (1:200.000), the Pre-Molasse sequence in the study area is represented by Palaeogene layers of carbonate and evaporite rocks (limestone, dolomite and gypsum), and detrital rocks with carbonate intercalations (claystone, siltstone, sandstone, limestone with shells and marlstone). The Molasse assemblage is formed by an alternation of Miocene rocks -red and reddishbrown sandstone, siltstone and claystone (Boldshuan Formation), grey and red-grey sandstone, brown-red, siltstone and claystone (Khingou Formation)-, and fewer Pliocene sediments -grey-brown siltstone, claystone, sandstone, gravel sandstone and conglomerate-.

3.3.3. Archaeological evidence

Ancient Termez is considered to have been one of the great centres of northern Bactria during the Seleucid/Greco-Bactrian periods. The original settlement consisted of a military fortress (Citadel) built by the Seleucids in the first half of the 3rd century B.C to control the river-crossing at this point of the Amu Darya (Figure 3.5). The Citadel remained occupied during the Greco-Bactrian and Yuezhi periods, but it occupied only half of the structures visible today (Leriche & Pidaev, 2007; Leriche, 2013).

The alluvial plain was also settled during the Greco-Bactrian and Yuezhi periods, as demonstrated by recent archaeological works and radiocarbon analyses carried out by

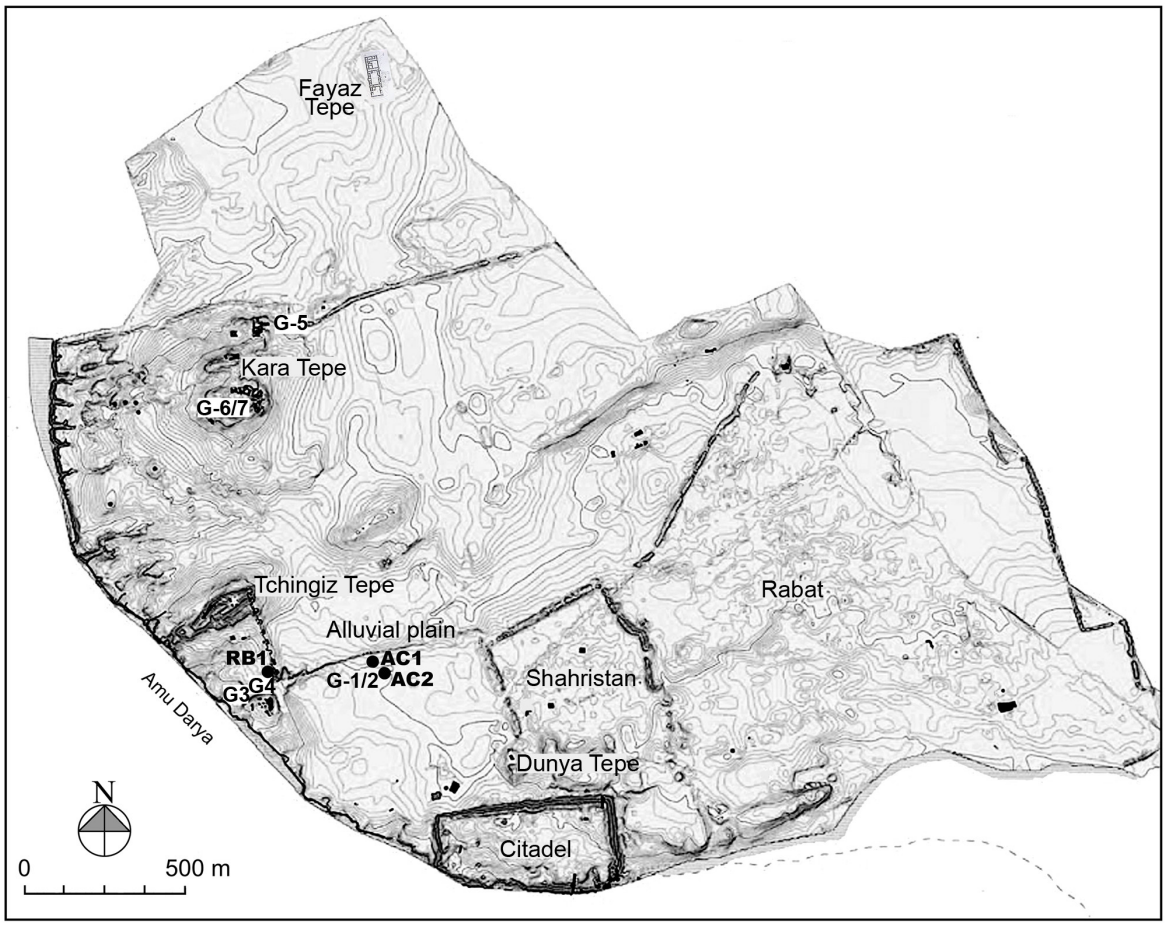

Figura 3.5: General plan of Termez showing the location of sectors AC1, AC2 and RB1 and the sites at which the seven clayey sediments (G-1 to G-7) were collected (cartographic base: Leriche & Pidaev, 2007). *Figure 2 in the original.*

the Spanish & Uzbek IPAEB team led by J. M. Gurt Esparraguera and S. R. Pidaev. The stratigraphic archaeological excavations in sectors AC1 and AC2 (Figure 3.5) did not uncover any dwelling structures, but they did find evidence of the ancient canal built to transport water from the Surkhan Darya to the Amu Darya. In sector AC2, two large jars/containers were found in situ, in the stratum (SU33) over the sandstone bedrock of the southern canal bank. 14C dating of charcoal remains from SU33 provided two dates for the first settlement of this area, cal B.C 352-295 (1σ, 27.4 %) and cal B.C 211-156 (1σ, 30.0 %) (Table 3.1). Although a precise chronology has yet to be established, the settlement must have predated the fall of the Greco-Bactrian kingdom. However, level SU20, which covers SU33, has been dated to the 1st century A.D, cal A.D 24-83 (1σ, 68.3 %), indicating that the sector was occupied during the Yuezhi period and, as evidenced by the stratigraphic sequence, also during the Kushan and Islamic periods. In sector AC1, the earliest stratigraphic level (SU12) has been dated by radiocarbon analysis to the 1st century A.D, cal A.D 16-79 (1σ, 77.6 %). This suggests the early pottery contexts can be ascribed to the late period of nomadic occupation.

A nomadic presence was also evident in the south-eastern area of the Tchingiz Tepe fortress (sector RB1; Figure 3.5). The earliest level (SU5), which is related to the construction of the curtain wall, was dated by 14C analysis to the 2nd century B.C, cal B.C 205 $\pm$ 91 (1σ, 59.6 %) (Martínez Ferreras et al., 2014). Like the Citadel and the floodplain, Tchingiz Tepe remained occupied during the Kushan Empire. During this period, Termez became an important religious centre, hosting several Buddhist monastic complexes such as Kara Tepe, Fayaz Tepe and Tchingiz Tepe (Abdullaev, 2013). However, there is no evidence of pottery workshops associated with the earliest occupations of the site, although kilns at Tchingiz Tepe and Kara Tepe demonstrate that there was a local production of tableware during the Kushan and Kushano-Sasanian periods (Martínez Ferreras et al., 2014: 437-439; Gurt Esparraguera et al., 2015; Tsantini et al., 2016).

Cuadro 3.1: Radiocarbon dates from sectors RB1 and AC2; Lab No.: Laboratory number; Radiocarbon Dating Laboratory (UBAR) of the University of Barcelona. Mass spectrometry measurements (MS) performed at the National Centre of Accelerators (CNA) in Seville; 1σ /2σ age, calibrated ages, 1σ /2σ range; P: the probability of the true calibrated date. *Table I in the original.*

Sample ID	Sample material	Lab. No.	δ ^{13}C (ppm)	^{14}C Age (yr B.P.)	1σ Age (B.C./A.D.)	P	2σ Age (B.C./A.D.)	P
AC2-SU33	Bones	UBAR-1127	-20.83	2155 ± 40 BP	cal BC 352-295	27.4 %	cal BC 360-273	32.6 %
		CNA1123			cal BC 229-220	3.1 %	cal BC 262-88	60.0 %
					cal BC 211-156	30.0 %	cal BC 76-57	2.8 %
					cal BC 136-114	7.8 %		
AC2-SU20	Bones & Charcoal	UBAR-1125	-12.01	1940 ± 25 BP	cal AD 24-83	68.30 %	cal AD 3-125	95.40 %
		CNA1121	-21.07					
		UBAR-1126						
		CNA1122						
AC1-SU12	Bones	UBAR-1242	-18.95	1955 ± 35 BP	cal AD 5-14	5.8 %	cal BC 38-9	8.2 %
		CNA2254			cal AD 16-79	62.5 %	cal BC 3-cal AD 93	77.6 %
							cal AD 97-125	9.6 %
RB1-SU5	Charcoal	UBAR-989	-31.11	2130 ± 45 BP	cal BC 343-324	7.3 %	cal BC 356-285	17.8 %
		CNA366			cal BC 205-91	59.6 %	cal BC 255-249	0.5 %
					cal BC 67-63	1.4 %	cal BC 234-44	77.1 %

Cuadro 3.2: Inventory of the samples analysed from the Citadel (TC), sectors AC1 (TP-1) and AC2 (TP-2) in the alluvial plain and sector RB1 at Tchingiz Tepe (TTT); P: plate; B: bowl; C: cup; PT: platter; T: top; J: jar; U/Ct: Urn/Container; G-B: Greco-Bactrian; G-B/Y: Greco-Bactrian/Yuezhi; Y: Yuezhi; s.: slipped; ^{14}C-SU: Stratigraphic units with radiocarbon date. *Table II in the original.*

Prototype	Period	Samples
P-1	G-B/Y	Pale s. (TC-1, TC-2), non-s. (TC-3), orange s. (TP2-7/textsuperscript{14}C-SU20);Parallels: Kampyr T., Dalverzin T., Kurganzol, Dzhiga T., Ai-Khanoum
P-2	G-B	Non-s. (TC-4), pale s. (TC-5), orange s. (TC-6, TC7); Parallels: Kampyr T., Dalverzin T., Kurganzol, Dzhiga T.
P-3	G-B/Y	Black s. & stamped palms (TC-8)
P-4	G-B/Y	Orange s. (TP2-11/textsuperscript{14}C-SU20); Parallels: Mirzakultepe, Kurganzol, Dzhiga T., Ai-Khanoum
P-5	Y	Reddish s. (TP2-21/SU17); Parallels: Mirzakultepe, Dzhiga T.

Prototype	Period	Samples
P-6	Y	Greyish s. & burnished lines (TP2-8/textsuperscript{14}C-SU20, TP1-1/14C-SU12, TTT-1/14C-SU5); Parallels: Mirzakultepe, Kampyr T.
B-1	G-B/Y	Non-s. (TC-9, TC-10), orange s. (TC-11, TC-12, TP1-8/ SU11), red s. (TP2-9/textsuperscript{14}C-SU20); Parallels: Dalverzin T., Kurganzol, Ai-Khanoum, Kampyr T., Dzhiga T.
B-2	G-B/Y	Non-s. (TP2-1/textsuperscript{14}C- SU33), dark brown s. (TP2-16/SU17, TP2-17/SU17); Parallels: Kurganzol, Ai-Khanoum, Mirzakultepe, Dzhiga T.
B-3	Y	Orange s. (TP2-10/textsuperscript{14}C-SU20); Parallels: Mirzakultepe
B-4	Y	Brown s. (TP2-19/SU17)
B-5	Y	Dark brown s. (TP2-20/SU17)
B-6	G-B/Y	Greyish paste (TP2-18/SU17); Parallels: Kurganzol, Dzhiga T., Mirzakultepe, Ai-Khanoum
B-7	G-B/Y	Orange s. (TP2-22/SU17); Parallels: Ai-Khanoum
C-1	G-B	Reddish s. (TC-14) ; Parallels: Kampyr T., Dalverzin T., Kurganzol, Dzhiga T.
C-2	G-B	Non-s. (TC-15, TC-16, TC-17) ; Parallels: Kampyr T., Dalverzin T., Kurganzol, Dzhiga T.
C-3	Y	Light red s. (TP1-4/textsuperscript{14}C-SU12); Parallels: Mirzakultepe, Dalverzin T., Dzhiga T.
C-4	Y	Light red s. (TP1-7/SU11)
C-5	Y	Orange s. (TP1-9/SU11, TP1-10/SU11); Parallels: Mirzakultepe, Dalverzin T.
C-6	G-B	Pale s. (TC-13)
C-Bases	Y	Brownish s. (TP2-15/textsuperscript{14}C-SU20), reddish s. (TP1-5/14C-SU12); Parallels: Mirzakultepe, Dalverzin T.
PT-1	G-B	Orange s. (TP2-12/textsuperscript{14}C-SU20); Parallels: Kampyr T.
PT-2	Y	Non-s. (TC-18, TTT-2/textsuperscript{14}C-SU5); Parallels: Mirzakultepe, Dzhiga T.
PT-3	G-B/Y	Reddish-brown s. (TP2-23/SU17, TP2-24/SU17); Parallels: Kurganzol, Dzhiga T.
PT-4	G-B/Y	Orange-brown s. (TP2-25/SU17); Parallels: Dalverzin T., Mirzakultepe
PT-5	Y	Non-s. & incised lines (TP1-6/textsuperscript{14}C-SU12); Parallels: Mirzakultepe , Dalverzin T.
T-1	Y	Non-s. (TP2-26/SU17)
J-1	G-B	Non-s. (TC-20); Parallels: Kurganzol, Dzhiga T.
J-2	G-B	Pale s. (TC-21), non-s. (TC-22); Parallels: Kurganzol, Mirzakultepe, Dalverzin T.
J-3	G-B	Non-s. (TP2-2/textsuperscript{14}C-SU33)
U/Ct-1	G-B	Orange s. (TC-19); Parallels: Kurganzol
U/Ct-2	G-B/Y	Red-orangish s. & incised lines (TP2-3/SU28, TP2-13/textsuperscript{14}C-SU20); Parallels: Mirzakultepe
U/Ct-3	G-B/Y	Reddish s. (TP2-4/SU28)
U/Ct-4	G-B/Y	Reddish s. (TP2-5/SU28); Parallels: Mirzakultepe
U/Ct-5	G-B/Y	Non-s. (TP2-6/SU22)
Bases	Y	Greyish s. (TP2-14/textsuperscript{14}C-SU20, TP1-2/14C-SU12, TP1-3/14C-SU12, TTT-3/14C-SU5); Parallels: Mirzakultepe, Ai-Khanoum

3.3.4. Materials

The archaeometric analysis was performed on 61 slipped and non-slipped wares from the Citadel (coded TC), sectors AC1 and AC2 (TP1 and TP2, respectively) in the alluvial plain, and sector RB1 (TTT) in Tchingiz Tepe (Table 3.2). However, three samples could not be examined by X-ray fluorescence (WD-XRF) and X-ray diffraction (XRD) analyses because they were too small. Additionally, thin-section analyses were conducted on 30 selected samples. The sherds were contextualised based on the stratigraphic sequence and 14C absolute dating and then categorised, classified and labelled within prototypes by examining their main morphological and measurable attributes (Figure 3.6). Each prototype (i.e., P-1 to P-6 for plates; C-1 to C-6 for cups, etc.) includes wares from the same functional category presenting common profiles and depicting morphological tendencies rather than specific, distinguishable traits (types). In addition, morphological comparisons (parallels) were established with pottery from other contemporary sites in the region to examine the significance of these prototypes in the regional framework.

The 22 wares analysed from the Citadel (TC) were recovered during the excavations conducted by S. R. Pidaev (1991a). Most are dated to the Seleucid and Greco-Bactrian periods and consist of plates, cups, bowls, platters and urns or containers. The specimens present considerably morphological uniformity (Table 3.2). Some prototypes (plates P-1, P-2 and P-3, bowls B-1, cups C-1, C-2 and C-6, jars J-1 and J-2, and urns/containers U/Ct-1) recall the vessels of the Hellenistic tradition that characterised the region (Houal, 2013: 424-426) while only a few can be attributed to the Yuezhi people. Also, 36 sherds were selected from the two sectors excavated by the IPAEB team in the alluvial plain, 10 from AC1 (TP1) and 26 from AC2 (TP2). Sampling was completed with three sherds recovered during the excavations conducted by this team in 2008 in sector RB1 at the Tchingiz Tepe fortress (TTT). All these vessels comprise prototypes commonly attributed to the nomadic groups (i.e., plates P-4, P-5 and P-6, bowls B-2 to B-7, cups C-3, C-4 and C-5, platters PT-1 to PT-5, jars J-3 and urn/containers U/Ct-2 to U/Ct-5), and exhibit considerable morphological diversity (Figure 3.6).

The raw materials analysed correspond to seven clayey sediments collected in three different areas (Figure 3.5): two in sector AC2 in the alluvial plain (G-1 and G-2), two from the south-western slope of Tchingiz Tepe (G-3 and G-4), and three in Kara Tepe (G-5 in the southern area of the pottery workshop, and G-6 and G-7 in two different clayey levels within an artificially carved monastic cave in the southern hill).

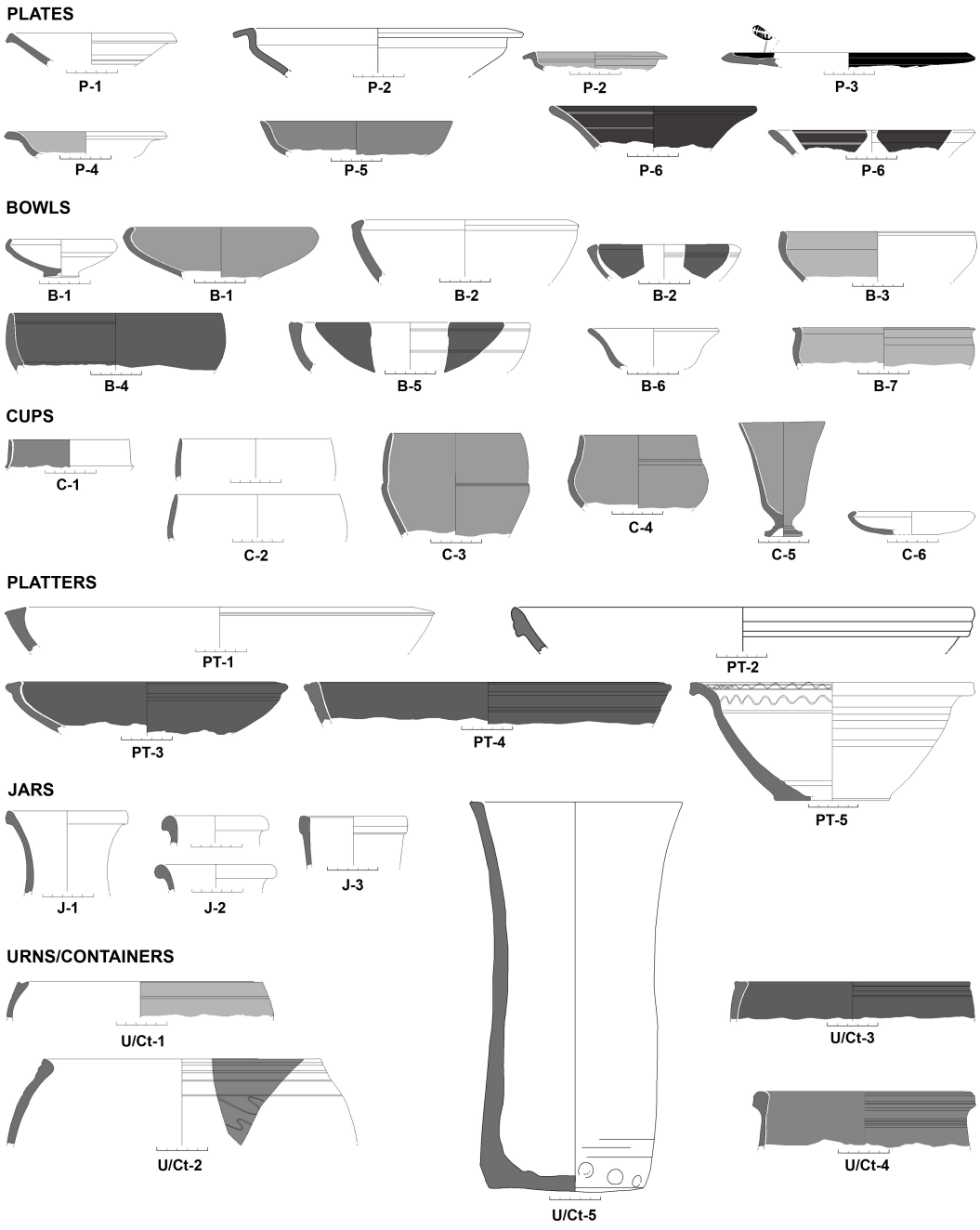

Figura 3.6: Main ceramic prototypes examined. Scale bar: 10 cm. *Figure 3 in the original.*

3.3.5. Methods

Radiocarbon analysis was performed on charcoal and bone samples from specific archaeological contexts (Table I). The radiometric measurements were carried out at the Radiocarbon Dating Laboratory (UBAR) of the University of Barcelona, and mass spectrometry measurements (AMS) were performed at the National Centre of Accelerators (CNA) in Seville (Spain). All dates were calibrated using the software Calib 6.0 together with the IntCal09 database (Stuiver & Reimer, 1993; Reimer et al., 2009).

The investigation of the pottery and clayey samples included chemical, mineralogical and petrographic analyses using WD-XRF, XRD and thin-section optical microscopy (OM). WD-XRF and XRD were performed on all the pottery sherds (powdered specimens) from Termez except TC-6, 11, and 14. The analyses were carried out at the CCiT-UB laboratory of the University of Barcelona following procedures described elsewhere (Martínez Ferreras et al., 2016). A PW 2400 spectrometer with an Rh excitation source was used for chemical analysis; the mineralogical composition was examined using two different diffractometers: a Siemens D-500 and a Panalytical X'Pert PRO alpha 1. Oriented aggregates-XRD were performed on the raw clayey sediments (unfired, powdered samples) using two different diffractometers: a Siemens D-500 and a Bragg-Brentano Panalytical X'Pert Diffractometer system. Semi-quantitative estimations of the mineral phases were determined using the reflective powers method proposed by Schultz (1964).

The petrographic analysis was carried out on 30 selected pottery samples using an Olympus BX41 polarising microscope and the image analysis software AnalySIS FIVE. The petrographic fabrics were defined taking into account the characteristics of the matrix (groundmass) and the microstructure (micromass). We paid particular attention to the identification and description of the aplastic inclusions (frequency, size, shape, distribution, and type) in the fine (< 0.125 mm) and coarse (> 0.125 mm) fractions, as well as to the frequency, size and shape of the voids. The analysis included the petrographic examination of the clayey sediments (thin sections of dried briquettes made with raw clay) and of two fragments of the rocky sedimentary basement at Tchingiz Tepe. Moreover, the clayey sediments were experimentally fired at both 800 and 950^{o}C. These fired samples were then examined by XRD and thin-section OM to evaluate the mineralogical changes that occur during firing.

Surface treatments were investigated on eleven selected wares (TC-6/8, TP2-7/8/19/21 and TP1-1/4/7/8/10) at the NCSR "Demokritos" in Athens (Figure S1, included in appendix A.1.1). Fresh fractured samples were examined by optical stereo-microscopy and using a FEI, Quanta Inspect D8334 scanning electron microscope coupled with an energy dispersive X-ray spectrometer (SEM-EDS). The samples were observed both in secondary electron and in backscattering modes in order to evaluate the microstructures of the ceramic bodies and surfaces. Additionally, at least three areas of both the body and the surface of each sample (typically c. 50×50 µm2 of the body and ca. 50×20 µm2 of the surface) were analysed with EDS to evaluate the compositional similarity/dissimilarity of the materials.

3.3.6. Results and discussion

3.3.6.1. Analysis of the raw materials

Chemical analysis

The chemical analysis performed by WD-XRF reveals some compositional differences between the seven clayey materials, although they all correspond to Ca-rich sediments (CaO from 7 to 11 wt %) (Figure 3.7, Table 5.1). G-3 presents the highest CaO concentration (16.4 wt %), and the lowest Fe_2O_3 (3.6 wt %), Al_2O_3 (9.8 wt %), TiO_2 (0.45 wt %) and MgO (1.8 wt %) contents. G-2 is similar in composition to G-3; however, the Fe_2O_3, Al_2O_3, TiO_2, and MgO contents and the concentrations of most of the trace elements are slightly higher. G-5 constitutes the sediment with the lowest CaO concentration (6.6 wt %) and the concentrations of SiO_2, Na_2O and Zr exceed those observed in the rest of the raw materials and wares. G-1 and G-4 exhibit similar CaO (11-12.4 wt %) and MgO (> 3 wt %) values; however, the former is characterised by higher P_2O_5, Ba, Nb, and Sr contents, and the latter by higher Fe_2O_3, Al_2O_3, Na_2O and K_2O concentrations. G-6 and G-7 have a similar chemical composition, but G-7 presents slightly higher Fe_2O_3, Al_2O_3 and K_2O values.

Petrographic analysis

Thin-section OM analysis of two fragments of the geological basement of Tchinguiz Tepe identified the substrate as being of sandstone (litharenite) (Figure 3.8, a). The substrate is formed of abundant, sub-angular to sub-rounded grains ($\leq$ 0.8 mm diameter) in carbonated cement. More specifically, calcite (micrite, microsparite and sparite) and

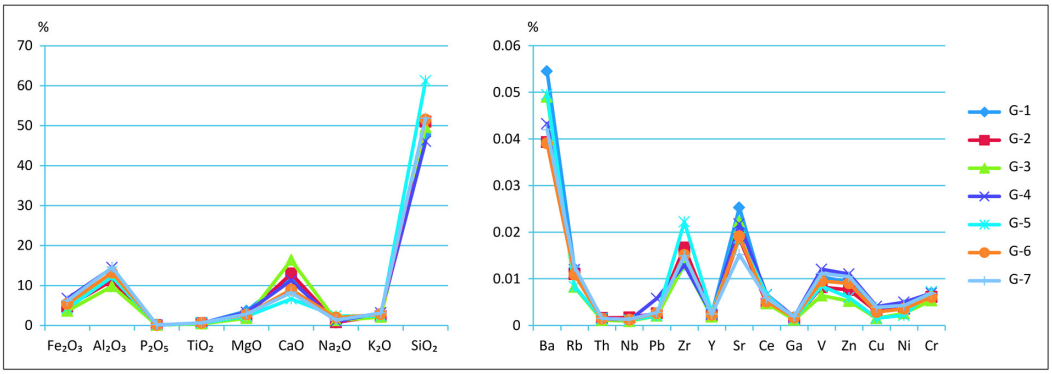

Figura 3.7: Chemical composition of the clayey sediments G-1 to G-7; a) major and minor elements; b) trace elements. *Figure 4 in the original.*

crystals of quartz, plagioclase and K-feldspar are predominant; phyllosilicates, opaque minerals and fragments of metamorphic rocks (schist and quartzite) are frequent; volcanic rocks and amphibole are common; pyroxene and other heavy minerals, including zircon and garnet, are rare.

Petrographic examination of the unfired clayey sediments reveals slight differences in the textural characteristics in terms of the frequency and size of coarse inclusions as well as the particle size of the groundmass (Table 3.3). G-4 has the finest groundmass followed by G-7, while G-3 and G-5 present the coarsest materials.

The two samples taken from the alluvial plain are Ca-rich sediments, although the clay fraction is more abundant in G-1 (Figure 3.8, b-c). The latter contains less than 5 % of compositionally heterogeneous grains set in a brown-orange groundmass. The coarsest clasts correspond to quartz, plagioclase, K-feldspar, and to a lesser degree, metapelites (schists) and calcite crystals. Additionally, the smallest grains include phyllosilicates and oxides. Plant root imprints appear as tubular to irregular voids. G-2 is a silty type of sediment formed from silt to fine-sand grained fragments and a few medium-sized inclusions set in a brown-greenish groundmass. The inclusions comprise sub-angular to sub-rounded crystals of quartz (reaching sizes up to 0.8 mm) together with small amounts of calcite, biotite, feldspar and muscovite.

The two samples taken from the southern escarpment of Tchingiz Tepe differ primarily in the grain size of their respective groundmasses. G-3 is a silty-sandy type of sediment with a brown-greenish groundmass, especially enriched in carbonate mineral phases, and presents various inclusions up to 0.5 mm (Figure 3.8, d-e). These include quartz,

Kfeldspar, plagioclase, micas (biotite and muscovite) and calcite. This sample also contains some rounded inclusions up to 1 mm in size of carbonate-rich silty sediment. In contrast, sample G-4 corresponds to very fine Ca-rich clayey sediment with less than 2 % of coarse inclusions. These comprise feldspars, quartz and calcite crystals together with fragments of metapelite (schists) and quartzite. As in sample G-1, G-4 also contains root imprints, providing evidence of ancient pedogenic processes.

The three samples collected in Kara Tepe also differ in the amount and size of their aplastic inclusions (Figure 3.8, f-h). G-5 is texturally similar to G-3 constituting a siltysandy type of sediment with large amounts of both fine and coarse inclusions (0.1 to 1.0 cm grain size). The latter include quartz, feldspars, calcite, slate/phyllite and schist fragments as well as biotite, muscovite and chlorite. G-6 is similar to G-2 constituting a Ca-rich silty type of sediment with a light-brown groundmass and fine- to medium-sand grained inclusions. The most prevalent grains are sub-angular to sub-rounded fragments of quartz, K-feldspar, plagioclase and metamorphic rocks, together with calcite, muscovite, biotite, oxides and chlorite. All the inclusions are smaller than 0.5 mm, with a mean size ca. 0.1-0.2 mm. Finally, sample G-7 is similar to G-6 but finer. It contains a Ca-rich clayey groundmass with a few aplastic inclusions ($< 1\,\%$) of quartz, feldspars, muscovite, biotite, some metapelite fragments and oxides, with maximum sizes of 0.1 mm (with a mean ca. 0.05 mm).

Examination of the experimental raw materials (fired at 800 and 950^{o}C) under the polarising microscope reveals a gradual textural change in the groundmass of the fired products. Samples fired at 950^{o}C show a higher degree of vitrification than those fired at 800^{o}C and, obviously, the original clay. A major mineralogical characteristic is the absence of calcite in the samples fired at 950^{o}C, whereas it is present (in the form of micrite) at 800^{o}C. Moreover, muscovite is observed at both 800 and 950^{o}C, although its presence decreases with increasing temperature.

Cuadro 3.3: Petrographic characteristics of the raw materials analysed. Bt: biotite; Cal: calcite; Chl: chlorite; Kfs: K-feldspar; Ig rk.: igneous; Meta rk.: metamorphic rocks; Ms: muscovite; Phyl: phyllite; Pl: Plagioclase; Qtz: quartz; Sch: schist; Sl: slate. *Table III in the original.*

Sample	**Groundmass**		**Inclusions**							**Voids**	
	Colour	Micro-structure	Frequency	Predominant inclusions	Other inclusions	Accessories	Range size of inclusions	Sorting	Angularity	Frequency	Shape
G-1	Brown-orange	Calcareous clayey-silty	Low	Qtz, Cal	Kfs, Ms,	Bt, Chl, Meta rk. (sch), oxides	0.1 - 0.5 mm	Moderate to good	Subangular to subrounded	Moderate	Subrounded to irregular
G-2	Brown-green	Calcareous silty	Low to moderate	Qtz, Cal, Ms	Kfs, Pl, Bt	Oxides, Meta rk.	0.1 - 0.5 mm (some reaching 0.8 mm)	Moderate	Subangular to subrounded	Low	Subrounded
G-3	Light brown	Calcareous silty-sandy	Moderate	Qtz, Cal, clay pellets	Kfs, Bt, Ms, Chl	Oxides, Pl	0.05 - 0.5 mm (clay pellets up to 1.5 mm)	Poor	Subangular to subrounded	Moderate	Subrounded to irregular
G-4	Brown-orange	Calcareous clay	Very low	Cal, Qtz	Ms, Meta rk. (sch), Kfs, Pl	Oxides, Ig rk.	0.1 - <0.4 mm (rarely up to 0.6 mm)	Good	Subangular	Moderate	Elongated to irregular
G-5	Light brown	Calcareous silty-sandy	Moderate	Qtz, Kfs, Meta rk. (sl/phyl), Cal	Meta rk. (sch), Bt, Ms, Chl	Ig rk., oxides	0.05 to 0.7 mm	Poor	Subangular to subrounded	Moderate	Subrounded to irregular
G-6	Brown-green	Calcareous silty	Low	Qtz, Cal, Meta rk.	Kfs, Pl, Ms	Bt, oxides	0.1 - <0.6 mm (some above 1 mm)	Moderate to good	Subangular to subrounded	Low	Irregular
G-7	Brown-green	Calcareous clayey-silty	Very low	Qtz, Cal	Oxides, Ms, Kfs, Pl	Bt	0.05 - <0.3 mm	Good	Subrounded	Moderate to low	Subrounded

Mineralogical analysis

The main crystalline phases identified by XRD in the raw sediments are quartz, calcite, clay minerals, plagioclase, K-feldspar, dolomite and iron oxides. X-rays of the oriented aggregates enabled us to identify the clay mineral fraction, which includes illite, kaolinite, montmorillonite and chlorite (Figure 3.9). Estimated abundances of these mineral phases, based on the semiquantitative evaluation of the XRD patterns, are reported in Table 3.4. Muscovite is the most common clay mineral fraction in the raw sediments analysed, with the exceptions of G-3 and G-5. Indeed, these last two samples have the lowest clay minerals content. Quartz is especially abundant in all the samples, with XRD estimations ranging from 27-45 wt %. Such results are in line with the petrographic observations (quartz is a prevalent mineral phase in all the clayey sediments) and the XRF results (SiO_2 ranges from 46.1-61.2 wt %). The highest calcite content detected by XRD corresponds (in order of abundance) to G-3, G-2, G-1 and G-4. These are, in turn, the raw materials with the highest CaO percentages (ranging from 11.3-16.4 wt %) and those which present abundant carbonate content, as observed by optical microscopy. Additionally, dolomite was identified in G-1 (4 wt %) and G-5 (2 wt %). Samples G-2 and G-3 have the lowest aluminosilicate mineral phase contents (i.e., clay minerals, K-feldspar and plagioclase). This finding agrees with the XRF analyses in which both samples record the lowest Al_2O_3 values (11.3 and 9.8 wt %, respectively).

XRD results of the fired products at 800 and 950ºC show that at the lower temperature calcite is significantly present whereas gehlenite and diopside are not detected. In contrast, calcite is absent at 950ºC, while gehlenite and diopside are notable mineral (firing) phases (Figure 3.10, a)

3.3.6.2. Analysis of the raw materials

Chemical analysis

The chemical sub-composition of the 58 vessels analysed by WD-XRF is shown in Table 5.1. The compositional variation matrix (CVM) was then calculated according to J. Buxeda (1999) to determine the total variation (tv) within the data set. The value resulted (tv = 0.436) is moderately high and characteristic of a relatively monogenic assemblage (Table 5.2) (Buxeda & Kilikoglou, 2003). When the CVM included the clayey sediments, tv appears somewhat higher (tv = 0.545) suggesting that the chemical

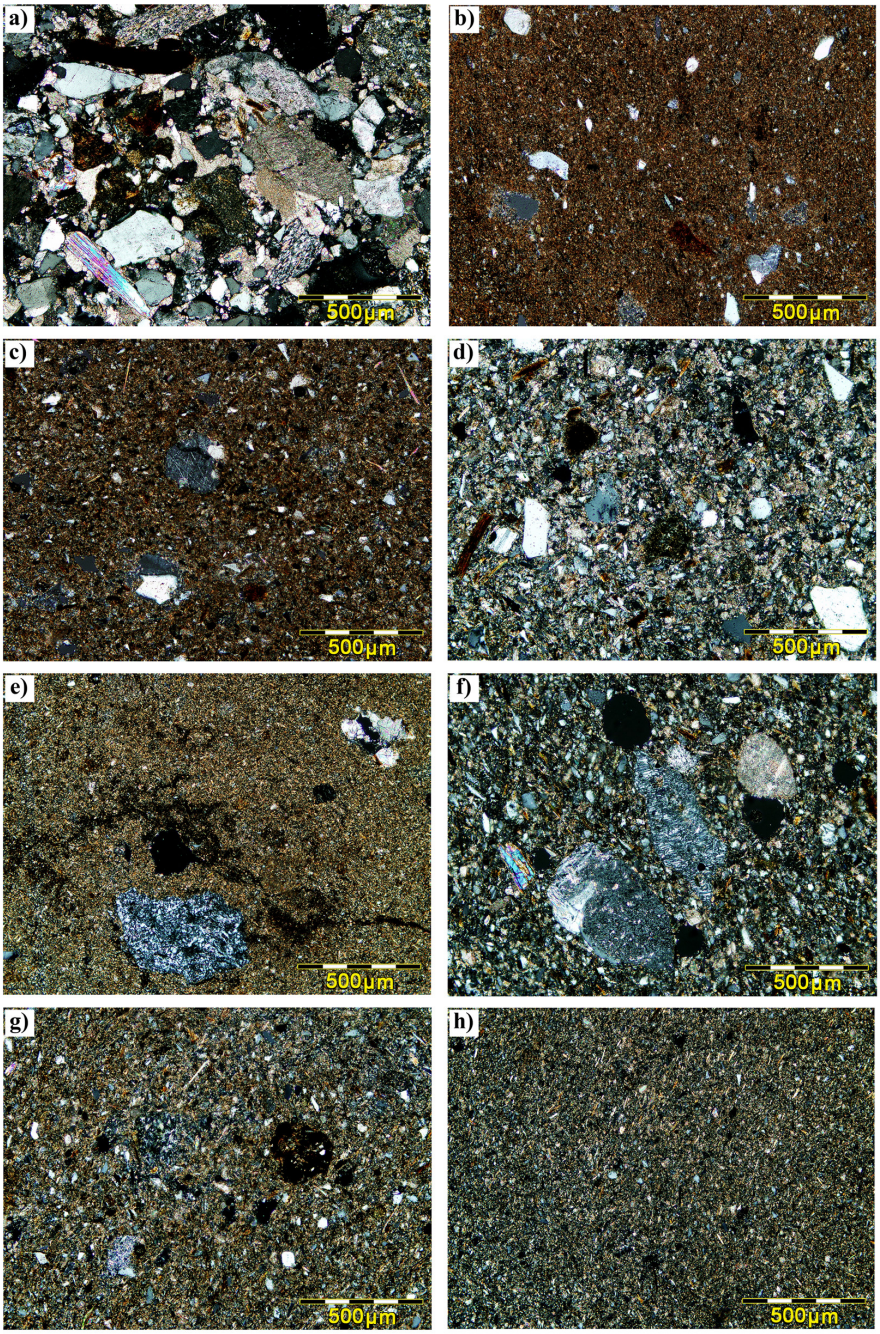

Figura 3.8: Photomicrographs of thin sections (100x, cross-polarised light): a) fragment of sandstone from the geological substrate at Tchingiz Tepe; b) clay G-1; c) clay G-2; d) clay G-3; e) clay G-4; f) clay G-5; g) clay G-6; h) clay G-7. Scale bars: 500 μm. *Figure 5 in the original.*

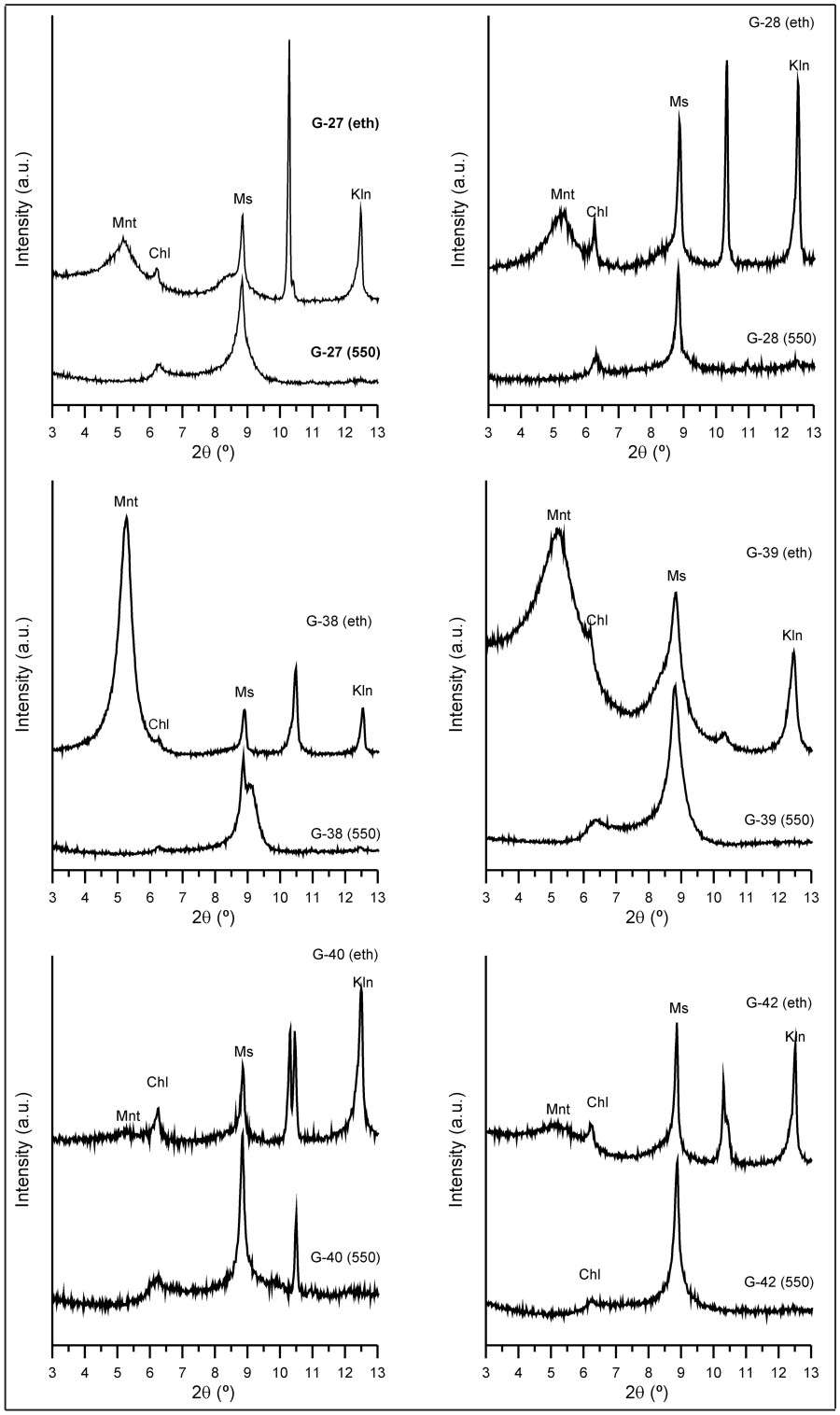

Figura 3.9: Oriented aggregates XRD of the raw materials (G1 to G-6) in which the clay mineral phases are represented. Chl: chlorite; Kln: kaolinite; Mnt: montmorillonite; Ms: Muscovite. *Figure 6 in the original.*

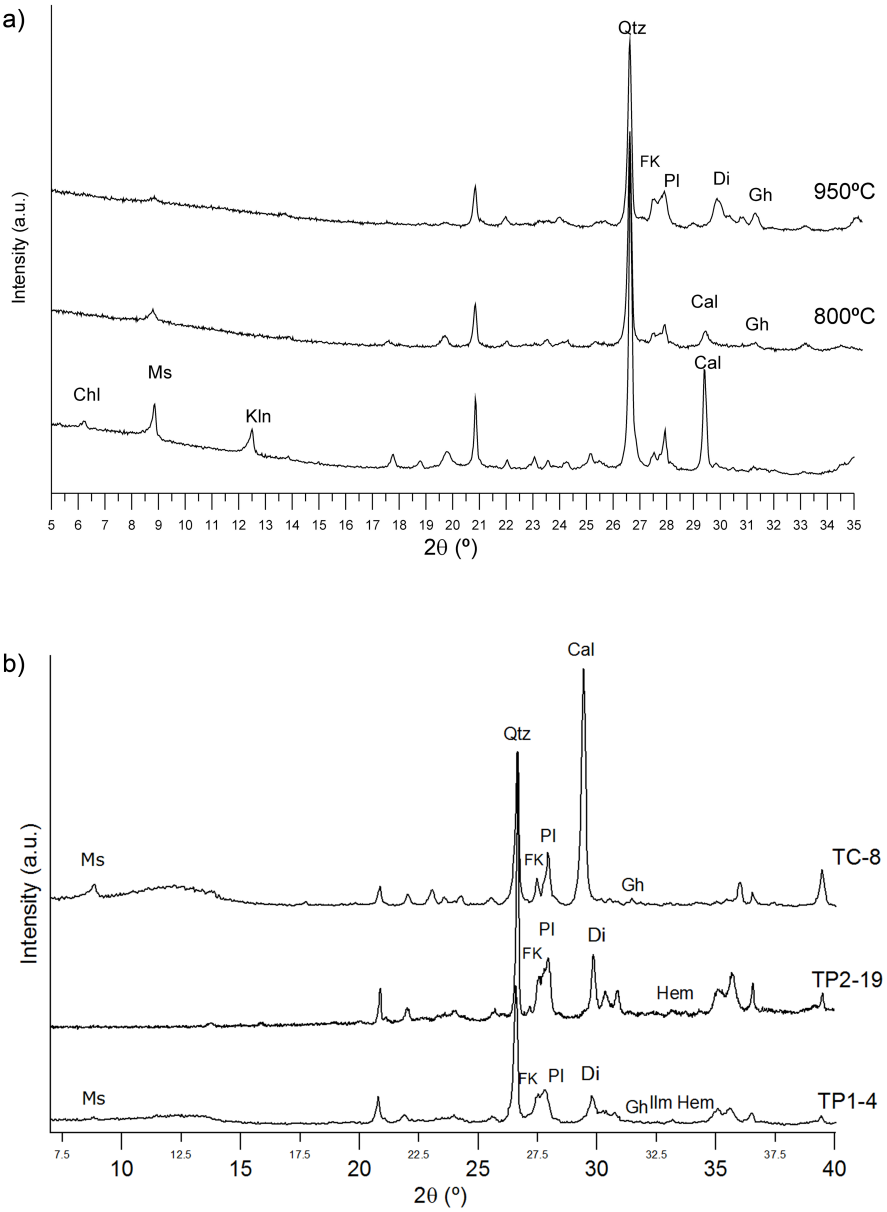

Figura 3.10: a) Powder XRD patterns of sample G-7 fired at 800 and 950ºC; b) Powder XRD patterns of three representative ceramics; Cal: calcite; Chl: chlorite; Di: diopside; Gh: gehlenite; Hem: hematite; Ilm: Ilmenite; Kfs: K-feldspar; Kln: kaolinite; Ms: muscovite; Pl: plagioclase; Qtz: quartz. *Figure 7 in the original.*

Cuadro 3.4: Semiquantitative estimation of the mineral phase concentrations (in wt %) detected by XRD; Cal: calcite; Chl: chlorite; Dol: dolomite; Hem: hematite; Kfs: K-feldspar; Kln: kaolinite; Mnt: montmorillonite; Ms: muscovite; Pl: plagioclase; Qtz: quartz. *Table IV in the original.*

Sample	Qtz	Kfs	Pl	Hem	Cal	Dol	Clay minerals			
							Mnt	Chl	Kln	Ms
G-1	27	3	11	0	22	4	2	5	8	17
G-2	45	4	13	2	23	0	1	1	4	6
G-3	36	9	16	0	29	0	4	0	2	3
G-4	30	10	8	2	20	0	3	6	6	16
G-5	33	19	29	0	12	2	0	1	2	2
G-6	41	6	12	0	16	0	2	3	6	15
G-7	34	8	14	0	16	0	0	4	7	18

composition of the vessels and clays is not very different (Table 5.3). The CVM also gives the ratio τ_i, that is, the sum of variances calculated for each element, and the tv/τ_i, which indicates the contribution of each element to the total variation.

The highest τ_i values are provided by P_2O_5, Pb, CaO, Na_2O, Sr, and Cu. The $\tau_{P_2O_5}$ value is assumed to be related to the high P_2O_5 concentrations in specific wares (especially in TC-10 but also in TC-12/19/22, TP1-9 and TP2-20). Phosphorus enrichment in these sherds might be the consequence of post-depositional contamination in the soil, given that it is an element which commonly appears perturbed in pottery deposited in anthropic environments (Maritan et al., 2009). The Pb concentrations of the pottery sherds differ slightly, with the highest value recorded in clay sediment G-4 probably being responsible for the τ_{Pb} ratio. Moreover, the high τ_{Cu} value appears to be due to the higher concentrations of Cu in some wares from the alluvial plain (TP1-5/6/7/8/9/10 from AC1 and TP2-7/9/11/21/22/26 from AC2).

Differences in the Cu content might be attributed to both the diversity of raw materials used in the manufacture of the vessels and the weathering processes to which specific vessels have been exposed. Differences in the CaO concentration of the vessels are not significant, with all of them corresponding to calcareous pastes (CaO between 6-13 wt %). This means the τ_{CaO} value may, in part, be attributed to the high CaO content exhibited by the clayey sediment G-3. The τ_{Na_2O} value, on the other hand, might be related to differences in the Na_2O concentrations of the sherds. Sample TC-9 exhibits the highest content, being similar to that found in clayey sediment G-5, while some

vessels from sector AC1 present the lowest concentrations. These data suggest the occurrence of weathering processes related to the crystallisation of salts in those sherds presenting the highest Na_2O concentrations. This contamination process has previously been described in archaeological ceramics found at Termez and in other settlements located in the Amu Darya-Surkhan Darya floodplain (Martínez Ferreras et al., 2016; Tsantini et al., 2016). Samples TC-21 and TP2-25 also show high Na_2O content together with the lowest K_2O and Rb concentrations. This correlation may be related to the crystallisation of analcime as a secondary phase (Schwedt et al., 2006), as detected by XRD analysis (see below).

Differences in the Sr content of the clayey sediments and the pottery vessels are responsible for the high τ_{Sr} value. However, the high variation in Sr can also be explained by the different CaO values detected in the samples. These two elements are usually subject to interferences attributable to their being alkaline-earth metals (Buxeda, 1999: 306-307). The calculation of the CVM excluding P_2O_5, Na_2O, Pb, Sr, and Cu provides a very low tv value (0.136), which is characteristic of a monogenic data set. When the seven raw clays are taken into account, the tv increased only moderately (0.182), which indicates a significant match between wares and raw materials.

We applied principal component analysis (PCA) to the sub-composition: Fe_2O_3, Al_2O_3, TiO_2, MgO, CaO, K_2O, SiO_2, Ba, Rb, Th, Nb, Zr, Y, Ce, Ga, V, Zn, Ni and Cr. The data were transformed into additive log-ratios using the component with the lowest τ_i value (Al_2O_3) as the divisor (Buxeda, 1999). The biplot shows the distribution of the wares and the clayey sediments according to the similarity of their respective chemical compositions (Figure 3.11). Although this two-dimensional representation is inconclusive, two main groups can be distinguished. One includes most of the wares from the Citadel (TC) associated with the clayey sediment G-4 from the Tchingiz Tepe southern escarpment. These wares contain slightly lower Th, Nb, V, Zn, and Cr concentrations than the ceramics from the alluvial plain. This group includes the greyish base TTT-3, while the urn/container TC-19, dated to the late Greco-Bactrian/Yuezhi period, is more distanced due to lower Nb and Ni content. In the other group, most of the vessels from sectors AC1 and AC2 cluster near the clayey samples G-6 and G-7 from the southern hill at Kara Tepe. Three plates of prototypes P-1 (TC-2/3) and P-2 (TC-7) from the Citadel and two vessels (TTT-1/2) from Tchingiz Tepe also match with this group. In contrast, a greyish base (TP1-2), the two cups of prototype C-5 (TP1-9/10), and a bowl/platter (TP2-9) are separated somewhat (bottom-left) because

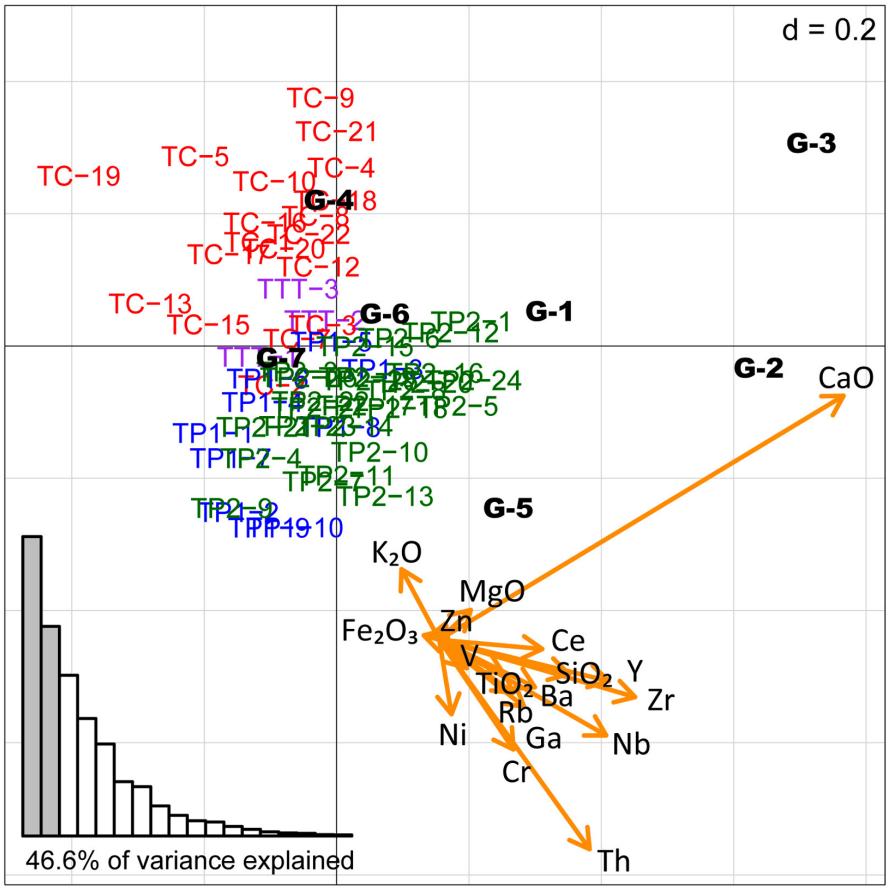

Figura 3.11: Biplot of the first two principal components considering the wares and the clayey sediments from Termez. *Figure 8 in the original.*

they exhibit slightly lower CaO and Y values, and higher Ba, Th, and Cr content.

Petrographic analysis

In general, petrographic observations of the wares under the microscope point to similar textural and mineralogical composition and characteristics (Table 3.5). The clay-rich groundmass occurs primarily in varying shades of brown colour with orange-red hues and the degree of vitrification of the matrix also differs depending on the firing temperature. In general, the ceramic bodies with no or little calcite present a higher degree of vitrification than those with significant amounts of calcite. The presence of voids also differs from low to moderate and high, consisting primarily of vughs with irregular to elongated shapes. The frequency of the fine and coarse fractions ranges from moderate to high. They include quartz, K-feldspar, plagioclase and metamorphic rock fragments as prevalent inclusions together with variable amounts of calcite (principally micrite),

Cuadro 3.5: Petrographic characteristics and composition of the wares analysed. Am: amphibole; Bt: biotite; Cal: calcite; Gh: gehlenite; Inc: inclusions; Ig rk.: igneous rocks; Kfs: K-feldspar; Meta rk.: metamorphic rocks; Ms: muscovite; Pl: plagioclase; Px: pyroxene; Qtz: quartz. *Table V in the original.*

Pottery samples	**Groundmass**		**Inclusions**						**Voids**				**Comments**
	Colour	Micro-structure	Degree of vitrification	Frequency	Predominant inclusions	Other inclusions	Accessories	Range size of inclusions (mm)	Sorting	Angularity	Frequency	Shape	
TC-4/8/9/18/20	Dark brown (8), brown-orange (4, 9), brown-reddish (18, 20)	Clay rich-sparse to common, very fine incl.	Moderate	Moderate to high	Qtz, Kfs, PlCal (micrite)	Meta rk., Ms, Bt Cal (micrite)	Oxides, Am, PxCal (micrite) (18), Ig. rk.	0,05 to ≤ 0.6 (>1 in TC-20)	Moderate	Subangular to subrounded	Moderate to low (8)	Irregular to elongated	Heterogeneous firing (20)
TC-1/13	Brown-reddish	Clay rich-sparse, very fine incl.	Moderate to high	Moderate to high	Kfs, Pl, Qtz, Cal (micrite)	Meta rk., Ms, Bt, Px, Am, Cal (micrite)	Oxides, Ig. rk.	0,05 to ≤ 0.4-0.5	Moderate	Subangular to subrounded	Moderate to low	Rounded to irregular	
TC-2/7/19	Brown-reddish (19), brown-orange(2,7)	Clay rich-sparse, very fine incl.	High	Moderate	Qtz, Kfs, Pl	Meta rk, Bt, Ms.	Px, Am, Cal (micrite), oxides	0,05 to ≤ 0.6-0.7	Moderate	Subangular to subrounded	Moderate to low	Irregular	Heterogeneous firing (19)
TC-21	Light brown	Clay rich-rare, very fine incl.	Moderate	Moderate ↓	Qtz, Kfs, Pl,	Meta rk, Cal (micrite)	Ms, Px, oxides	≤ 0.05 to ≤ 0.5	Moderate	Subangular to subrounded	Moderate	Irregular	
TP1-1/10, TP2-14/18	Dark brown. Brown-orange (10)	Clay rich-sparse, very fine incl.	Moderate	Moderate ↑	Qtz, Kfs, Pl	Cal (micrite), Meta rk., Bt, Ms	Ig. rk., Am, Px?, oxides	0.1 to ≤ 0.8	Moderate	Subangular to subrounded	Low to moderate	irregular	Heterogeneous firing (14, 18).
TP2- 2	Brown-orange	Clay rich-rare, very fine incl.	High	High	Qtz, Kfs, Pl	Meta rk., Ms	Ig. rk.?, oxides	≤ 0.1 to ≤ 0.7	Moderate↑	Subangular to subrounded	Moderate to high	Irregular	Heterogeneous firing
TP2-1	Brown-reddish	Clay rich-rare, very fine incl.	Moderate	Moderate	Qtz, Kfs, Pl	Meta rk., Cal (micrite)	Ms, Bt, Px?, oxides	0.1 to ≤ 0.8	Moderate↑	Subangular to subrounded	Moderate to high	irregular	Heterogeneous firing

Pottery samples	Groundmass		Inclusions						Voids				Comments
	Colour	Micro-structure	Degree of vitrification	Frequency	Predominant inclusions	Other inclusions	Accessories	Range size of inclusions (mm)	Sorting	Angularity	Frequency	Shape	
TP1-4/8, TP2-21	Brown-orange, Brown-reddish (21)	Clay rich-rare, very fine incl.	Moderate to high	Moderate	Qtz, Kfs, Pl	Meta rk., Ms, Bt	Oxides, Am, Px	0.2 to ≤ 0.8	Moderate	Subangular to subrounded	Moderate	Irregular to elongated	No Cal is observed. Heterogeneous firing (21)
TP1-6/7	Brown-orange (6), Brown-reddish (7)	Clay rich-common, very fine incl.	High	High	Qtz, Kfs, Pl	Meta rk., Bt, Ms	Am, Px, oxides	≤ 0.05 to ≤ 0.5	Moderate[ɬ]	Subangular	Moderate	Elongated to irregular	No Cal is observed
TP1-2,TP2-20	Dark brown (2), Brown orange (20)	Clay rich-sparse to common, very fine incl.	Moderate	High	Qtz, Kfs, PlCal (micrite)	Bt, Meta rk., Cal (micrite)	Ms, oxides, Px, Am	≤ 0.05 to ≤ 0.8	Moderate to poor	Subangular to subrounded	Low to moderate	Irregular to elongated	Heterogeneous firing (2)
TP2-19/23/25	Light brown (19), Brown orange (23/ 25)	Clay rich-rare, very fine incl.	High	Low (25) to moderate	Qtz, Kfs, Pl	Meta rk.	Oxides, Ms	≤ 0.1 to ≤ 0.6	Moderate[†]	Subangular to Subrounded	Moderate to low	Irregular to elongated	Heterogeneous firing (23, 25)
TT-1/2/3	Brown-reddish (1). Dark brown (2,3)	Clay rich-sparse to common, very fine incl.	Moderate	Moderate (1, 2) to high (3)	Qtz, Kfs, Pl, Cal (micrite)	Meta rk. (2, 3), Ms, Bt, Cal (micrite)	Oxides, Px, Am, Ig. rk.?	0,05 to ≤ 0.4(3)-0.7(1)	Moderate	Subrounded	Low to moderate	subrounded to irregular	Groundmass with a coarser grainsize (especially in TT3)

biotite, muscovite, pyroxene, amphibole and oxides. The coarse fraction mainly exhibits a moderate sorting and displays sub-rounded to sub-angular shapes.

Despite the common petrographic features presented by the wares analysed, several textural characteristics are specific to groups or productions. Each of the petrographic fabrics includes vessels from what is essentially a specific chrono-spatial context. For instance, most of the Seleucid/Greco-Bactrian wares from the Citadel (TC) have a slightly smaller size range of aplastic inclusions (Table 3.5). Compared to the rest of the vessels, they also present the highest calcite (micrite) concentration (Figure 3.12, a-c). The presence of this phase suggests a firing process in which decomposition of primary calcite and transformation into micrite occurred. Calcite is absent only in TC-2 and TC-19, while it is an accessory phase in TC-7 and TC-18. Besides calcite and partially/totally decomposed Ca-microfossils, the prevalent phases are quartz, Kfeldspar, plagioclase and metamorphic fragments. All the wares from the Citadel also display abundant muscovite, biotite and, to a lesser degree, (clino)pyroxenes, amphiboles and igneous fragments. Samples TC-1, 4, 8, 9, 19 and 20 show dissimilar groundmass colours, providing evidence of heterogeneous firing.

The vessels from the alluvial plain are slightly coarser, and their main aplastic inclusions include crystals of quartz, K-feldspar, plagioclase and metamorphic rock fragments. In contrast to the specimens from the Citadel, overall, these wares display smaller amounts of muscovite and biotite, especially those samples from sector AC2. Thus, muscovite is absent in TP2-19/25 and occurs as an accessory phase in TP2-1/20/23. Biotite presents a similar behaviour: it is completely absent in samples TP2-19/23/25 and occurs as an accessory phase in TP2-1. Calcite (micrite) is abundant in TP1-1/2/10, and in TP2-1/14/18/20, whereas it is absent in TP1-4/6/7 and TP2-2/19/20/21/23/25. Additionally, samples TP2-1/19/20/21/23/25 and TP1-2/4/8 are characterized by the absence of (clino)pyroxene or amphibole as well as by that of igneous fragments. Therefore, several petrographic groups can be recognised among the wares analysed from sectors AC1 and AC2, based on the presence or absence of specific mineral phases (Table 3.5, Figure 3.12).

The three samples from sector RB1 at Tchingiz Tepe present a different variable size and frequency of inclusions, although they each exhibit a groundmass with a coarser particle size (Figure 3.12). Sample TTT-3 differs because it contains the highest frequency of coarse and fine inclusions as well as the lowest maximum sizes (below 0.4 mm). Based on

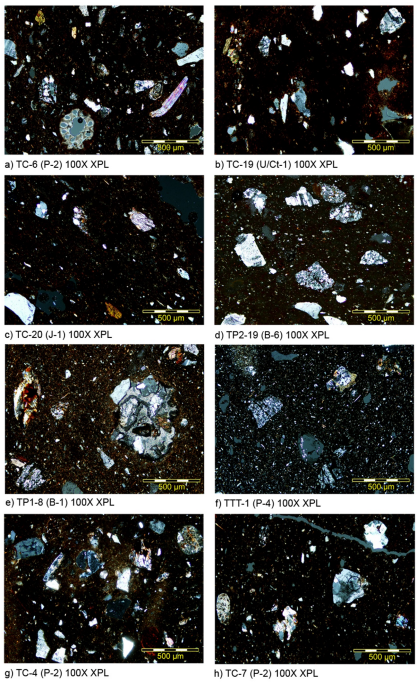

Figura 3.12: Photomicrographs of thin sections (100x, cross-polarised light) of representative sherds of ceramic artifacts from Termez. Scale bars: 500 μm. *Figure 9 in the original.*

its composition and textural characteristics, it resembles samples TC-8 from the Citadel and TP1-2 from the sector AC1. The wares TTT-1 and TTT-2 are more homogenous in all aspects.

Mineralogical analysis

Quartz, plagioclase and K-feldspars are the primary phases detected in all the diffractograms examined, while muscovite, calcite, diopside and gehlenite are identified only in certain pottery sherds (Table 3.6). Iron oxides in the form of hematite are identifiable to different degrees in all the samples that exhibit brownish-reddish to light brown ceramic bodies. The vessels presenting greyish pastes can be assumed to contain magnetite, with the iron oxide having developed in reducing firing conditions. However, this phase is not readily identifiable in the diffractograms owing to its low intensity, probably due to the crystals' small grain size; moreover, magnetite almost coincides with the other mineral phases (e.g., diopside) that are common in the specimens analysed. Ilmenite has been detected as firing phase in all the samples except TC1/18/20.

Cuadro 3.6: The five mineralogical groups identified according to the XRD mineral phases and the equivalent firing temperatures (EFT) estimated. In bold the greyish fabrics; Anl: analcime; Cal: calcite; Di: diopside; Gh: gehlenite; Hem: hematite; Ilm: ilmenite; Kfs: Kfeldspar (orthoclase); Mag: magnetite; Ms: muscovite; PL: plagioclase (albite); Qtz: quartz; sec: secondary. *Table VI in the original.*

	Samples	**XRD** Qtz	**mineral** Pl	**phases** Kfs	Di	Gh	Ms	Cal	Hem	Mag?	Ilm	Anl	**EFT**
1	TC-19, TP2-26	x	x	x			x	x	x		x		$\leq$ 800ºC
	TP1-3	x	x	x			x	x	x	x			$\leq$ 800ºC
2	TP2-3/11	x	x	x	x		x	x	x				800-850ºC
	TC-8	x	x	x		x	x	x		x	x		800-850ºC
	TC-18/20	x	x	x	x	x	x	x	x				$\backsim$ 850ºC
	TC-4/5/9/10/12, TP1-9/10, TP2-1/4/5/6/7/10/12/13/15/16/22, TTT-2	x	x	x	x	x	x	x	x		x		$\backsim$ 850ºC
	TP1-1, TP2-8/14, TTT-1	x	x	x	x	x	x	x		x			$\backsim$ 850ºC
	TP1-2, TTT-3	x	x	x	x		x	x		x	x		$<$ 900ºC
3	TC-2/3/7/13, TP1-4/6/ 8, TP2-21	x	x	x	x	x	x		x		x		900-950ºC
	TC-1	x	x	x	x	x	x		x				900-950ºC
4	TC16/17, TP1-7, TP2-17/20	x	x	x	x	x		(sec)	x				$>$ 1000ºC
	TP2-18	x	x	x	x	x		(sec)		x			$>$ 1000ºC
	TC-21, TP2-25	x	x	x	x		x		x		x	x	$>$ 1000ºC
5	TP2-2/19/23, TP1-5	x	x	x	x				x		x		$>$ 1000ºC

According to the mineral assemblages detected by XRD, five main groups or mineralogical categories can be distinguished (Figure 3.10, b). Group 1 includes those wares that present quartz, plagioclase, K-feldspar, calcite and illite-muscovite. The iron oxides are very poorly developed and appear either as a primary phase or as an early firing phase.

Group 2 ceramics comprise the same primary phases, albeit in different proportions together with some firing phases. Thus, most of the vessels also exhibit diopside (except TC-8) and gehlenite (except TP1-2, TP2-3/11 and TTT-3), as well as hematite or

magnetite, as firing phases. Group 3 vessels include the same primary phases as groups 1 and 2 with the exception of calcite. There are fewer phyllosilicates, and hematite, diopside and gehlenite appear as the main firing phases. Muscovite is absent in groups 4 and 5 samples and calcite, when detected, can be considered a secondary phase. Iron oxides and diopside are more intense while gehlenite is only detected in group 4 samples, except in TC-21. The latter specimen and TP2-25 also contain analcime as a secondary phase. This zeolite usually crystallises in calcareous pottery fired at a very high temperature (Schwedt et al., 2006).

It is known that clayey pastes undergo significant mineralogical and textural modifications upon firing (Rice, 1987). Knowledge of the stability of specific minerals as a function of temperature allows us to estimate the equivalent firing temperatures (EFT) of the vessels under analysis (Table 3.6). Furthermore, it is widely accepted that calcite is still stable at 800ºC yet completely absent at 900ºC, suggesting total decomposition occurs within this range, although this also depends on the duration of firing (e.g., Boynton, 1980; Maniatis, Simopoulos & Kostikas, 1981; Cultrone et al., 2001; Maggetti, Neururer & Ramseyer, 2011; Fabbri, Gualtieri & Shoval, 2014). Calcite decomposes into lime, which then reacts with Si to produce new Ca-silicates, such as gehlenite and diopside. Gehlenite can initially be crystallised at temperatures ranging from 800-850ºC. However, its stability is maximum at temperatures around 850-950ºC (e.g., Cultrone et al. 2001, Ricciardi, Messiga & Duminuco, 1999; Trindade et al., 2009; Maggetti, Neururer & Ramseyer, 2011). The stability field of gehlenite depends on the SiO_2 saturation of the reaction (i.e., the higher the Si content, the lower the equilibrium temperature at which gehlenite is stable). Thus, while it is stable at 950ºC, it is totally decomposed at temperatures of 1050-1100ºC (Moroni & Conti, 2006).

Initial formation of diopside also occurs at ca. 800-850ºC, albeit in very low concentration, but it forms rapidly at 900-950ºC at the dolomite-quartz interface. Moreover, phyllosilicates normally disappear at temperatures between 1000-1100ºC. The occurrence of iron oxides in the Ca-rich clays is closely related to the production of gehlenite and diopside. When carbonates decompose and react to form these two mineral phases, hematite is able to nucleate as nano-sized particles and grow within micro-domains corresponding to former chlorite flakes (Nodari et al., 2007).

Taking into account the stability of these mineral phases, the EFT estimated for all the sherds clustered in group 1 is below 800ºC, since diopside and gehlenite have not

crystallised (Table 3.6). This estimation is further supported by the results obtained from the analysis of the experimental (fired) clayey sediments. Both, the mineral phases identified by XRD and the degree of vitrification determined by thin section analysis link the vessels from this group to samples G-1 and G-7 fired at 800ºC. A slightly higher EFT (ca. 850ºC) seems more probable for the group 2 wares. The presence of calcite suggests firing temperatures below 900ºC, but the occurrence of diopside and gehlenite points to temperatures up to 800/850ºC. The absence of diopside in TC-8 and of gehlenite in TP2-3/11 may indicate slightly lower firing temperatures (above 800ºC and below 850ºC). The same applies to the group 3 vessels, in which phyllosilicates are decreased and calcite has totally decomposed, suggesting an EFT around 900-950ºC. This temperature is compatible with the high degree of vitrification as presented by the raw materials G-1 and G-7 fired at 950ºC. The complete decomposition of phyllosilicates in the samples clustered in groups 4 and 5 points to an EFT above 1000ºC.

3.3.6.3. Analysis of the surface treatments

Optical microscopy

The eleven samples selected for the SEM analysis of their surface layers included one black (TC-8), two grey (TP1-1 and TP2-8), two reddish (TC-6 and TP2-21), two light reddish (TP1-4/7), three orange (TP1-8/10, and TP2-7) and one brown (TP2-19) coated vessels (Figure S1, included in appendix A.1.1). Under the optical stereo-microscope, the surface colours, in general, appear to be more intense than those of their respective bodies although no considerable differences in shades were observed. Indeed, this homogeneity indicates that, even though the ceramic colours can be assumed to have been controlled by the kiln atmosphere (oxidising or reducing), the kilns were operated in somewhat basic conditions, without alternating the kiln atmosphere during the same firing cycle.

Microstructure

The SEM-EDS analysis shows that, in all cases, both the external and internal surfaces of the wares examined present slip layers, with thicknesses ranging between 10-30 µm (Figure 3.13). Smooth interfaces between the slip layers and ceramic bodies indicate that these were burnished before the slips were applied. Furthermore, the slipped surface of plate TC-6 presents an additional paint layer corresponding to a dark brown streak on

the surface.

The slip layers exhibit a more compact microstructure and a considerably higher degree of vitrification than those shown by ceramic bodies. In general, while the latter present initial vitrification, the slip layers show extensive to intermediate vitrification (Table 3.7). Considering that the ceramics were produced from what are effectively calcareous clays, the degree of vitrification observed in the ceramic bodies indicates that the kilns would have been typically operated at firing temperatures in between 800-1000 °C, confirming estimates based on XRD. The higher degree of vitrification observed in the surface layers can be attributed primarily to the smaller particle sizes of the slip material and, in some cases, to a higher content of potassium, which acts as flux (see below).

Chemical composition

The results from the SEM-EDS analysis of the composition of the bodies and surfaces of the eleven samples investigated do not present a uniform picture regarding the enrichment or depletion of specific elements (Table 3.7). To assess these processes, we have generated ternary diagrams with the average contents of SiO_2, Al_2O_3 and the sum of MgO and CaO (Figure 3.14, a) and calculated ratios over SiO_2 and Al_2O_3 concentrations (Figure 3.14, b-c). All the fragments examined, except two grey (TP1-1 and TP2-8), a light red (TP1-4) and the brown (TP2-19) slipped sherds, exhibit a surface enrichment of K_2O. The slips of four reddish-orangish slipped vessels (TC-6, TP1-7/8, and TP2-7) and the greyish plate TP2-8 also present higher Al_2O_3 than the respective ceramic bodies, while it is lower in the surfaces of samples TC-8, TP2-21 and TP1-1. Samples TC-6, TP1-7/8/10 and TP2-7/21) show a coinciding surface depletion of CaO and MgO. However, TP1-8/10 and TP2-21 present different surface and body ratios of Al_2O_3 and SiO_2. While the ratio is higher in the slip of TP1-8 and TP1-10, it is slightly lower in TP2-21. As discussed, the potassium concentration is considerably higher in the latter. The slips of these three sherds, as well as the black and greyish coatings of samples TC-8 and TP1-1 respectively, also exhibit higher Fe_2O_3 content. In contrast, CaO is slightly higher in the slips of samples TC-8, TP1-1/4 and TP2-19, which also present an equivalent or relatively lower MgO content in the slip than that shown in the ceramic.

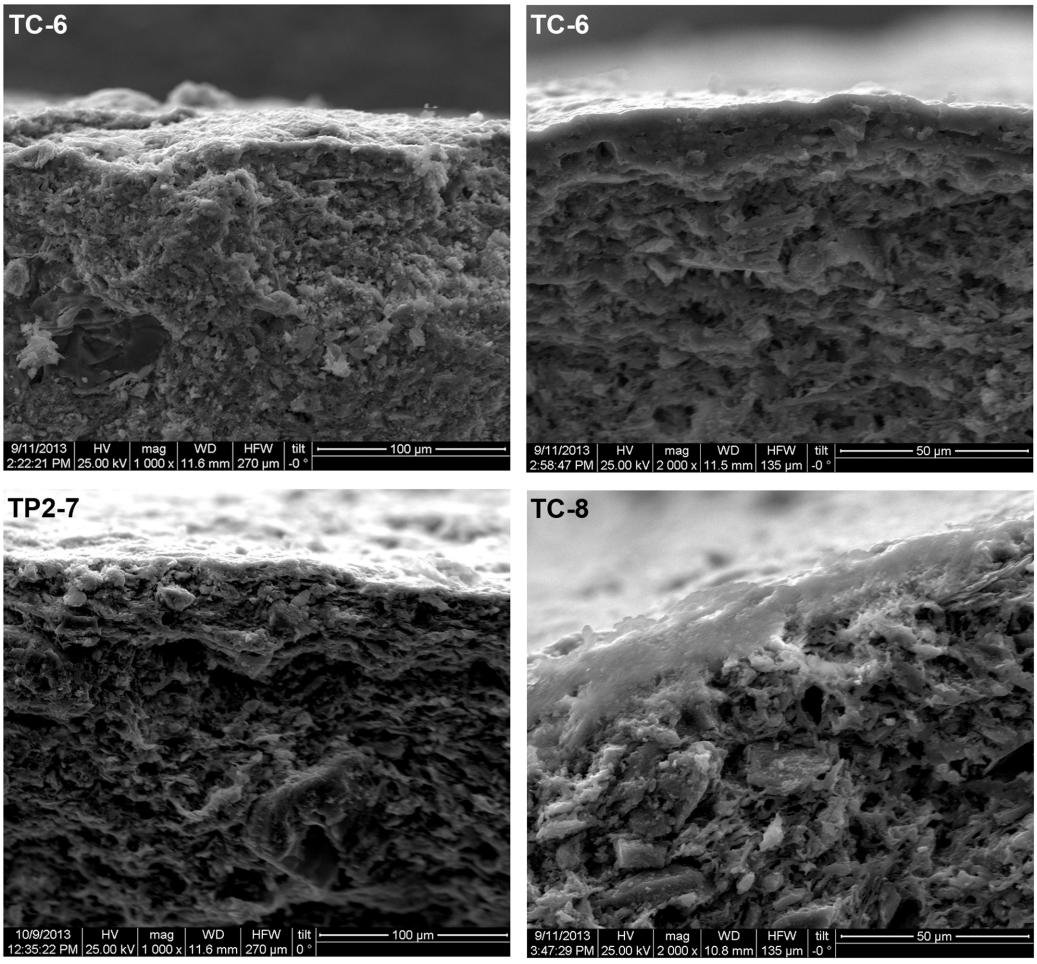

Figura 3.13: SEM micrographs in secondary electron mode: a) TC-6: external surface with thin paint layer. b) TC-6: slip layer with intermediate vitrification. c) TP2-7: slip layer with extensive vitrification. d) TC-8: thin slip layer. *Figure 10 in the original.*

Cuadro 3.7: The four groups (S1 to S4) of slipped wares identified according to the mean of the chemical composition (wt %) and the standard deviations (sd) calculated from multiple SEM-EDS measurements of areas in body and slip. The observed degrees of vitrification were: IV - initial vitrification, EV - extensive vitrification and IMV - intermediate vitrification. *Table VII in the original.*

S	Sample	Vitrification	Thickness(Ï¼m)		Na2O	MgO	Al2O3	SiO2	P2O5	SO3	Cl2O	K2O	CaO	TiO2	Fe2O3	NA
S1	TC-6(red)	body	IV	-	mean	1.2	3.8	14.1	45.3	1.1	1.1	0.1	4.2	19.3	0.8	8.6
					sd	0.2	0.3	1.3	3.1	1.1	0.4	0.1	0.5	4.3	0.4	0.9
		slip	IMV	~ 10-20 (ext.)	mean	2.4	1.9	17.3	52.5	0.5	1.3	0.3	8.7	7.4	0.9	6.2
				~ 20-30 (int.)	sd	0.6	0.3	0.9	3.3	0.2	0.8	0.1	0.7	4.3	0.1	0.4
		paint	IMV	~ 10	paint	3.6	2.0	19.1	52.5	0.2	2.0	0.2	7.4	6.9	0.8	5.2
	TP1-7(light red)	body	EV	-	mean	1.2	3.8	17.5	53.3	0.3	0.2	0.3	3.0	10.8	0.9	8.1
					sd	0.2	0.4	1.0	0.8	0.1	0.1	0.1	0.2	0.7	0.3	0.8
		slip	EV to IMV	~ 10 (ext.)	mean	2.6	3.4	18.7	56.1	0.2	0.2	0.3	3.4	6.8	0.7	7.5
				~ 10 (int.)	sd.	1.2	0.5	1.7	0.7	0.2	0.1	0.0	0.8	1.2	0.2	1.7
	TP1-8(orange)	body	IV	-	mean	1.0	3.2	14.8	57.4	0.3	0.4	0.3	3.0	11.2	1.2	6.9
					sd.	0.2	0.5	0.5	3.3	0.1	0.2	0.3	0.7	2.8	0.9	0.7
		slip	EV to IMV	~ 20-30 (ext.)	mean	1.1	3.6	15.6	52.5	0.4	0.5	0.3	3.6	7.7	0.8	13.5
				~ 10-20 (int.)	sd	0.2	0.7	1.2	4.0	0.1	0.2	0.1	1.8	5.5	0.2	8.5
	TP1-10(orange)	body	IV to EV	-	mean	0.8	3.6	16.4	54.7	0.6	0.2	0.2	3.3	10.2	0.9	8.5
					sd	0.2	0.5	1.4	3.2	0.4	0.1	0.1	0.4	2.4	0.2	1.7
		slip	EV to IMV	~ 20-30 (ext.)	mean	1.6	3.1	16.6	51.8	0.3	0.4	0.4	4.8	5.6	0.8	14.3
				~ 20-30 (int.)	sd.	0.1	0.3	2.0	3.3	0.1	0.1	0.2	0.0	2.7	0.1	1.2
	TP2-7(orange)	body	IV	-	mean	1.0	3.9	16.7	51.8	0.3	0.3	0.2	4.1	8.3	1.1	11.8
					sd	0.3	0.2	1.0	3.6	0.2	0.1	0.1	0.3	1.6	0.2	4.0
		slip	EV to IMV	~ 20-30 (ext.)	mean	0.9	2.8	19.3	58.5	0.2	0.3	0.2	5.3	1.9	0.9	9.3
				~ 20-30 (int.)	sd	0.4	0.4	2.2	4.9	0.2	0.2	0.1	1.6	1.0	0.2	0.9
	TP2-21(red)	body	IV	-	mean	1.1	3.9	16.6	53.0	0.2	0.6	0.1	3.3	12.0	0.7	8.2
					sd.	0.1	0.1	0.4	1.0	0.2	0.2	0.1	0.6	0.5	0.1	1.0
		slip	EV to IMV	~ 10-20 (ext.)	mean	2.6	3.2	15.8	50.6	0.2	1.8	0.8	6.0	6.3	0.7	11.6
					sd	0.3	0.1	0.6	2.1	0.1	0.6	0.4	0.8	0.2	0.1	1.4
S2	TP1-4(light red)	body	EV	-	mean	1.0	3.8	16.9	55.0	0.3	0.2	0.2	2.7	11.1	0.9	7.5
					sd	0.1	0.4	0.4	1.1	0.1	0.1	0.0	0.3	1.3	0.1	0.6
		slip	EV to IMV	~ 40 (ext.)	mean	1.1	4.0	16.7	53.6	0.2	0.3	0.3	2.5	12.2	1.0	7.7
				~ 20-30 (int.)	sd	0.3	0.3	1.7	2.9	0.2	0.2	0.2	0.1	0.8	0.3	0.4
	TP2-19(brown)	body	IV to EV	-	mean	1.1	3.8	15.5	57.7	0.4	0.2	0.1	2.6	11.2	0.8	6.4
					sd.	0.2	0.5	1.1	2.8	0.2	0.1	0.1	0.2	0.9	0.1	0.7
		slip	EV	~ 10 (ext.)	mean	1.4	3.3	15.9	57.3	0.4	0.7	0.1	2.3	11.8	0.6	6.0
				~ 10 (int.)	sd	1.3	0.8	3.4	6.1	0.1	0.9	0.1	1.1	4.7	0.2	1.9

S	Sample	Vitrification	Thickness (Ï¼m)		Na2O	MgO	Al2O3	SiO2	P2O5	SO3	Cl2O	K2O	CaO	TiO2	Fe2O3	NA
S3	TC-8(black)	body	IV	-	mean	1.1	3.1	16.3	54.5	0.6	0.5	0.2	4.2	11.2	0.8	7.0
					sd	0.3	0.4	1.1	1.6	0.4	0.1	0.1	0.3	1.3	0.1	0.5
		slip	EV	~ 10-20 (ext.)	mean	1.3	3.0	12.8	41.6	5.0	1.0	0.9	5.1	13.0	0.7	13.3
				~ 10-20 (int.)	sd	0.2	0.5	2.5	5.5	3.8	0.7	0.4	1.3	5.3	0.2	3.1
	TP1-1(grey)	body	IV	-	mean	1.0	3.6	15.4	55.4	0.3	0.2	0.2	3.7	9.7	0.8	9.2
					sd	0.2	0.3	0.9	3.4	0.2	0.2	0.2	0.3	1.1	0.2	3.0
		slip	EV to IMV	~ 20-30 (ext.)	mean	1.3	3.1	14.4	50.8	0.6	0.7	1.2	3.7	10.9	1.1	11.7
				~ 20-30 (int.)	sd.	0.3	0.3	1.0	2.9	0.3	0.5	0.9	1.3	1.3	0.4	1.2
S4	TP2-8(grey)	body	IV	-	mean	0.9	2.8	14.6	57.5	1.0	0.2	0.1	3.4	11.1	0.7	7.4
					sd	0.2	0.2	0.7	2.6	0.6	0.2	0.1	0.5	1.3	0.2	1.4
		slip	EV	~ 20-30 (ext.)	mean	1.5	2.6	15.3	60.5	0.5	0.3	0.1	2.9	9.9	0.5	5.7
				~ 20-30 (int.)	sd	1.3	0.6	2.7	4.8	0.2	0.1	0.1	1.0	2.7	0.2	1.2

Surface and the body chemical data allow us to distinguish four main groups of specimens (S1 to S4) (Table 3.7). The first comprises six vessels (TC-6, TP1-7/8/10, and TP2-7/21) with a red-orangish slip, which contains higher concentrations of alkali metals and lower concentrations of alkaline earth metals. To some extent, this pattern can be achieved with the refinement of the clays used for the construction of the ceramic body through elutriation, that is, removing coarser components, such as carbonates. However, the compositional differences detected between bodies and coatings are significant and suggest the use of different recipes (Noll, 1991: 125). Thus, the vessels of group S1 exhibit slightly diverse Fe_2O_3 values, being higher in the slip than it is in the body in samples TP1-8/10 and TP2-21, while lower in samples TC-6, TP1-7 and TP2-7. Moreover, the slips of all these samples, except TP2-21, present similar or higher values of Al_2O_3. In the case of TC-6, TP1-7 and TP2-7, aluminium concentration is considerably higher in the slip, while the corresponding iron concentration is low, indicating that different clays must have been used for the slip (Figure 3.14, c). Similar recipes to those identified within group S1 have been recognised in the red, brown and black slips of coeval tableware of Hellenistic tradition produced in Kampyr Tepe (Martínez Ferreras et al., 2016). Moreover, these recipes are equivalent to those found in the coatings of some contemporary Mediterranean productions, including the Campanian A wares from south Italy and Sicily, which are characterised by high amounts of alkali metals and low concentrations of alkaline earth metals (Montana et al., 2013).

The second group (S2) comprises the light red slipped cup TP1-4 and the brown slipped

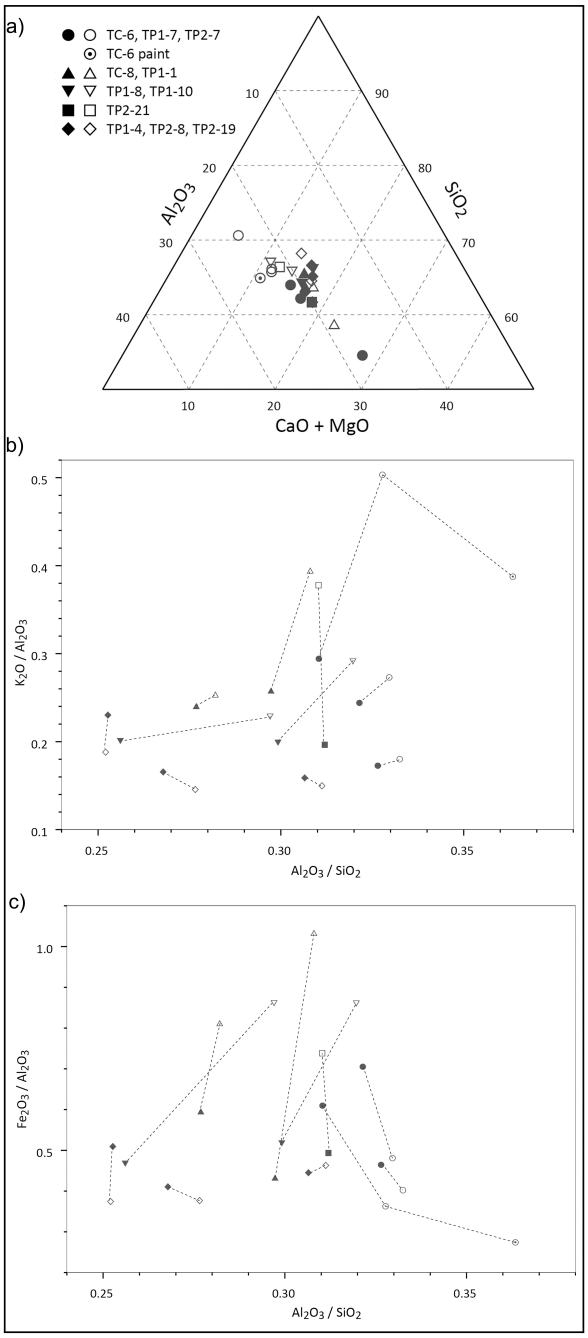

Figura 3.14: a) Ternary diagram with SiO_2, Al_2O_3 and CaO+MgO concentrations. The black symbols correspond to average concentrations in the body and the white symbols to average concentrations in the slip. b) Ratios K_2O/Al_2O_3 versus Al_2O_3/SiO_2. c) Ratios Fe_2O_3/Al_2O_3 versus Al_2O_3/SiO_2. *Figure 11 in the original.*

bowl TP2-19 (Table 3.7). Their slips exhibit a higher CaO content, similar MgO, and a lower concentration of Fe_2O_3 and alkali metals than in the ceramic bodies. Interestingly, group S3 comprises the greyish plate TP1-1 and the black slipped plate with stamped palms TC-8. The surfaces of these specimens have a higher CaO content than that of their bodies, while the K_2O concentration is equivalent or higher in the surface. Here again, these differences suggest the use of a different fine, iron-rich clay for the slip, in this case calcareous. Furthermore, a significant enrichment of P_2O_5 (ca. 5 wt %) was detected in the slipped surface of sample TC-8, while the body presents a similar level of phosphorus to that observed in the other ceramics. Phosphorus enrichment could be indicative of the addition of bone ash to the slip. A similar pattern is observed in the grey slipped surfaces of the grey body wares produced in Eastern Sicily (Mirti, 2000; Mirti & Davit, 2001). Group S4 comprises the greyish slipped plate TP2-8. Its slip contains higher Al_2O_3 and SiO_2 values and lower amounts of alkali metals and alkaline earth metals, compared to the body.

3.3.7. Conclusions

Both the chrono-typological classification, performed here using reliable stratigraphic and 14C data, and the archaeometric analysis, carried out on the wares and the raw materials, have enabled us to undertake a complete characterisation of the main ceramic prototypes used in different sectors of ancient Termez from the Seleucid/Greco-Bactrian period to that of the Yuezhi nomadic migrations. Regarding the provenance of the vessels, the WD-XRF analysis reveals the presence of two main pottery productions that present very small chemical variations. Indeed the tv value calculated is low, indicating that all the wares analysed form a fairly homogeneous assemblage. Moreover, the composition of the samples clustered in these groups resembles that of the clayey sediments collected at the site, with the exceptions of G-2, G-3 and G-5. Specifically, the chemical composition and the textural characteristics of G-3 and G-5 both differ significantly from those of the studied wares. Their groundmass is excessively sandy, a characteristic that is evident not only in the pristine materials but also in the fired products at 800ºC and 950ºC. Similarly, sample G-5 presents some metapelitic (slate/phyllite) inclusions that are not detected in any of the other wares studied. Clayey sediment G-2 differs because, together with G-3, it exhibits the lowest aluminosilicate mineral phase contents. In contrast, both the chemical composition and the textural characteristics displayed by

clayey sediments G-4, G-6 and G-7 (and G-1 to a lesser degree) provide the best fit with the chemical and petrographic properties of the wares studied. In addition, the lithological composition of the aplastic inclusions identified in the ceramic products is compatible with the main geological constituents of the area, as demonstrated by an examination of the clays and the sandstone substrate of Tchingiz Tepe. Therefore, the clayey sediment used in the manufacture of these vessels was most probably procured from the Neogene deposits in the confluence of the Amu Darya and the Surkhan Darya valleys. This suggests that most of the wares analysed are of local origin; however, the absence of any evidence of pottery workshops in Termez during this period means this claim should be treated with caution and leads us to attribute a local/regional provenance to these wares.

The significantly lower content (or absence) of coarse inclusions in the clays compared to that of the wares can be explained if a temper was added during paste processing. The bimodality observed among the vessels' aplastic inclusions lends further support to this hypothesis. Nevertheless, as has been suggested in the case of the tableware produced at Kara Tepe in Termez during the Kushan period (Tsantini et al., 2016), the clay was, in all likelihood, unintentionally mixed during extraction, since the sedimentary stratigraphy is composed of successions of clayey, silty and sandy layers of different widths. Such mixture would also explain why the coarse inclusions of the wares are in general larger than those found in the raw materials analysed, especially in those presenting the greatest compositional similarity to the vessels.

In general, each production links wares from distinct periods and from clearly different sectors of Termez. For example, one group comprises most of the vessels of Hellenistic tradition from the Citadel and a few wares from the alluvial plain. This distribution proves the simultaneous occupation of both settlements in Termez at some point, as suggested by radiocarbon dating. This group represents the earliest pottery among the wares analysed, an assemblage that includes non-slipped and slipped plates, bowls and cups with a typical 'Greek' profile, platters and jars. Such artefacts are usual in the Seleucid/Greco-Bactrian contexts of Kampyr Tepe, Dalverzin Tepe, Kurganzol, Dzhiga Tepe, Ai-Khanoum and Merv. The second group comprises most of the wares from the alluvial plain, two from Tchingiz Tepe and three from the Citadel. Most of these specimens were recovered in contexts that have been accurately dated by 14C, covering from the Greco-Bactrian to the Yuezhi periods. Apart from a number of specific plate, bowl and platter types, most of the vessels in this group correspond to a large repertoire

of bowls of prototypes B-3, B-4, B-5, B-6 and B-7, cups C-3, C-4, C-5 and C-6, plates P-4 and P-5, urns/containers, platters and the greyish bowls and plates of nomadic tradition. The differences detected between their composition and that of the earlier vessels are probably related to the procurement of more diverse raw materials and to slight differences in the processing of the paste.

Apart from the slight chemical and petrographic differences observed between the respective groups, the archaeometric characterisation points to a high technological standardisation in the procurement and processing of raw materials over the period considered, with all the wares analysed being fine-medium calcareous fabrics. As for modelling, all the sherds analysed comprise wheel-thrown pottery. However, Termez's Yuezhi population introduced a new pottery repertoire more closely related to the service and consumption of food and drink, including the greyish slipped bowls and plates with the polished lines of prototype P-6, and the cups of prototypes C-3, C-4, and C-5. These wares replaced the earlier plates of prototypes P-1 and P-2 and the cups of prototypes C-1 and C-2, characteristic of the Greco-Bactrian period in ancient Bactria. No significant differences were observed in the surface treatments applied by the two different cultural groups to the vessels. The identification of several recipes suggests the use of different procedures -probably technological traditions- to coat the vessels, which appear to have coexisted in the period under analysis. Indeed, the identification of the same pattern in wares dated both to the Hellenistic/Greco-Bactrian and Yuezhi periods (i.e., groups S1 and S3) indicates that these recipes endured over a long time span. The reddish-orangish slips of group S1 wares contain high concentrations of alkali metals, while the black-greyish slips of group S3 are characterised by the presence of high concentrations of alkaline earth metals. The latter also present greater concentrations of iron oxides in the slips, but at a level that indicates the selection of an iron-rich clay rather than the deliberate mixing with iron oxides (Noll, Holm & Born, 1975). In contrast, groups S2 and S4 comprise vessels dated solely to the Yuezhi period and should correspond to recipes belonging to the nomadic tradition. The slips of group S2 present higher amounts of alkaline earth metals and lower concentrations of alkali metals and iron oxides, while the greyish plate from group S4 contains high concentrations of Al_2O_3 and SiO_2, and low amounts of alkali and alkaline earth metals. This difference suggests the use of different finer clayey materials, probably illitic, in the coatings. Apart from the specific use of illitic clays, subject also to decantation, the potassium content may have been further boosted with plant ash or, even, bone ash to facilitate

the vitrification of the surface, since it acts as flux (Noll, Holm & Born, 1975). The high levels of phosphorous in the black slip of the plate with stamped palms TC-8 also points to the mixing of clay with bone ash (Rice, 1987: 97).

The firing process of the vessels would have reached temperatures that ranged from 800 to 1000/1100ºC using both oxidising and reducing atmospheres. In fact, in both Greco-Bactrian and Yuezhi traditions, a single atmosphere was maintained during the firing process. These firing conditions would have been equivalent to those identified in the pottery production at the nearby site of Kampyr Tepe dated to the Seleucid and Greco-Bactrian periods (Martínez Ferreras et al., 2016). Therefore, it appears that the oxidising-reducing-oxidising single firing cycle, characteristic of some black coated pottery productions from the Mediterranean (i.e., Attic and Campanian A and B wares), was not performed by Bactrian potters (Maniatis, Aloupi & Stalios, 1993; Montana et al., 2013). As far as the firing process is concerned, a technological association can be established nevertheless between the black and greyish slipped wares analysed and the Campanian C wares produced in Sicily in the Hellenistic period (Mirti, 2000; Mirti & Davit, 2001), which also present black or greyish coated surfaces over greyish ceramic bodies.

Although the morphological and technological characteristics of some of the wares analysed resemble certain contemporary types of Mediterranean tableware, the existence of any technological/cultural interactions between the Mediterranean and the Hellenistic settlements of northern Bactria still requires a more exhaustive examination. This study does contribute to providing a better understanding of this phenomenon and of the cultural changes introduced by the nomadic tribes from the mid- or late 2nd century B.C. The morphological changes observed in the pottery used from these dates at Termez point to shifts in the processing and consumption practices regarding liquid and solid foodstuff. However, the technological processes involved in pottery manufacture appear to have remained rather standardised across the Greco-Bactrian and the nomadic pottery traditions. The absence of any determinant technological changes would seem to corroborate the accepted view that pottery was produced by specialised itinerant potters, and that the Greco-Bactrian pottery workshops continued to operate with the arrival of the nomadic tribes.

Acknowledgments

This study was carried out as part of the research conducted by Verònica Martínez Ferreras within the Juan de la Cierva (JCI-2011-10963) and the Ramón y Cajal programs (RYC-2014-15789) funded by the Spanish Ministry of Economy and Competitiveness (MINECO). Financial support for research for this paper was provided under three research projects led by J.M. Gurt Esparraguera (HAR2008-01730, funded by the Spanish Ministry of Science and Innovation, MICINN) and V. Martínez Ferreras (CAMOTECCER HAR2012-32653 and CERAC HAR2016-75133-C3-1-P funded by MINECO). The research was also supported by the Simulpast-CSD2010-00034, project Consolider-Ingenio program-MICINN, led by M. Madela (J.M. Gurt Esparraguera as coordinator of Group 4). The authors thank the anonymous referees for their helpful comments on earlier drafts of this paper.

References

Abdullaev, K. (2013). The Buddhist culture of Ancient Termez in old and recent finds. *Parthica*, 15, 157-187.

Anderson, M.J., & Walsh, D.C.I. (2013). PERMANOVA, ANOSIM, and the Mantel test in the face of heterogeneous dispersions: What null hypothesis are you testing? *Ecological Monographs*, 83, 557-574.

Bernard, P. (1994). The Greek kingdoms of Central Asia. In: J. Harmatta, B.N. Puri & G.F. Etemadi (Eds.), *History of Civilizations of Central Asia. Vol. II. The development of sedentary and nomadic civilizations: 700 B.C. to A.D. 250* (pp. 99-129). Paris: UNESCO Publishing.

Bolelov, S.B. (2001). Goncharnaya mastyerskaya III-II vyekov do H.E. na Kampyrtepa. In E.V. Rtveladze (Ed.), *Matyerialy Tokharistanskoy Ekspyeditsii. Arkhyeologichyeskiye isslyedovaniya Kampyrtepa*, vol. 2 (pp. 15-30). Tashkent: Academy of Fine Arts of Uzbekistan, San'At.

Bolelov, S.B. (2011). Proizvodstvyennyy tsyentr epokhi Ellinizma na Tsitadyeli Kampyrtepa. *Matyerialy Tokharistanskoy Ekspyeditsii. Arkhyeologichyeskiye isslyedovaniya Kampyrtepa*, vol. 8 (pp. 48-79). Yelyest: Academy of Fine Arts of Uzbekistan, San'At.

Bourgeois, O., Cobbold, P.R., Rouby, D., & Thomas, J.C. (1997). Least squares restoration of Tertiary thrust sheets in map view, Tajik depression, central Asia. *Journal of Geophysical Research*, 102, B12, 27553-27573.

Boynton, R. S., (1980). *Chemistry and Technology of Lime and Limestone* (2nd ed.). New York: Wiley.

Buxeda i Garrigós, J. (1999). Alteration and contamination of archaeological ceramics: the perturbation problem. *Journal of Archaeological Science*, 26, 295-313.

Buxeda i Garrigós, J., & Kilikoglou, V. (2003). Total variation as a measure of variability in chemical data sets. In L. Van Zelts (Ed.), *Patterns and Process: a Festschrift in honour of Dr. Edward V. Sayre* (pp. 185-198), Suitland, Maryland: Smithsonian Centre for Materials Research and Education.

Cultrone, G., Rodriguez-Navarro, C., Sebastian, E., Cazalla, O., & De la Torre, M.J., (2001). Carbonate and silicate phase reactions during ceramic firing. *European Journal of Mineralogy*, 13, 621-634.

Enoki, K., Koshelenko, G.A., & Haidary, Z. (1994). The Yüeh-Chich and their Migrations. In: J. Harmatta, B.N. Puri & G.F. Etemadi (Eds.), *History of Civilizations of Central Asia. Vol. II. The development of sedentary and nomadic civilizations: 700 B.C. to A.D. 250* (pp. 171-189). Paris: UNESCO Publishing.

Fabbri, B., Gualtieri, S., & Shoval, S. (2014). Review. The presence of calcite in archeological ceramics. *Journal of the European Ceramic Society*, 34, 1899-1911.

Gardin, J.C. (1973). Les Céramiques. In: P. Bernard (Ed.), Fouilles d'Aï-Khanoum I (Campagnes 1965, 1966, 1967, 1968) (pp. 121-188). *Mémoires de la Délégation Archéologique Française en Afghanistan* 21. Paris.

Gurt Esparraguera, J.M., Ariño Gil, E., Martínez Ferreras, V., & Pidaev, Sh.R. (2015). The Buddhist occupation of Tchingiz Tepe (Termez, Uzbekistan) in the Kushan period through the ceramic contexts. *Archaeological Research in Asia*, 3, 19-33.

Houal, J.-B. (2013). La céramique de Termez des époques antique et médiévale. In J. Bendezu-Sarmiento (Dir.), *L'Archéologie Française en Asie Centrale, Nouvelles recherches et enjeux socioculturels* (pp. 423-442). Cahiers d'Asie Centrale 21/22. Paris: De Boccard.

Leith, W., & Alvarez, W. (1985). Structure of the Vakhsh fold and thrust belt, Tadjik SSR: geological mapping on a Landsat image base. *Geological Society of America Bulletin*, 96, 875-885.

Leriche, P. (2013). L'apport de la Mission Archéologique Franco-Ouzbèque (MAFOuz) de Bactriane du Nord à l'histoire de l'Asie Centrale. In J. Bendezu-Sarmiento (Dir.), *L'Archéologie Française en Asie Centrale, Nouvelles recherches et enjeux socioculturels* (pp. 135-164). Cahiers d'Asie Centrale 21/22. Paris: De Boccard.

Leriche, P. (2007). Bactria, land of a thousand cities. In: G. Hermann & J. Cribb (Eds.), *After Alexander. Central Asia before Islam* (pp. 121-153). Proceeding of the British Academy 133. Oxford: Oxford University Press.

Leriche, P., & Pidaev, Sh.R. (2007). Termez in Antiquity. In: G. Hermann & J. Cribb (Eds.), *After Alexander. Central Asia before Islam* (pp. 179-211). Proceeding of the British Academy 133. Oxford: Oxford University Press.

Lyonnet, B. (2013). La céramique hellénistique en Asie centrale. In: N. Fenn & Ch. Römer-Strehl (Eds.) *Networks in the Hellenistic World. According to the pottery in the Eastern Mediterranean and beyond* (pp. 351-368). BAR International Series 2539. Oxford: British Archaeological Reports.

Maggetti, M., Neururer, Ch., & Ramseyer, D. (2011). Temperature evolution inside a pot during experimental surface (bonfire) firing. *Applied Clay Science*, 53, 500-508.

Mandelshtam, A.M. (1975). *Pamyatniki kochyevnikov kushanskogo vryemyeni v syevernoy Baktrii*. Trudy tadzhiskoy arkhyelogichyeskoy ekspyeditsii Instituta Arkheologii AN CCCP i Instituta Istorii, VII. Leningrad: Academy of Sciences of USSR, Nauka.

Maniatis, Y., Simopoulos, A., & Kostikas, A. (1981). Mössbauer study of the effect of calcium content on iron oxide transformations in fired clays. *Journal of American Ceramic Society*, 64, 263-269.

Maniatis, Y., Aloupi, E., & Stalios, A.D. (1993). New evidence for the nature of the Attic Black gloss. *Archaeometry*, 35, 23-34.

Maritan, L., Angelini, I., Artioli, G., Mazzoli, C., & Saracino, M. (2009). Secondary phosphates in the ceramic materials from Frattesina (Rovigo, North-Eastern Italy). *Journal of Cultural Heritage*, 10, 144-151.

Martínez Ferreras, V., Ariño Gil, E., Gurt Esparraguera, J.M., & Pidaev, Sh.R. (2014). The enclosure of Tchingiz Tepe (ancient Termez, Uzbekistan) during the Kushan and Kushan-Sassanian periods. Archaeological stratigraphy and 14C dating analyses. *Iranica Antiqua*, 49, 413-474.

Martínez Ferreras, V., Gurt Esparraguera, J.M., Hein, A., Pidaev, Sh.R., Rtveladze, E.V., & Bolelov, S. (2016). Tableware in the Hellenistic tradition from the city of Kampyr Tepe in ancient Bactria (Uzbekistan). *Archaeometry*, 58-5, 736-764.

Marínez Ferreras, V., Angourakis, A., Hein, A., Gurt Esparraguera, J.M., Sverchkov, L.M., Sánchez del Corral, A. (in press). Pottery in Hellenistic tradition from ancient Bactria: The Kurganzol fortress (Uzbekistan, Central Asia). *Journal of Archaeological Science: Reports*, doi: 10.1016/j.jasrep.2016.11.049.

Mirti, P. (2000). X-Ray microanalysis discloses the secrets of ancient Greek and Roman potters. *X-Ray Spectrometry*, 29, 63-72.

Mirti, P., & Davit, P. (2001). Technological characterization of Campanian pottery of type A, B and C and of regional products from ancient Calabria (southern Italy). *Archaeometry*, 43, 19-33.

Montana, G., Tsantini, E., Randazzo, L., & Burgio, A. (2013). SEM-EDS analysis as a rapid tool for distinguishing Campanian A ware and Sicilian imitations. *Archaeometry*, 55, 591-608.

Morel, J.-P. (1981). *Céramique campanienne. Les formes*. Bibliothèque des Écoles Françaises d'Athènes et de Rome 244. Rome.

Moroni, B., & Conti, C. (2006). Technological features of Renaissance pottery from Deruta (Umbria, Italy): an experimental study. *Applied Clay Science*, 33, 230-246.

Nekrasova, E.F., & Pugachenkova, G.A. (1978). Kyeramika Dalverzintepe, In G.A. Pugachenkova & E.V. Rtvladze (Eds.), *Dalverzintepe. Kushanskiy gorod na yugye Uzbekistana* (pp. 143-161). Academy of Sciences of the Soviet Socialist Republic of Uzbekistan. Tashkent: Fan.

Nikolaev, V.G. (2002). Afghan-Tajik depression, Architecture of sedimentary cover and evolution. *Russian Journal of Earth Sciences*, 4, 399-421.

Nodari, L., Marcuz, E., Maritan, L., Mazzoli, C., & Russo, U. (2007). Hematite nucelation

and growth in the firing of carbonate-rich clay for pottery production. *Journal of the European Ceramic Society*, 27, 4665-4673.

Noll, W., Holm, R., & Born, L. (1975) Painting of Ancient Ceramics. *Angewandte Chemie* 14, 602-613.

Noll, W. (1991). *Alte Keramiken und ihre Pigmente*. Stuttgart: E. Schweizbart'sche Verlagsbuchhandlung.

Pidaev, S.R. (1984). Kyeramika Dzhiga-tepe (iz raskopok 1976 g.). In I.T. Kruglikova (Ed.), *Matyerialy Sovyetsko-Afganskoy arkhyeologichyeskoy ekspyeditsii* (pp. 112-124). Dryevnyaya Baktriya 3. La Bactriane Ancienne 3. Moscow: Academy of Sciences of USSR, Nauka.

Pidaev, S.R. (1991a). Kyeramika gryeko-baktriyskogo vryemyeni s gorodishcha starogo Termeza (pp. 210-224). *Sovyetskaya Arkhyeologiya* (Otdyelnyy ottisk) 1. Moscow: Academy of Sciences of USSR.

Pidaev, S.R. (1991b). Syeroglinyanaya kyeramika Mirzakultepa. In A.A. Askarov (Ed.), *Istoriya matyerialnoy kultury Uzbekistana*, vol. 25 (pp. 88-98). Tashkent: Academy of Sciences of the Republic of Uzbekistan, Fan.

Puschnigg, G. (2013). The Dynamics of Exchange and Innovation in the Oasis City of Merv. In: N. Fenn & Ch. Römer-Strehl (Eds.), *Networks in the Hellenistic World. According to the pottery in the Eastern Mediterranean and beyond* (pp. 339-350). BAR International Series 2539. Oxford: British Archaeological Reports.

Reimer, P.J., Baillie, G.L., Bard, E., Bayliss, A., Beck, J.W., Bertrand, C.J.H., Blackwell, P.G., Buck, C.E., Burr, G.S., Cutler, K.B., Damon, P.E., Edwards, R.L., Fairbanks, R.G., Friederich, M., Guilderson, T.P., Hogg, A.G., Hughen, K.A., Kromer, B., McCormac, G., Manning, S., Ramsey, C.B., Reimer, R.W., Remmele, S., Southon, J.R., Stuiver, M., Talamo, S., Taylor, F.W., Van der Plicht, J. & Weyhenmeyer, C.E. (2009). IntCal04 Terrestrial Radiocarbon Age Calibration 0-26 cal kyr BP. *Radiocarbon*, 46, 1029-1058.

Riccardi, M.P., Messiga, B., Duminuco, P.,(1999). An approach to the dynamics of clay firing. *Applied Clay Science*, 15, 393-409

Rice, P.M. (1987). *Pottery Analysis*. A Sourcebook. Chicago: The University of Chicago Press.

Sánchez del Corral, A. & Thum, H. (2012). Geomorphology and Late Holocene morphogenesis of Tchinguiz Tepe hill (Old Termez, Uzbekistan, Central Asia). *Quaternary International*, 281, 89-104.

Schultz, L.G. (1964). *Quantitative Interpretation of Mineralogical Composition from Xray and Chenical Data for the Pierre Shale*. Washington: Geological Survey Proffesional Paper 391-C.

Schwedt, A., Mommsen, H., Zacharias, N., & Buxeda, J. (2006). Analcime crystallization and compositional profiles-comparing approaches to detect postdepositional alterations in archaeological pottery. *Archaeometry*, 48, 237-251.

Stuiver, M. & Reimer, P. J. (1993). Extended 14C data base and revised Calib 3.0 14C age calibration program. *Radiocarbon*, 35, 215-230.

Sverchkov, L.M. (2008). The Kurganzol Fortress (on the History of Central Asia in the Hellenistic Era). *Ancient Civilizations from Scythia to Siberia*, 14 (pp. 123-191). Leiden: Koninklijke Brill NV.

Trindade, M.J., Dias, M.I., Coroado, J., & Rocha, F. (2009). Mineralogical transformations of calcareous rich clays with firing: A comparative study between calcite and dolomite rich clays from Algarve, Portugal. *Applied Clay Science*, 42, 345-355.

Tsantini, E., Martínez Ferreras, V., Ariño Gil, E., Gurt Esparraguera, J.M. & Pidaev, Sh.R. (2016). Pottery production in the Buddhist communities in Central Asia: The Kushan-Sassanian pottery workshop of Kara Tepe (Termez, Uzbekistan). *Archaeometry*, 58, 35-56.

Yachminnikov, Y.U., & Nikolaev, V.G. (1990). Seismic survey data on the sediment cover structure in the Surkhandarya Depression. *Geotectonics*, 24, 53-58.

3.4. Presenting multivariate statistical protocols in R using wine Roman amphorae productions in Catalonia, Spain

Esta sección corresponde al siguiente artículo:

Angourakis, A., Martínez Ferreras, V., Torrano, A., Gurt, J.M. (2018). Presenting multivariate statistical protocols in R using wine Roman amphorae productions in Catalonia, Spain. *Journal of Archaeological Science*, 93:150-165.

Los anexos correspondientes a esta publicación se encuentran en la sección A.1.2 del Apéndice.

Resumen Existen varias técnicas analíticas que pueden funcionar como fuentes de datos para caracterizar las cerámicas arqueológicas. Estas fuentes de datos no son necesariamente alternativas sino más bien complementarias entre sí. Informan sobre diferentes aspectos de la cerámica en relación con el origen de las materias primas y los procesos tecnológicos involucrados. Sin embargo, cuando los estudios integran más de una fuente de datos, a menudo lo hacen a través de la descripción textual y la argumentación, no a través de un análisis estadístico combinado.

Nuestro objetivo es ayudar a superar esta situación presentando cuatro protocolos para explorar datos sobre cerámica arqueológica. Estos protocolos cubren cuatro vías diferentes para interrogar muestras de cerámica: (1) definición de grupos de referencia químicos (RG) usando composiciones geoquímicas, por ejemplo, proporcionadas por el análisis de Fluorescencia de Rayos X (WD-XRF); (2) definición de los grupos de materiales mediante la examinación de imágenes petrográficas, tales como la microscopía óptica de sección delgada; (3) definición de procedencia utilizando la suma integral de las dos últimas fuentes de datos; y (4) definición de procedencia utilizando datos geoquímicos y una selección de variables petrográficas que se consideran indicativas del origen de las materias primas y independientes de factores humanos. Demostramos su rendimiento aplicándolos a un conjunto de datos de ánforas romanas de vino bien estudiadas de Cataluña, NE España, y contextualizando los resultados. Además, al comparar los resultados de los protocolos, replanteamos la conclusión de Baxter et al. (2008) que

un enfoque de “modo mixto” es preferible al análisis de datos de diferentes fuentes por separado.
Los protocolos son el producto sintético de varios métodos estadísticos multivariables desarrollados con fines similares en otras disciplinas, como la Geología y la Ecología. Para permitir a los futuros usuarios replicar nuestro análisis y aplicar los protocolos, publicamos en línea dos paquetes R que contienen todos los procedimientos necesarios, desde la limpieza de datos hasta la generación de gráficos. También ofrecemos en los apéndices un tutorial para usar estos recursos y los scripts de ejemplo.

Resum Hi ha diverses tècniques analítiques que poden funcionar com a fonts de dades per caracteritzar les ceràmiques arqueològiques. Aquestes fonts de dades no són necessàriament alternatives sinó més aviat complementàries entre si. Informen sobre diferents aspectes de la ceràmica en relació amb l'origen de les matèries primeres i els processos tecnològics involucrats. No obstant això, quan els estudis integren més d'una font de dades, sovint ho fan a través de la descripció textual i l'argumentació, no a través d'una anàlisi estadística combinat.
El nostre objectiu és ajudar a superar aquesta situació presentant quatre protocols per explorar dades sobre ceràmica arqueològica. Aquests protocols cobreixen quatre vies diferents per interrogar mostres de ceràmica: (1) definició de grups de referència químics (RG) usant composicions geoquímiques, per exemple, donades per l'anàlisi de Fluorescència de Raigs X (WD-XRF); (2) definició dels grups de materials mitjançant la examinació d'imatges petrogràfiques, com ara la microscòpia òptica de secció prima; (3) definició de procedència utilitzant la suma integral de les dues últimes fonts de dades; i (4) definició de procedència utilitzant dades geoquímiques i una selecció de variables petrogràfiques que es consideren indicatives de l'origen de les matèries primeres i independents de factors humans. Hem demostrat el seu rendiment aplicant-los a un conjunt de dades d'àmfores romanes de vi ben estudiades de Catalunya, NE Espanya, i contextualitzant els resultats. A més, en comparar els resultats dels protocols, replantegem la conclusió Baxter et al. (2008) que un enfocament de “manera mixta” és preferible a l'anàlisi de dades de diferents fonts per separat.
Els protocols són el producte sintètic de diversos mètodes estadístics multiva-

riables desenvolupats amb fins similars en altres disciplines, com la Geologia i l'Ecologia. Per permetre als futurs usuaris replicar la nostra anàlisi i aplicar els protocols, publiquem en línia dos paquets R que contenen tots els procediments necessaris, des de la neteja de dades fins a la generació de gràfics. També oferim en els apèndixs un tutorial per fer servir aquests recursos i els scripts d'exemple.

Journal of Archaeological Science 93 (2018) 150–165

Contents lists available at ScienceDirect

Journal of Archaeological Science

journal homepage: www.elsevier.com/locate/jas

Presenting multivariate statistical protocols in R using Roman wine amphorae productions in Catalonia, Spain

Andreas Angourakis[a,*], Verònica Martínez Ferreras[a], Alexis Torrano[b], Josep M. Gurt Esparraguera[a]

[a] ERAAUB, Department of Prehistory, Ancient History and Archaeology, University of Barcelona, C/Montalegre, 6, 08001, Barcelona, Spain
[b] BSC/CNS, Barcelona Supercomputing Center/Centro Nacional de Supercomputación, Carrer de Jordi Girona, 29-31, 08034, Barcelona, Spain

ARTICLE INFO

Keywords:
Ceramics
Archaeometric characterization
Geochemical composition
Petrography
Multivariate statistics
R
Roman amphorae

ABSTRACT

Several analytic techniques can provide data for characterizing archaeological ceramics. These data sources are not alternative but rather complementary to each other. They report on different aspects of ceramics concerning the origin of raw materials and the technological processes involved. However, when studies integrate more than one data source, they often do it through textual description and argument, not through a combined statistical analysis.

We aim to help to overcome this situation by presenting four protocols for exploring data on archaeological ceramics. These protocols cover four different paths when interrogating ceramic samples. Protocol 1 aims to assist the definition of chemical reference groups using geochemical compositions, for instance, given by X-ray fluorescence analysis (WD-XRF). Protocol 2 focuses on fabric groups using petrographic examinations, such as in thin-section optical microscopy. Protocol 3 offers a hybrid assessment of provenance, using the integral sum of the two data sources. Last, Protocol 4 consists of the same approach as Protocol 3 but using geochemical data and a selection of petrographic variables that are considered indicative of the origin of raw materials and independent of human factors. We demonstrate their performance by applying them to a well-studied Roman wine amphorae dataset from Catalonia, NE Spain, and contextualising the results. Through a comparison of the results produced by these protocols, we restate the conclusion of Baxter et al. (2008) that a 'mixed mode' approach is preferable to analysing data from different sources separately. Moreover, we argue that treating geochemical data as compositional and petrographic semi-quantitative observations as ordinal variables, when calculating dissimilarity, offers a more complete image of ceramic materials.

The protocols are the synthetic product of several multivariate statistical methods developed for similar purposes in other disciplines, such as geology and ecology. To allow future users to replicate our analysis and apply the protocols, we published online two R packages containing all necessary procedures, from data cleaning to plotting. We also offer in the appendices a tutorial and the example scripts.

1. Introduction

Pottery provenance and technology are well-studied fields in archaeology since they largely contribute to the economic, social and cultural reconstruction of past societies. The examination of the composition and the morphological and technical characteristics of pottery vessels allows making many inferences about them, their creators and users. Typically, we are capable of assessing their provenance and performance characteristics, which informs on the technological skills and traditions involved in their manufacture, trade relationships, the expectations of consumers, etc. (Schiffer and Skibo, 1997, 1987; Sillar and Tite, 2000). Under this perspective, the ultimate goal is to reconstruct the system entangling potters' decisions and constraints—i.e., *chaîne opératoire* (Cressell, 1990; Gosselain, 1995; Lemonnier, 1976)—which have both universal and contextual components (Sillar and Tite, 2000).

Archaeology is today conceptually and technically well equipped to address this system, given enough evidence (Tite, 2008). Since the 1960s, the incorporation of scientific methods in the study of ancient pottery has been a significant advance in the fields of study (Rice, 1987; Shepard, 1956). Provenance analysis is used to locate specific pottery designs and technological patterns in particular places and periods, as well as trade relationships between different areas. The use of different archaeometric techniques to assess provenance, such as chemical

* Corresponding author.
E-mail address: andros.spica@gmail.com (A. Angourakis).

https://doi.org/10.1016/j.jas.2018.03.007
Received 10 November 2017; Received in revised form 12 March 2018; Accepted 22 March 2018
0305-4403/ © 2018 Elsevier Ltd. All rights reserved.

Abbreviations

alr, clr, ilr	additive, centered, isometric log-ratio
CA	correspondence analysis
CHEM	geochemical data
FGs	fabric groups
IND	tag for site-wise outliers (e.g., FEU-IND2 is the second outlier in the Fenals)
NI	neighbour interchange approach to measure dissimilarity in ordinal variables
NMDS	non-metric multidimensional scaling
PCA	principal components analysis
PCoA	principal coordinates analysis
PETRO	mineralogical and petrographic data
PGs	provenance groups
RGs	chemical reference groups
RPCA	robust principal component analysis
RRD	relative rank difference approach to measure dissimilarity in ordinal variables
WD-XRF	X-ray fluorescence analysis

Amphorae formal types:

D1	Dressel 1
D2/4	Dressel 2/4
D7/11	Dressel 7/11
L2	Lamboglia 2
Ob.74	Oberaden 74
P1	Pascual 1
T1, T3	Tarraconense 1 and 3

analysis and thin section optical microscopy, has shown different levels of results (i.e., from workshop to regional attribution). The potential of each technique will depend on the nature of the samples, the research questions, and the background knowledge available. The use of reference resources (e.g., databases, publications, and geological charts) is recommended to get more discriminative results at a small-scale, such as for recognising productions within a workshop. Moreover, through a wide range of spectroscopic and microscopic methods, archaeologists can investigate the technological processes involved in pottery manufacture (the procurement and processing of raw materials, forming, finishing, firing, and surface treatments). When approaching pottery artefacts from a long-term perspective, we can address the evolution of pottery making and style, possibly discerning specific cultural and technological patterns.

However, contributions are often limited to a partial characterization according to the technical and theoretical backgrounds of the researchers involved. Usually, the plethora of possible analyses will not reach their potential, if not sufficiently integrated with other methods, including those generating qualitative and semi-quantitative data. The need for data integration was already acknowledged in several foundational archaeometric studies (Perlman and Asaro, 1969; Sayre, 1976; Shepard, 1965). Nonetheless, it was not until the 2000s that the statistical and computational sophistication was enough to offer more transparent, effective, fast, and accessible solutions.

To our knowledge, the clearest examples of the integration of data on archaeological ceramics are the works of Rice and Saffer (1982) and Baxter et al. (2008). Both papers successfully illustrate the benefits of combining petrographic and geochemical data to improve classifications based on macroscopic features. Our contribution builds on their conclusions, as we also aim to demonstrate the virtues and limitations of "mixed-mode" analyses. Based specifically on Baxter et al. (2008), we explored different paths to achieve integration. We focused on statistical methods developed in other disciplines (Filzmoser et al., 2009; Pavoine et al., 2009; Podani, 1999), that exploit computational resources while moving towards reproducible research (Gandrud, 2016; Marwick, 2017). Regarding the processing of geochemical data, we side with those authors that have advocated for log-ratios (Aitchison, 1982; Buxeda i Garrigós, 1999; Martín-Fernández, 2015; Pawlowsky-Glahn and Buccianti, 2011) rather than some form of standardization (e.g., log-scaled). Though not favouring log-ratios, Baxter (2008) summarized this debate with refreshing clarity, identifying arguments that are still valid today.

We synthesize our explorations by presenting a multivariate methodology implemented in R (R Core Team, 2015), which is an entirely free and open-source statistical software widely used in academia. We published an R package online, *cerUB* (Angourakis and Martínez Ferreras, 2017), containing the code required for applying this methodology to comparable datasets. We encourage further extensions and improvements by the community, as we were allowed to do so, particularly regarding the contribution of Pavoine et al. (2009).

The greatest challenge for mixed-mode integration is that, while the geochemical composition is strictly quantitative, both mineralogical and petrographic compositions often go through qualitative assessments in archaeological studies. The methodology we present deals exclusively with qualitative petrographic data (see Appendix A). However, we acknowledge that there are quantitative approaches to petrographic (i.e., point-counting) and mineralogical (i.e., digital image) analyses that are increasingly being used on archaeological ceramics (Quinn, 2013, sec. 4.2.3; Stoltman, 1989). Although beyond the scope of our current proposal, these analyses will be considered for developing additional protocols in the future.

Once we designed a pottery database reflecting these and other aspects (section 2.2), we explored separate datasets involving different working hypotheses (e.g., provenance diversity, technological change). After much exploration, we define four statistical protocols of multivariate analysis to measure and represent dissimilarity between individual ceramics (section 2.3). The first three address respectively the geochemical composition (protocol 1), the petrographic characterization with data inferred from the mineralogical and petrographic compositions (protocol 2), and both data sources simultaneously (protocol 3). Protocol 4 differs from protocol 3 by selecting variables considered indicative of provenance.

We apply each protocol on a collection of Roman wine amphorae to demonstrate their performance in measuring and visualizing dissimilarity between archaeological ceramics. The collection includes samples found in fifteen workshops in Catalonia, NE Spain, and three shipwrecks sunk along the coast towards Narbonne, SE France (section 2.1). Both workshop productions and amphorae from the ships' cargoes were fully characterized in previous studies (Martínez Ferreras, 2014; Martínez Ferreras et al., 2015, 2013).

Through this approach we expect (a) to provide the analyst with a straightforward image of the pottery variability, thus aiding archaeological classification; and (b) to facilitate the identification of the most relevant factors among variables, to guide future finer analyses. Ultimately, we intend this methodology to be a useful tool for assessing the context of pottery-making, as well as the transport of materials for trade or tribute and the technological change among past societies.

2. Material and methods

2.1. Archaeological materials

The sample consists of a total of 236 Roman wine amphorae (Fig. 1, Table 1): 175 found in 15 workshops located in different production areas of the Catalan littoral and pre-littoral depressions, which initiated

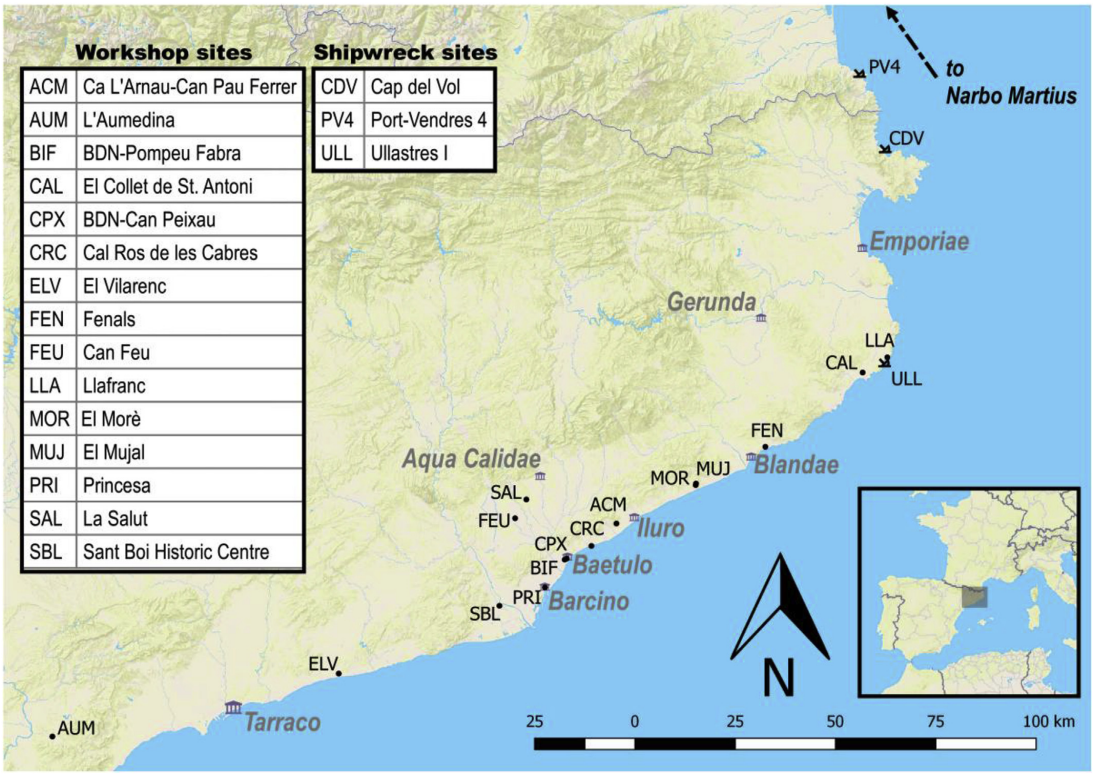

Fig. 1. The location of the main Roman settlements in the Catalan coast (NE Spain), the fifteen amphora workshops and the three shipwrecks included in the analysis.

pottery activity at different times; and 61 recovered in three shipwrecks along the coast towards Narbonne, France.

From c. 100/75 BC to 25 AD, the manufacture of amphorae in the region focused on wine production and export, feeding the maritime trade routes and reaching several port cities, such as *Narbo Martius* (Narbonne) in *Galia Narbonensis* (Martínez Ferreras, 2015).

The collection includes several typological forms of transport amphorae corresponding to specific periods and production areas. The first amphora design consists of a copy of the Dressel 1 (D1) prototype which was by far the most common Italian amphora for wine trade in the western Mediterranean. It existed in the Laietan region (nowadays El Maresme) especially in a few workshops located around the Roman city of *Iluro* (Mataró) such as in ACM. Another isolated production of the D1 type has been identified at La Salut (SAL), located in the western pre-littoral area near the Ripoll River Basin. The area of *Iluro* was also the focus of the introduction in *c*. 50 BC of new variants of an amphora prototype called Tarraconense 1 (T1), in sites such as ACM and MUJ. The workshops at ELV and SAL also produced other variants, which progressively replaced the D1 type.

Shortly after, around 40/30 BC, a new amphora design, the Pascual 1 (P1) type was adopted in the Laietan region, in the outskirts of the Roman city of *Baetulo* (nowadays Badalona) (CPX, BIF) and at the lower Llobregat River Valley (SBL). Production of P1 amphorae spread further throughout the territory, which mirrored the peak of wine industry and trade during Augustus' reign. From that time, it was produced in the pottery workshops that emerged in newly organized territories and cities, such as *Barcino* (Barcelona) (PRI), *Aqua Calidae* (Caldes de Montbui), the western pre-littoral (FEU), or in the north-eastern (LLA, CAL, FEN, MUJ, MOR) and southern (AUM, ELV) areas.

From 30/20 BC most of the production areas in *Hispania Tarraconensis* started to imitate another Italian prototype for the wine trade, the Dressel 2/4 (D2/4). The manufacture of other minor types such as the Oberaden 74 (Ob74) and Dressel 7/11 (D7/11) designs began at this time, the production of which was limited to the northern and southern areas (Martínez Ferreras, 2014; Miró, 1988).

D1, T1, and P1 types were mainly directed for supplying local and Gaul markets, although the latter also reached military camps in Germania and the southern coasts of Britannia. Even if some D2/4 were traded to Gaul, this type appears to have been mainly diffused at a local and regional level or sent to Italy and other areas of the Roman Empire.

The three shipwrecks selected show the trade *in transito* between a port of departure in NE Spain and a port of destination in southern France, probably at Narbonne (Fig. 1). The Port Vendres 4 is one of the several shipwrecks recovered at Port Vendres, south France. Dated to 40/30 BC, it contained an assemblage of Roman wine amphorae from Italy (D1 and L2) and NE Spain (P1), suggesting a trade shipment from a port in the central Catalan coast, probably *Iluro* or *Baetulo*, (Martínez Ferreras et al., 2015). Contrary, Els Ullastres (Palafrugell) and Cap del Vol (Port de la Selva), located in the northern Catalan coast, comprise homogeneous cargoes including only P1 amphorae. Most of the

Table 1
The pottery workshops and shipwrecks investigated.

Site	Location	Category	Chronology	Amphorae types
AUM Aumedina	Tivissa (Ribera d'Ebre)	Wine centre and pottery workshop	30 BC – 1st c. AD	P1, D7/11, Ob.74
ELV El Vilarenc	Calafell (Baix Penedès)	*Villa*, wine centre and pottery workshop	40/30 BC – 50 AD	D1, T1, T3, P 1, Flat base
SBL Barri Antic	S. Boi Llobregat (Baix Llobregat)	*Villa*, pottery workshop	50 BC – 1/10 AD	P1, D2/4
FEU Can Feu	S. Quirze Vallès (Western Vallès)	*Villa*, wine centre and pottery workshop	20/10 BC – 50 AD	P1, D2/4
SAL La Salut	Sabadell (Western Vallès)	*Villa*, wine centre and pottery workshop	50/25 BC – 1/10 AD	D1, T1
PRIN Princesa	Barcelona (Barcelonès)	Suburban pottery workshop	20/10 BC – 1st c. AD	P1
CPX Can Peixau	Badalona (Barcelonès)	Suburban pottery workshop	40/30 BC – 10/20 AD	P1
BIF Pompeu Fabra	Badalona (Barcelonès)	Suburban pottery workshop	40 BC – 25/50 AD	P1, D2/4
CRC Cal Ros Cabres	El Masnou (Maresme)	*Villa*, wine centre and pottery workshop	30/20 BC – 1st c. AD	P1
ACM CAN Pau Ferrer	Cabrera de Mar (Maresme)	Amphorae accumulation	100/75 BC	D1
ACM Ca l'Arnau	Cabrera de Mar (Maresme)	Industrial complex, pottery workshop	100/75 BC – 20/30 AD	D1, T1, P1
MOR El Moré	S. Pol de Mar (Maresme)	Industrial complex, wine centre and pottery workshop	30/20 BC – 10/20 AD	P1, D2/4
MUJ El Mujal	Calella (Maresme)	*Villa*, wine centre and pottery workshop	30/20 BC – 70 AD	T1, P1
FEN Fenals	Lloret de Mar (La Selva)	*Fundus*, pottery workshop	30/20 BC – 70/80 AD	P1, D2/4
CAL Collet S. Antoni	Calonge (Baix Empordà)	*Fundus*, pottery workshop	30/20 BC – 60/70 AD	P1
LLA Llafranc	Palafrugell (Baix Empordà)	Industrial complex, wine centre and pottery workshop	30/20 BC – 1st c. AD	P1, D7/11
PV4 Port-Vendres 4	Port-Vendres (Pyrénées-Orientales)	Shipwreck	40/30 BC	P1 and Italian D1 and L2
ULL Els Ullastres	Palafrugell (Baix Empordà)	Shipwreck	25/1 BC	P1
CPV Cap del Vol	Port de la Selva (Alt Empordà)	Shipwreck	10 BC/5 AD	P1

containers have been associated with the pottery workshops located on the outskirts of *Baetulo* and particularly, with BIF (Table 2). Therefore, these two case studies are evidence of the prevalence of the wine amphorae produced at *Baetulo* (Badalona) in the maritime trade to Gaul during the Augustan Age.

2.2. Data formatting

We design a database to enclose and relate common aspects of the study of archaeological pottery from an archaeometric perspective, namely the geochemical, mineralogical, and petrographic compositions, the latter two being registered as qualitative data. However, other important attributes relevant to archaeological interpretations, such as the shape, surface treatment, and mechanical properties could be introduced, if data is available.

The chemical analysis by WD-XRF, the mineralogical analysis by XRD, and the petrographic analysis through thin section optical microscopy allowed the identification of specific chemical reference groups (RGs) along the period of activity of the workshops (Table 2; Martínez Ferreras, 2014).

The geochemical composition was investigated through WD-XRF using a Philips PW 2400 spectrometer with an Rh excitation source. A total of 25 oxides and trace elements was measured, out of which 16—Fe_2O_3, Al_2O_3, TiO_2, MgO, CaO, SiO_2, Th, Nb, Zr, Y, Ce, Ga, V, Zn, Ni, and Cr—were deemed fit for the analysis of all samples.

The mineralogical composition was examined through XRD using both a Siemens D-500 and a Panalytical X'Pert PRO alpha 1 diffractometers. The crystalline phases were evaluated using the PANalytical HighScore X'Pert software and synthesized as an ordinal variable expressing the approximate firing temperature. Both WD-XRF and XRD measurements were performed at the CCiT-UB laboratory of the University of Barcelona.

The petrographic measurements were performed through the observation of thin-sections under the polarising optical microscope Olympus BX41, using a digital camera Olympus DP70 and the Analysis Five software. Petrographic data concerns the composition and characteristics of the matrix (groundmass) and the microstructure (micromass), especially the frequency, size, shape, type, and distribution of non-plastic inclusions (Whitbread, 1995). The frequency of non-plastic inclusions and voids were estimated by using the comparative tables offered by Matthew et al. (1991). Petrographic analysis registered a total of 115 variables, out of which 46 were not considered in this study, due to their dependence on known post-depositional perturbations (Buxeda i Garrigós, 1999; Maritan et al., 2009; Maritan and Mazzoli, 2004; Schwedt et al., 2006), the absence of variance within the selected samples (e.g., a mineral component inexistent in all samples), or because their information involves higher levels of interpretation (e.g., colour, forming technique, whether there was a mixture of clays).

In previous studies, we defined fabric groups (FGs), which are broader than RGs, based solely on petrographic data. Provenance groups (PGs), collapse RGs and FGs into a wider spatial criterion: e.g., "AUM" means "was made in L'Aumedina's workshop". In all classifications, we tag the site-wise outliers (IND) separately from the general site groups.

A complete list of petrographic variables names and their values can be consulted in Appendix A.

Table 2
The amphorae examined with indication of the pottery workshops, the groups or productions identified at each one and the average found for CaO and MgO at each group.

Sites	RG	Amphorae types/samples[a]	CaO %	MgO %
AUM	AUM-1	P1: AUM-4, 8, 11, 12; D7/11: AUM-14; Ob.74: AUM-17, 20	4.9	5.5
(n = 10)	AUM-2	P1: AUM-5, 10	12.3	4.3
	AUM-IND	P1: AUM-9	5.6	4.3
ELV	ELV-1	D1: ELV-2; T3: ELV-7, 9, 15, 52	15.4	3.2
(n = 18)	ELV-2	T3: ELV-45; T1: ELV-51; Flat base: ELV-47, 49	15.7	3.5
	ELV-3	D1: ELV-1; P1: ELV-16, 19, 20, 23, 24, 26, 36	10.7	3.4
	ELV-IND	T3: ELV-28	23.5	2.9
SBL	SBL-1	P1: SBL-1, 6, 11, 24, 28, 32	9.2	1.8
(n = 11)	SBL-2	D2/4: SBL-38 e.s. CALAM, SBL-40 e.s. QVA, SBL-42 e.s. QVA, SBL-43 e.s. SAB, SBL-45 e.s. TH	13.3	1.6
FEU	FEU-1A	D2/4: FEU-28, 29	4.9	1.8
(n = 20)	FEU-1B	P1: FEU-15, 17, 18, 19, 26	4.9	1.8
	FEU-2A	P1: FEU-1, 3, 5, 6, 8, 13, 14	14.6	1.8
	FEU-2B	Pointed bases: FEU-38 e.s. CE, FEU-39 e.s. CE, FEU-40 e.s. SEVE, FEU-41 e.s. H	12.5	1.7
	FEU-IND1	P1: FEU-9	1.7	2.3
	FEU-IND2	P1: FEU-16	4.9	1.7
SAL	SAL-1	D1: SAL-21; T1: SAL-11, 16; Pointed bases: SAL-25 e.s. MAA, SAL-28 e.s. H	6.4	1.5
(n = 11)	SAL-2	D1: SAL-22; T1: SAL-32	8.2	2.1
	SAL-IND1	Pointed bases: SAL-24 e.s. CA,	12.6	2.8
	SAL-IND2	SAL-26	2.3	1.9
	SAL-IND3	SAL-27	10.6	1.8
	SAL-IND4	SAL-29	7	3.7
PRINC	PRINC-1	P1: CSC-54, 55, 58, 59, 65, 66, 67, 70, 91	7.8	1.9
(n = 10)	PRINC-IND	P1: CSC-85	4.8	2.6
CPX	CP-A	P1: CPX-4, 8, 33, MRCCP1 e.s. M.PORCI	12.6	6
(n = 11)	CP-B	P1: CPX-10, 13, 18, 42, 48, MRCCP2 e.s. C.ANTESTI	10.3	4
	CP-IND	T1: MRCCP5 e.s. Q.MEVI	12	3.5
BIF	BIF-1	P1: BIF-12, 13, 15, 20	11	8.1
(n = 21)	BIF-2	P1: BIF-4, 5, 6, 9, 11, 21, 25, 28	12.3	5.6
	BIF-3	P1: BIF-19, 41, 48; D2/4: BIF-36, 37	14	7.2
	BIF-IND1	P1: BIF-26	6.3	3.6
	BIF-IND2	D2/4: BIF-35	2.9	1.7
	BIF-IND3	BIF-50	17.3	8.4
CRC	CRC-1	P1: CRC-2, 19	14.5	6.8
(n = 5)	CRC-2	P1: CRC-8, 18, 24	13.6	4.3
ACM	ACM-A	D1: ACM-73, 80, 86, 97, 99 Can Pau Ferrer	5.2	1.9
(n = 18)	ACM-B	D1: ACM-40, 45, T1D: ACM-59, T1E: ACM-3, 61, 63, P1?: ACM-31 Ca l'Arnau	5.4	1.5
	ACM-C	P1: ACM-1, 20, 71, 72 Ca l'Arnau	11.2	1.6
	ACM-IND1	D1: ACM-81 Can Pau Ferrer	7.9	2
	ACM-IND2	ACM-102 Can Pau Ferrer	5.6	1.6
MOR	MOR-1	P1: MOR-4, 5, 6, 10	7.8	1.8
(n = 11)	MOR-2	P1: MOR-8, 13, 15; D2/4: MOR-17	4.4	1.8
	MOR-3	D2/4: MOR-11, 18, Pointed base: MOR-20 e.s. CHR	1.8	1.6
MUJ	MUJ-1	P1: MUJ-24, 29	1.2	1.4
(n = 7)	MUJ-2	T1A: MUJ- 40, 41, 42, T1C: MUJ-33, 53	1.4	1.3
FEN	FEN-A	P1: FEN-11, 25, 26, 27, 29, 31	1.8	1
(n = 9)	FEN-B	D2/4: FEN-36, 37, 38	1	1.3
CAL	CAL-A	P1: CAL-2, 3, 25, 28, 32	13.8	1.6
(n = 6)	CAL-B	P1: CAL-5	5.2	1.6
LLA	LLA-A1	P1: LLA-9, D7/11: LLA-13	10	1.3
(n = 8)	LLA-A2	P1: LLA-16, 18, 24, 33, D7/11: LLA-10	5.5	1.3
	LLA-IND	P1: LLA-17	11.9	1.7
PV4	PV4-ACM	P1: PV4-1, 2, 4, 11, 16 e.s. TH + S	3.2	2.5
(n = 13)	PV4-MOR	P1 pointed base: PV4-38 e.s. CHR	1.5	1.5
	PV4-MUJ	P1 pointed base: PV4-8 e.s. AM	1.5	1.4
	PV4-BIF	P1: PV4-5, 7, 9	11.7	6.5
	PV4-IND1	P1: PV4-6	6.9	8.2
	PV4-IND2	P1: PV4-13	11.5	3
	PV4-IND3	P1: PV4-14	12.1	2.2
CDV	CDV-BIF	P1: CDV-1-11, 13–15, 17-20	11.4	6.6
(n = 19)	CDV-IND	P1: CDV-12	12.6	8.1
ULL	ULL-BIF	P1: ULL-1-4, 7, 9–11, 13–16, 18–20, 22	9	8.8
(n = 19)	ULL-IND1	P1: ULL-12	3.2	2.4
	ULL-IND2	P1: ULL-17	8.6	2.2
	ULL-IND3	P1: ULL-21	2.5	1.7

[a] e.s.: epigraphic stamp.

2.3. Statistical protocols

We defined four protocols using multivariate methods developed and used by mathematicians, geologists, and ecologists (Anderson and Walsh, 2013; Filzmoser et al., 2009; Pavoine et al., 2009; Podani, 1999).

Protocol 1 is designed for analysing geochemical compositions (CHEM) while protocol 2 aims to represent mineralogical and petrographic data (PETRO). Protocol 3 allows the combination of both types of data (CHEM & PETRO) and can be properly called a mixed-mode analysis, after Baxter et al. (2008). Protocol 4 is equivalent to protocol 3 but using a specific selection of variables deemed relevant for

Table 3
Statistical protocols.

	Protocol 1	Protocol 2	Protocol 3	Protocol 4
Data source	CHEM	PETRO	CHEM & PETRO	CHEM & $PETRO_{PROV}$
Transformation	ilr/clr	ranking	clr & ranking	clr & ranking
Distance	Euclidean	RRD/NI	Extended Gower distance (Euclidean & RRD)	Extended Gower distance (Euclidean & RRD)
Ordination	RPCA	PCoA/NMDS	PCoA	PCoA

identifying provenance (CHEM & $PETRO_{PROV}$), mainly those indicating mineralogical composition (see Appendix A, column "Provenance related"). Consequently, in contrast with protocol 3, protocol 4 do not include those variables that indicate the conditions of firing (i.e., maximum temperature, atmosphere and post-atmosphere, frequency and shape of voids) and forming (i.e., orientation, distribution, spacing, and sorting of inclusions). In addition to their data source, protocols vary in three key steps: data transformation, calculation of distance/dissimilarity, and ordination method (Table 3).

Focusing in CHEM, the protocol 1 first step is to transform counts or percentages given by WD-XRF readings into log-ratios (Aitchison, 1982; Buxeda i Garrigós, 1999; Martín-Fernández, 2015; Pawlowsky-Glahn and Buccianti, 2011). Once data is transformed using any log-ratio procedure (alr, clr, or ilr), it is possible to perform PCA using Euclidean distances between log-ratios. However, we do warn that using different log-ratio transformations, as well as any other transformation (normalization, logarithmic), must be taken into account carefully while interpreting results. For easiness and readability, we followed the approach of Filzmoser et al. (2009), which uses a combination of ilr transformation and RPCA. Such treatment empowers the visualization of compositional data, by compensating for distortions produced by outliers and closure. There are three R packages dedicated to compositional data, which can be used for further and more detailed compositional analysis (zCompositions: Palarea-Albaladejo and Martín-Fernández, 2015; robCompositions: Templ et al., 2011; compositions: van den Boogaart et al., 2014). The cerUB package uses the robCompositions package to handle compositional data.

When addressing PETRO in protocols 2, 3, and 4, we chose to preserve the original format of variables—i.e., ordinal variables. This practice contrasts with other approaches (Baxter et al., 2008; Cau Ontiveros et al., 2004; Ownby et al., 2014). These used binominal dummy variables instead, thus merely differentiating values (e.g., "common" ≠ "few") instead of accounting for their order (e.g., "common" > "few"). However, a special treatment is required to measure dissimilarity in ordinal variables. We explored two alternative approaches to this challenge, relative rank difference and neighbour interchange (NI and RRD; Appendix B; Podani, 1999). The essential trait of both methods is that ordinal values are converted into rank scores, which depend not only on ordering (i.e., the sequence of categories) but also on ties (i.e., observations falling into the same category).

Dissimilarities given by NI generally do not satisfy the axiom of triangle inequality (i.e., they are not metric). Therefore, NI can be used in protocol 2, dealing only with ordinal variables, but it is incompatible with the integration of Euclidean distances, as in protocols 3 and 4. In turn, RRD dissimilarities can be analysed with metric techniques and so we used this approach to measure dissimilarity in PETRO variables in protocols 2 through 4.

Protocols 2 through 4 calculate the overall dissimilarity between observations using a version of Gower's distance (Gower, 1971; Appendix B), extended and implemented in R language by Pavoine et al. (2009). Similarly to Baxter et al. (2008) 'mixed mode' approach, they named this methodology as the "mixed-variables coefficient of distance" which was presented with their original R code.

The extended Gower distance enables protocols 3 and 4 to combine CHEM and PETRO in the same distance coefficient. CHEM numeric variables contribute with Euclidean distances between pairs of clr, and PETRO ordinal variables with RRD between pairs of rank scores. By modifying Pavoine et al. (2009) original script, it was possible to equal the weights of the two sets of variables (CHEM, PETRO), so that the distance represents the exact middle ground between the patterns displayed in protocols 1 and 2. We then project the resulting distance matrix in 2D and 3D through PCoA.

The 2D and 3D projections generated by each protocol are complemented with PERMANOVA and PERMDISP2 tests (Anderson and Walsh, 2013), which together evaluate the significance of the separation between given groups. These tests are good supplements to ordination methods (PCA, PCoA) because both use the entire multidimensional variability present in distance matrices, part of which is invisible in graphic projections (biplots).

PERMANOVA assesses the probability of the null hypothesis of no difference among group centroids (i.e., small p values indicate significant separation). However, PERMANOVA is unreliable when there is heterogeneity of dispersions, which confounds effects of group location and dispersion. PERMDISP2 tests the null hypothesis of heterogeneity of dispersions, ignoring the position of group centroids. If homogeneity of dispersion can be assured (PERMDISP2: p-value < 0.05), PERMANOVA may be considered a reliable test for significant separation among groups. Both tests are possible using the *vegan* package in R (Dixon, 2003; Jari Oksanen et al., 2016): the *adonis* function and the *permtest* function (applied to *betadisper* function results).

The statistical protocols presented here include methods already available in one or more existing packages in R. However, we aim to facilitate their use for archaeologists. In this sense, accompanying this study, we present two R packages that are fully documented and freely available.

The *cerUB* package contains all necessary functions to follow the protocols and apply them to other comparable datasets (Angourakis and Martínez Ferreras, 2017). It includes the dataset presented here (amphorae), as a working example but also for ease of reproducibility.

The *biplot2d3d* package (Angourakis, 2017) combines the functionalities of several R packages to generate 2D and 3D projections of ordination methods (biplots; Gabriel, 1971), allowing for centralized control of many graphic parameters. We used four features particular to this package:

1. We opted to detach the location of the 'second' plot of a biplot (i.e., the arrows), move it to the bottom-right corner, and re-scale it to avoid overlapping points;
2. To reduce the number of variables represented in protocols using petrographic data (> 80 variables), we filtered those that did not project well in the first two dimensions (less than 50% of the maximum covariance among all variables).
3. We added a representation of eigenvalues (bottom-left corner), which are interpretable as the proportion of variance captured in every dimension (i.e., the first two or three bars being the dimensions of the plot). Additionally, we indicate this proportion as the percentage of variance explained by the visible dimensions.
4. We mark groups of observations with inertia ellipses, which correspond to 95% confidence ellipses whenever we assume that group members were drawn from normal distributions in the two dimensions displayed. We advise that this may not be reasonable for groups that are either too small or contain subgroups, in which case ellipses should be interpreted simply as graphic summaries of the group's cloud of points. We also add the "star" representation of groups, i.e. every point (group member) connected by a line to the group centroid.

We offer a full walkthrough for installing and using the *cerUB and*

biplot2d3d packages (Appendix C) and the corresponding R scripts (Appendix D); these are also available in a GitHub page (Angourakis and Martinez, 2018). Besides having published them in Zenodo.org, we maintain their open source code in GitHub repositories (github.com/Andros-Spica/cerUB, github.com/Andros-Spica/biplot2d3d). All analyses and plots presented here were made using R 3.4.1.

3. Results

3.1. Determining production centres

Aiming to test their usefulness for defining productions from pottery centres, we applied protocols 1 through 4 only to samples found in workshops. The classifications displayed in biplots and tested with PERMANOVA and PERMDISP2 vary depending on the range of the input data (i.e., RGs in protocol 1 and 3, FGs in protocol 2, and PGs in protocols 4).

In Protocol 1 (Fig. 2; the 3D biplot in Appendix E.1), the amphorae are distributed forming clusters consistent with the previously defined RGs. Most IND sherds are isolated or close to other sites' RGs. The main factors causing this distribution are the CaO and MgO values. As already detected, the P1 produced around *Baetulo* has the highest MgO content (Buxeda i Garrigós et al., 2002; Martínez Ferreras, 2014).

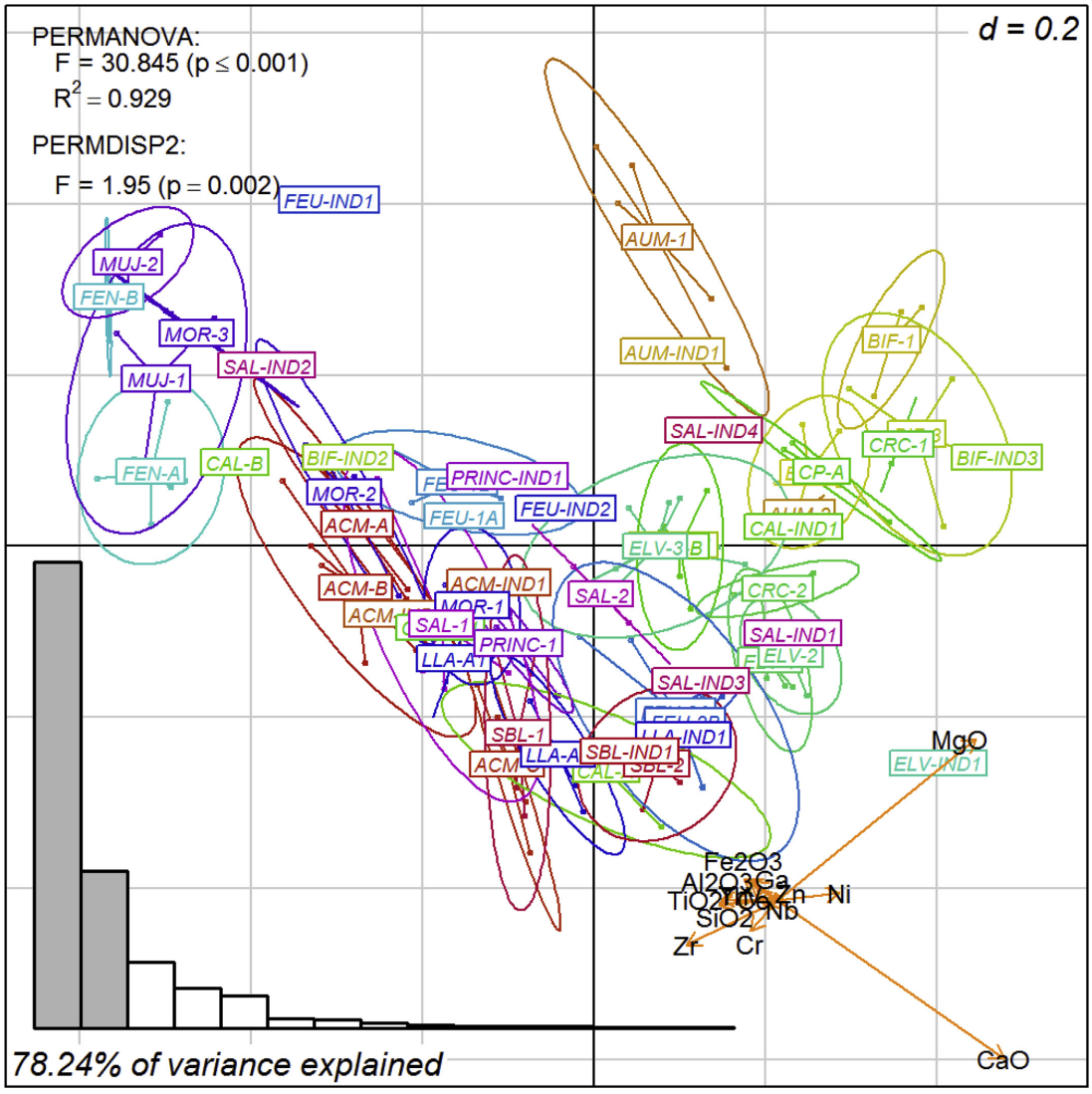

Fig. 2. Protocol 1 results concerning the samples of all amphorae workshops included in the study. The plot shows the best 2D projection, the horizontal and vertical axes respectively containing the first and second principal components. The RGs are labelled and distinguished by colour. (For interpretation of the references to colour in this figure legend, the reader is referred to the Web version of this article.)

Supplementary video related to this article can be found at http://dx.doi.org/10.1016/j.jas.2018.03.007.

Some workshops procured and processed raw materials differently. In CAL, the first D1 and T1 were produced using Fe-rich clays, while the latter P1 correspond to calcareous pastes. In MOR and FEU, the earlier P1 (MOR-1, FEU-2A, and FEU-2B) exhibit higher CaO content than the latter P1 and D2/4 (MOR-2, MOR-3, FEU-1A, and FEU-1B) which were made with Fe-rich clays. The variability within a workshop has usually been interpreted as a diversity of local raw materials used over time (Vila Socias et al., 2009). Such variability causes the RGs of some workshops to be relatively dispersed. Still, large clusters emerge with workshops geographically close, thus using similar raw materials; i.e., those located around *Blandae* (MUJ and FEN) or *Baetulo* (CPX, BIF and CRC; Buxeda i Garrigós et al., 2002; Martínez Ferreras, 2014; Vila Socias, 2011). In other cases, RGs of different production sites and areas overlap because they exhibit many similarities in their chemical composition, especially in CaO and MgO; i.e., ACM-C, SBL-1, and LLA-A2.

The low calcareous amphorae from the workshops located around *Iluro* and *Blandae* form another cluster. It comprises amphorae of the T1 (MUJ-2), P1 (MUJ-1 and FEN-A), and D2/4 (MOR-3 and FEN-B) types, also joined by one of the pointed bases from La Salut (SAL-IND2). This cluster exhibits the lowest CaO (1–2%) of the dataset, together with low MgO and high Fe_2O_3, Al_2O_3, SiO_2, Zr, and Y. Nevertheless, amphorae from FEN present lower TiO_2 and V, and higher Cr values. Most of the D2/4 from MOR (MOR-3) resemble these productions, although they exhibit lower Cr and higher Zn. The P1 from MOR (MOR-2) are low to border calcareous (4% CaO), while the earlier production of this type (MOR-1) appears to be calcareous (7–8% CaO).

In ACM, the production of different types of amphorae also entailed changes in raw materials procurement or processing. For instance, the D1 and T1 (ACM-A and ACM-B) exhibit 4–7% CaO and high Fe_2O_3, Al_2O_3, TiO_2, Y, and Ce. Their composition is similar to MOR-2, though with higher Cr. The P1 and D2/4 from FEU (FEU-1A and FEU-1B) resemble ACM's but containing higher Zn and Ni. We could attribute the P1 PRINC-IND found at Barcelona to FEU productions. The D1 and T1 from SAL (SAL-1) are border calcareous (6.4% CaO) with high TiO_2 and Zr. Instead, SAL-2 is more calcareous and exhibits lower Zr and Cr.

The P1 from PRINC (PRINC-1) and LLA (LLA-A1) are also border calcareous to calcareous with low Fe_2O_3 and Al_2O_3. LLA-A1 presents lower MnO, TiO_2, and MgO, and higher Cr. It differs from LLA-A2 because the latter exhibits higher CaO (10%). The calcareous P1 LLA-A2 is similar to CAL-A, ACM-C, and SBL-1. Ce is higher in ACM-C, while Ni and Cr are more abundant in SBL-1. The D2/4 from SBL (SBL-2) exhibits lower Zr and Cr, and present similarities with the P1 from FEU (FEU-2A and FEU-2B), except for their higher SiO_2. One of the pointed bases from SAL (SAL-IND-3) also resembles these two FEU RGs.

The P1 discussed above differ from those produced at the Besòs River Valley, through their MgO content. Amphorae from CP (CP-A and CP-B) and BIF (BIF-1, BIF-2, and BIF-3) consist of calcareous pastes (10–14% CaO) with low Al_2O_3, SiO_2, and Ga, and high MgO (4–8%). As previously suggested, amphorae from *Baetulo* resemble those found at CRC (CRC-1/2), located north of the Roman city (Buxeda i Garrigós et al., 2002).

Regarding the southern workshops near *Tarraco* (Tarragona), some RGs present a relatively unique chemical composition, i.e., the D1, T3, and flat-bottom amphorae from ELV-1 and ELV-2 and the P1 from AUM-1. The first two present calcareous pastes (15–16% CaO) with high Ni and low Al_2O_3, SiO_2, Ce, and Ga, while the third exhibits 5% CaO, the highest K_2O (5%), high MgO (5.5%) and Ni, and low SiO_2, Ba, Zr, and Ce. Nevertheless, the P1 from ELV-3 contain higher Ce and Zn and are closer to the P1 from CP-B. Moreover, the two amphorae included in group AUM-2 exhibit higher CaO (12%), Sr, and Cu and approach the products from *Baetulo*.

We mentioned the interesting cases of those IND sherds found in one workshop but allegedly produced in another. However, most INDs (AUM-IND1, FEU-IND2, BIF-IND1, BIF-IND3, ACM-IND1, and ACM-IND2) are linked with the RGs of their respective sites. They probably correspond to productions that were not well characterized, or were made in nearby workshops not yet investigated or discovered. Only two samples, FEU-IND1 and ELV-IND1, don't match with any RG and so their provenance remains indeterminate.

In protocol 2, the separation of FGs is more consistent with their textural characteristics and with the geographical location of the pottery workshops (Fig. 3; the 3D biplot in Appendix E.2). For instance, the amphorae from the southern workshops (AUM and ELV) are tightly clustered because they consist of fine to medium-fine fabrics with moderately abundant aplastic inclusions (≤ 0.5 mm grain-sized; lower L2; Fig. 4). The predominant inclusions are quartz (L43), K-feldspar, and plagioclase derived from granitoids. Foraminifers, micritic calcite (L27), and sparite in some samples, all presenting various states of decomposition, are frequent. Phyllosilicates (L36), metamorphic and sedimentary rock fragments (L24, L33) are common to few. The raw materials used were the local Pleistocene alluvial deposits and piedmont terrains constituted by marls, calcarenites, and biomicrites from the Miocene.

The coarser, low calcareous D1, T1, and P1 from the workshops located around *Iluro* and *Blandae* —ACM-1, MOR-1, MOR-2, MUJ-1, and FEN-1— appear on the opposite side. These workshops exploited raw materials from the Quaternary fluvial-torrential deposits extending in the narrow plain between the coastal mountains and the Mediterranean Sea. The clayey matrix is rich in iron oxides, and inclusions in the coarse fraction are moderately abundant, ranging in size from fine-grained to very coarse-grained sand (≤ 0.25–2 mm grain-sized; higher L2). They include predominant granitic rock fragments (L7) derived from the Carboniferous-Permian coastal mountain system and crystals detached from these rocks, mainly quartz, K-feldspar, plagioclase, and biotite together with few to common amphibole and epidote (Fig. 4). Partly or totally decomposed microfossils and calcite (micrite) are common to rare in fabrics ACM-1, MOR-1 and LLA-1. MOR-1 and MOR-2 exhibit few metamorphic rock fragments. Moreover, clinopyroxene crystals are present (few) in LLA-1 derived from the Quaternary alkaline-volcanic complex located to the west. Although overlapping in 2D, ACM-1 and LLA-1 are well differentiated in 3D.

A few P1 from CAL (CAL-2) are close to those of *Iluro* and *Blandae* because it corresponds to a medium coarse, border calcareous fabric with few microfossils and frequent crystals derived from granitoids. The other P1 from this workshop (CAL-1) are not too different, though they have a Ca-rich matrix with predominant inclusions of grain size fine to medium-fine (Vila Socias and Martínez Ferreras, 2015). Despite its finer inclusions, the petrographic composition of CAL amphorae resembles that of the P1 from ACM (ACM-2).

The fabrics attributed to the sites near the Ripoll River Basin (FEU-1, SAL-1, and SAL-2), as well as some “IND” sherds from these sites, are clustered because they consist in medium-to-coarse, border calcareous to calcareous fabrics. The clayey sediment is rich in iron oxides, with the presence of some nodules of calcite (micrite) and microfossils, especially in SAL-2. Most of the inclusions are metamorphic and sedimentary rock fragments, together with crystals derived from granitoids. They constitute the fluvial-torrential Miocene and Quaternary clayey sediments of the Ripoll River Valley formed by the erosion of the littoral and pre-littoral mountain ranges.

FEU-2 and the productions from the Lower Llobregat basin (SBL-1 and SBL-2) and Barcelona (PRINC-1) unite because they all are calcareous, coarse fabrics. FEU-2 comprises P1 and pointed bases with epigraphic stamps that were produced using Ca-rich clays with abundant medium to very coarse grain-sized aplastic inclusions. In this case, granitic and metamorphic rock fragments predominate, quartz and feldspars are frequent, and limestone and fragments of sedimentary rocks are scarce. The P1 from SBL-1 and PRINC-1 have in turn a Fe-rich clay matrix with carbonates and moderately abundant inclusions, which primarily consist of granitic rock fragments, crystals derived from these rocks, metamorphic rock fragments and, to a lesser extent,

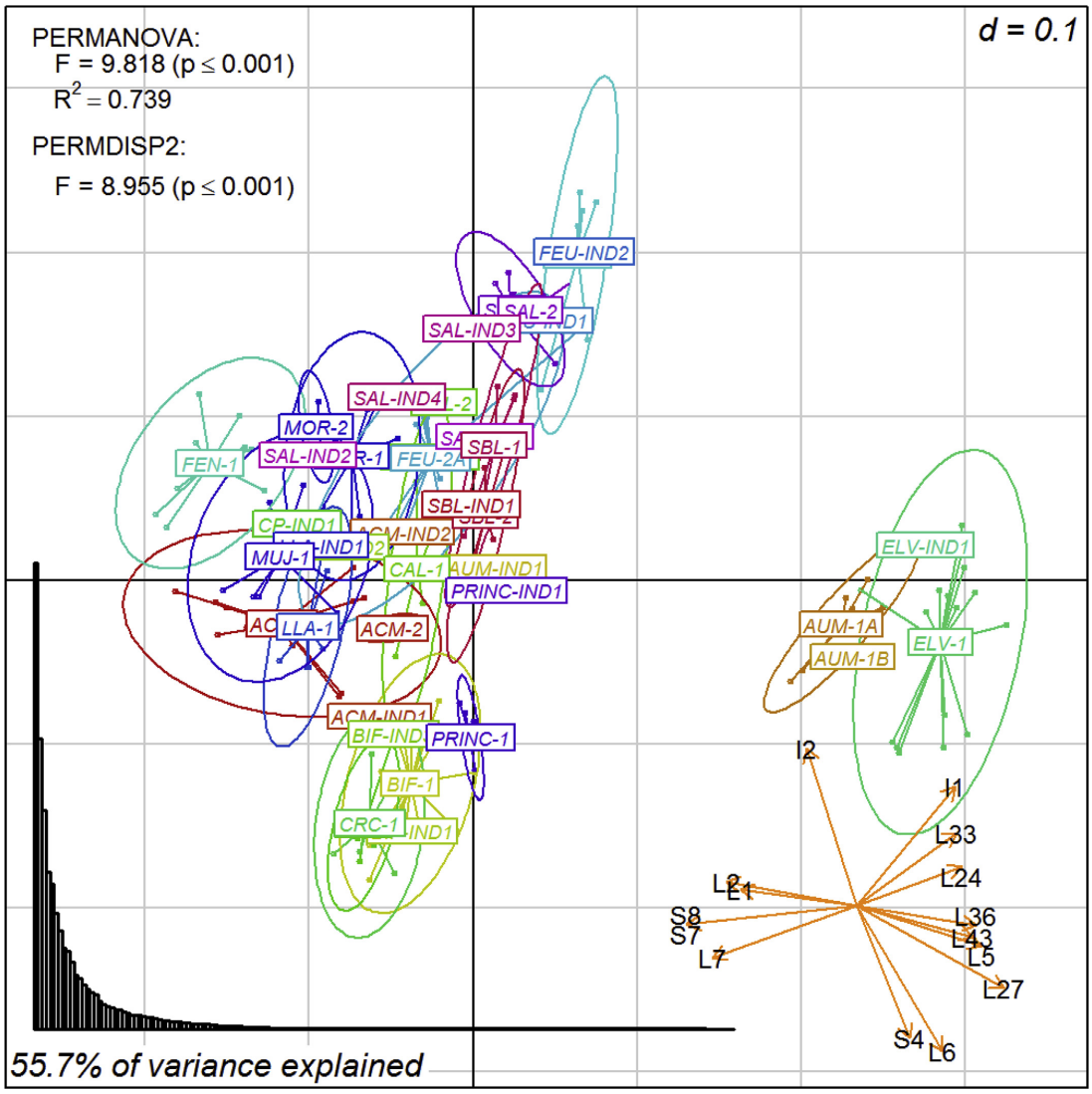

Fig. 3. Protocol 2 results concerning workshops samples. The plot shows the best 2D projection, the horizontal and vertical axes respectively containing the first and second principal coordinates. The FGs are labelled and distinguished by colour. Consult Appendix A for variable codes. (For interpretation of the references to colour in this figure legend, the reader is referred to the Web version of this article.)

sedimentary rock grains. The petrographic composition of the stamped pointed bases of group SBL-2 is similar to that of the P1 amphorae from the same site. These materials come from the Quaternary alluvial clayey sediments deposited in the Lower Valley of the Llobregat River.

The coarse FGs from CP and BIF, in *Baetulo* (CP-1 and BIF-1), and CRC (CRC-1) are clustered apart because they exhibit a characteristic calcareous matrix with aggregates of calcareous, silty sediment. The aplastic inclusions are relatively abundant and consist of coarse and very coarse granitic rock fragments and crystals derived from these rocks —quartz, plagioclase, K-feldspar, amphibole, and epidote— along with calcareous nodules (micrite). Sandstone and metamorphic rock fragments are few or absent at CP-1.

As expected, the petrographic variables related to firing (F1, F2, and F3) do not contribute much to the overall variance in this dataset, due to the relative technological homogeneity among these workshops. All individuals indicate oxidising firing and post-firing atmosphere, and their temperatures vary widely from 700 to 1100 °C within most workshops. Variables describing the shape and frequency of voids (V1 to V17), which are also related to firing, among other processes, are also not well projected in Fig. 4.

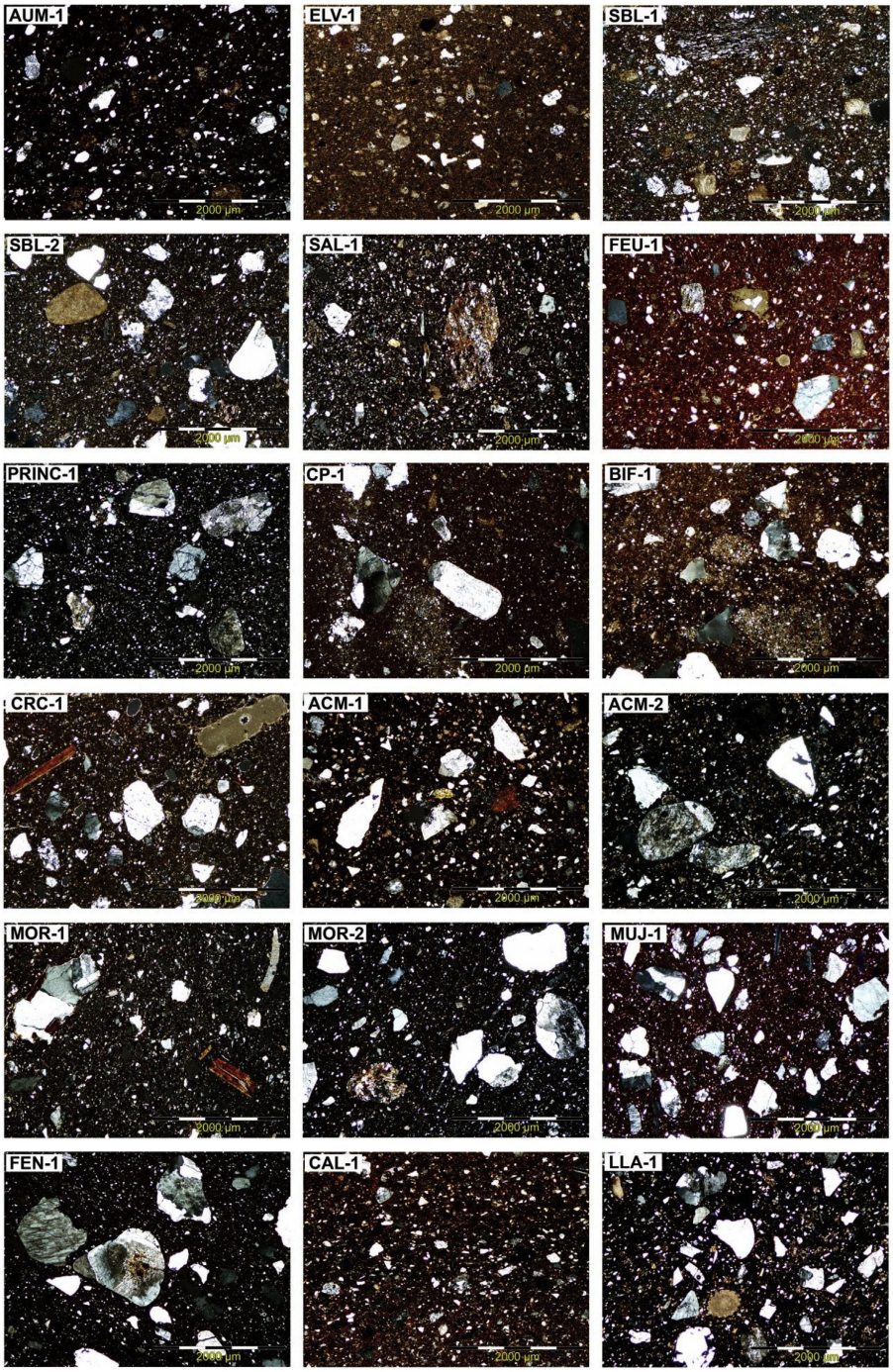

Fig. 4. Microphotographs of the FGs 40X, X.

Protocol 3 combines all CHEM and PETRO variables to return a more comprehensive picture of both the provenance and technological characteristics of pottery productions (Fig. 5, the 3D biplot in Appendix E.3).

The southern workshops (AUM and ELV) stand out from the others. The most distinctive characteristic is their fine fabrics, predominantly calcareous, with an abundance of carbonates, especially foraminifers, quartz, feldspars, and metamorphic and sedimentary rock fragments.

Workshops near *Iluro* and *Blandae* (ACM, MOR, MUJ, and FEN) differ because of their Fe-rich clays with coarse aplastic inclusions primarily derived from granitoids and abundant biotite, consistent with high Fe_2O_3, Al_2O_3, and SiO_2. The amphorae from the Lower Besòs Basin (CP, BIF and CRC), already well distinguished with protocols 1 and 2, are completely detached from the other workshops. In protocol 3, their position is due to both their petrographic properties (coarse fabrics with a predominance of carbonates and crystals and rock fragments derived from granitoids in a Ca-rich clay matrix) and their high CaO and MgO contents, which are consistent with the presence of dolomite outcrops in the area.

FEU and SAL form another cluster. The D1 and T1 from SAL are close to the border calcareous P1 and D2/4 from FEU (FEU-1A and FEU-1B). Less distinguished, the calcareous P1 and pointed bases with stamped marks from FEU (FEU-2A and FEU-2B) share significant compositional similarities with the D2/4 from SBL (SBL-2). They consist

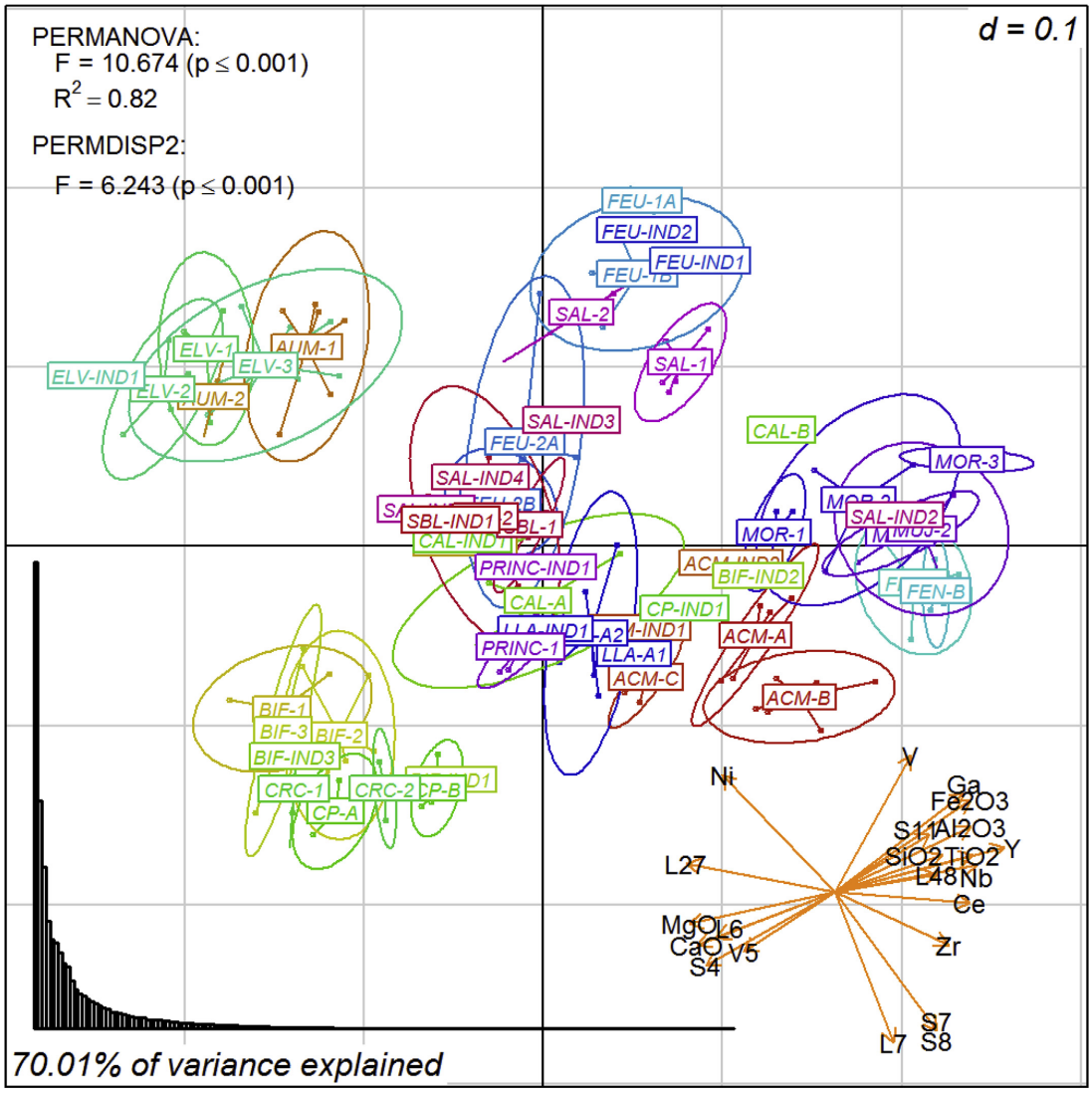

Fig. 5. Protocol 3 results concerning the workshops samples. The plot shows the best 2D projection, the horizontal and vertical axes respectively containing the first and second principal coordinates. The RGs and the site outliers are labelled and distinguished by colour. Consult Appendix A for petrographic variable codes. (For interpretation of the references to colour in this figure legend, the reader is referred to the Web version of this article.)

of calcareous, coarse amphorae, with granitoids, metamorphic and sedimentary rock fragments and carbonates resulting in high CaO and low Fe_2O_3, Al_2O_3, MgO, and Cr. The P1 from SBL (SBL-1) differ from SBL-2 because they contain higher Zr, Ni, and Cr. They chemically resemble the P1 of PRINC-1, but the lithological constituents of the aplastic inclusions are equivalent to those observed in the D2/4 from SBL-2.

The northern workshops (CAL and LLA) are difficult to individualize. The calcareous P1 (CAL-A and LLA-A2), which contain foraminifers and bivalves, match those of SBL-1 and PRINC-1. On the other hand, the border calcareous P1 and D7/11 of LLA-A1 are closer to the calcareous P1 of ACM-C.

In protocol 3, the contribution of petrographic data is most evident in aspects that are indicative of provenance rather than technology. However, in contrast with protocol 2, two technological variables do project well in the biplot plane: the frequency of microvesicles (V5) and the degree of sorting of inclusions in the coarse fraction (L6). Both of these variables differentiate well between individuals from MOR and MUJ (V5: few; L6: poorly-sorted) and BIF, CP, and CRC (V5: predominant; L6: moderately-sorted).

To assess the provenance as accurately as possible, protocol 4 considers only variables that characterize raw materials (CHEM & PETR-O_{PROV}; see Appendix A, column "Provenance related"). The resulting biplot (Fig. 6; the 3D biplot in Appendix E.4) were not as discriminative as expected. This is due to the still high multidimensionality of the

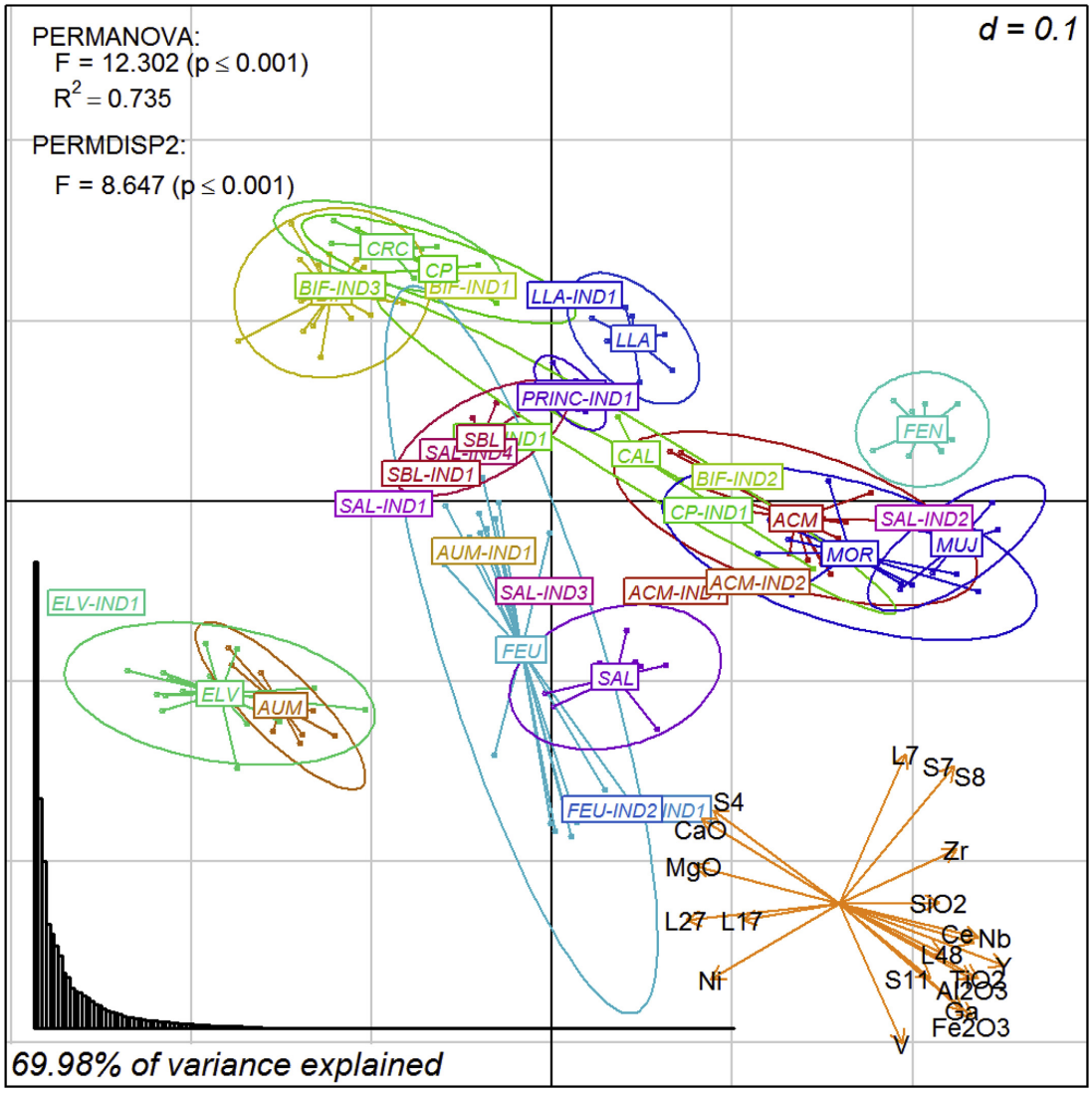

Fig. 6. Protocol 4 results concerning the workshops. The plot shows the best 2D projection, the horizontal and vertical axes respectively containing the first and second principal coordinates. The general PGs and the site outliers are labelled and distinguished by colour. Consult Appendix A for petrographic variable codes. (For interpretation of the references to colour in this figure legend, the reader is referred to the Web version of this article.)

data—note the many long arrows pointing different directions. Even so, several productions are individualised and most positions are consistent with the PGs.

Particularly well defined are the workshops placed near the Ebro River and *Tarraco* (AUM and ELV), in the lower Besòs River Basin near *Baetulo* (CP, BIF, CRC), and in the Laietan region near *Iluro* and *Blandae* (ACM, MOR, MUJ, FEN). CP, BIF, and CRC exploited Holocene deposits and Miocene marls from the plain that are deltaic, fluvial, torrential and marine. The presence of carbonates in the clayey pastes conferred pale brown to yellowish colours after firing. Instead, the amphorae produced in ACM, MOR, MUJ, and FEN consist in reddish fabrics because the Laietan potters employed the Fe-rich clayey sediments from Quaternary fluvial-torrential deposits that cover the littoral plain. These areas have specific geological constituents, and their amphorae productions are well differentiated while the variability within each zone is very low.

Unfortunately, not even protocol 4 can satisfactorily separate all productions within each region. Nonetheless, this treatment proved to be useful to discern among the amphorae manufactured in the Ripoll River Basin (FEU and SAL), even when they exhibit a high variability in shapes and composition within their workshops. It also allowed individualizing LLA, PRINC, and SBL, which overlap in other protocols. CAL remains the only workshop that overlaps in 2D with geographically unrelated productions.

3.2. Determining provenance: shipwreck case studies

Protocol 4 proved to be the most effective treatment for individualizing provenance. Therefore, we used it to explore the origin of amphorae from the three shipwrecks considered in this study.

As expected, the biplot (Fig. 7; the 3D biplot in Appendix E.5) shows that most of the P1 from CDV (CDV-BIF) and ULL (ULL-BIF), dated to the Augustan Age, match the amphorae produced at the lower Besòs River Basin (CP, BIF and CRC). Two of the containers with unknown origin from ULL (ULL-IND1/3) resemble the low calcareous productions from MUJ and FEN, while ULL-IND2 is closer to the productions of LLA. CDV-IND1 appears related to the amphorae produced at the lower Llobregat River Valley (SBL) and *Barcino* (PRINC). Despite the varied provenance of these amphorae, the port of departure of these ships was probably the coastal city of *Baetulo* since most of the cargo originated in the workshops found on the outskirts of the city (BIF, CP).

Dated in earlier times (between 40/30 BC), the provenance of the amphorae found in PV4 is more diverse. Some low and border calcareous amphorae (PV4-ACM, PV4-MOR, and PV4-MUJ) present similar chemical and petrographic composition with the products of different workshops located in the territory of *Iluro* and *Blandae* (i.e., ACM, MOR, and MUJ). Other vessels are associated with the workshops in *Baetulo* (PV4-BIF), and three (PV4-IND1/2/3) are isolated due to major chemical and petrographic differences compared to the PGs considered.

4. Discussion

The goal of this paper has been to present an explorative methodology for analysing the variability of archaeological ceramics. We intended to offer alternative protocols that drawn information from different data sources and follow different statistical treatments. Building on the conclusions of Baxter et al. (2008), we experimented with a new version of what they named the mixed-mode approach, i.e., the combination of geochemical composition and petrographic data into the same multivariate analysis. Their proposal included using raw chemical data and converting petrographic ordinal data into binominal dummy variables, and the application of PCA or CA for visualization. The approach we advocate here differs in that geochemical data is treated as compositional data, by applying log-ratio transformations, and that the ordinal variables normally used as petrographic data can contribute to more systematic analysis without sacrificing the ordering information. In this sense, our proposal employs techniques developed in other disciplines that, in our assessment, produce more satisfactory and integral images of ceramic materials.

Our confidence in the protocols presented here comes from their performance summarizing the variability of the Roman wine amphorae as shown above. Overall, there is a good match between prior classifications (RGs, FGs, and PGs) and the 2D/3D projections generated by each protocol. Additionally, all PERMANOVA and PERMDISP2 results are significant, under any reasonable criterion (in all cases p-values are much less than 0.01), meaning that the classifications given are satisfactory group hypotheses according to the distances calculated in each protocol.

Except in protocol 1 where there is much overlap, 2D projections consistently separated the two southern workshops (ELV, AUM), the three *Baetulo*-Besòs river workshops (BIF, CP, CRC), four of the Laietan workshops (ACM, MOR, MUJ, FEN), and, in lesser degree, the two inland workshops (SAL, FEU). The least differentiated groups were those containing samples from SBL, PRINC, and CAL, which never lay too far from the projection centre.

By comparing the results of the four protocols, we also aimed to present an independent confirmation of the main conclusion in Baxter et al. (2008), which states that the 'mixed mode' approach to archaeological ceramics is superior to considering data sources separately. Indeed, the results obtained with protocols 3 and 4 confirmed that integrating *chemical* and *petrographic* data can aid the characterization and detection of groups in space and time. Furthermore, we concluded that a more selective multivariate analysis is a better strategy for answering specific questions—i.e., choosing those variables known to indicate the provenance of materials in protocol 4.

To the date, several studies in pottery archaeometry use more than a single analytic method, typically WD-XRF and petrographic observations. In this sense, they are already following a mixed-mode approach. However, datasets originating from different sources are rarely put together into the same database or go through the same statistical analysis, if at all. We acknowledge the standalone value of every analytical technique, which may in many cases be enough for answering the archaeological questions at hand. Moreover, depending on the case study, there may be much redundancy between geochemical and petrographic data. This possibility mainly comes as a disincentive for performing chemical studies in addition to petrographic studies, which are less expensive. However, we insist that, whenever data or funding is available, the combination of more than one technique may bring up their potential. Redundancy is a risk that decreases with the number and variety of variables considered. Due to the intrinsic complexity of ceramic materials, pottery individuals are best compared and classified as polythetic classes, i.e., defined by many properties simultaneously (as argued by Rice and Saffer, 1982).

By publishing online the *cerUB* and *biplot2d3d* packages, we offer an opportunity for those researchers that have access to different analytic methods but lack the know-how required for applying and visualizing more sophisticated multivariate statistics (including ordinal variables). Moreover, by establishing these four protocols under the same framework, we allow for straightforward comparisons between their results, which is useful for defining and testing typologies based on different aspects of the data.

Despite what, in our opinion, are clear advantages of applying these protocols, we did detect possible caveats in doing so. First, the applicability of protocols 2 through 4 requires petrographic observations to be annotated in a database. Due to the amount of work this entails, petrographic variables may not be available for all archaeological samples recovered. However, it is indispensable that observations entering the database take the form of ordinal variables rather than other qualitative textual assessment. Additionally, the functions in *cerUB* package assume that petrographic data were named and entered following the same system used by us (Appendix A). However, as we have shown here, it is not necessary to input all petrographic variables in our list since protocols can manage any smaller set of variables.

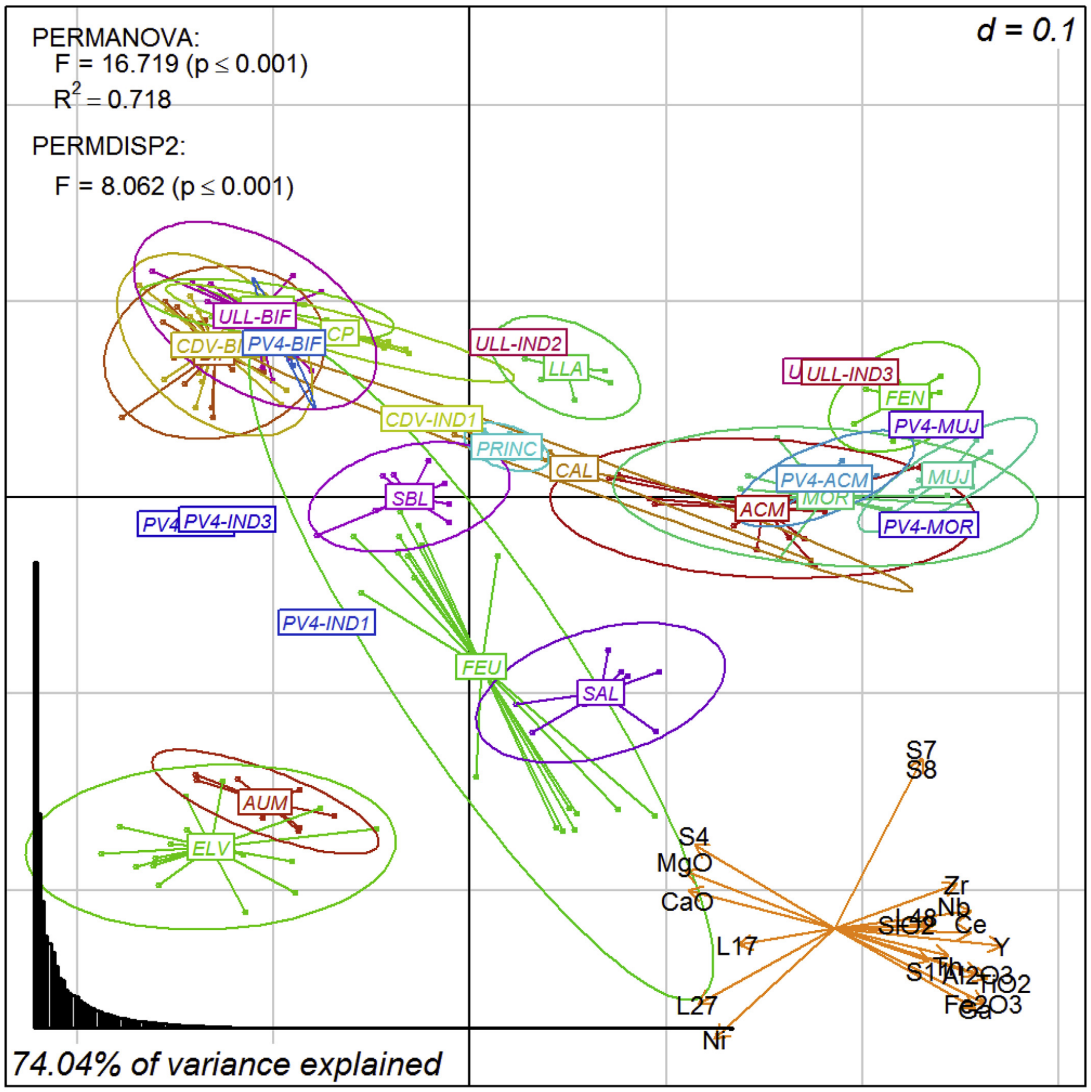

Fig. 7. Protocol 4 results concerning both workshops and shipwrecks samples. The plot shows the best 2D projection, the horizontal and vertical axes respectively containing the first and second principal components. The general PGs and the shipwreck outliers are labelled and distinguished by colour. Consult Appendix A for petrographic variable codes. (For interpretation of the references to colour in this figure legend, the reader is referred to the Web version of this article.)

Also, if the analyst has access to a reliable quantitative petrographic method (e.g., point-counting), other versions of protocols 2, 3, and 4 could be developed to only handle sets of numeric variables rather than using ordinal variables. In the case of using point counting, these alternative protocols would certainly be less complex, requiring solely the scaling to sample total (in case totals vary among samples) and a log-ratio transformation, given that the input data would be strictly compositional (as defined in Aitchison, 1982).

Another critical warning concerns the nature of multivariate representations (e.g., biplots), not only in our protocols but when using any ordination method (e.g., PCA, CA, PCoA). We cannot interpret a multivariate projection as bivariate. Multivariate means multi-dimensional, which implies that the distance between two points in two dimensions cannot account for their distance in a third dimension, the same way that a single blueprint cannot represent a two-story building. Biplots of the first two principal coordinates display the most complete 2D representation that the method can calculate with the data given.

For instance, in protocol 1 (Fig. 2), the 2D projection explains almost 80% of the total variability, which in turn is mostly contributed by CaO and MgO. In this case, we may read more safely the position of points in terms of more or less CaO or MgO content. Conversely, when there are many variables, the two most explicative dimensions may

correlate with several of them, what is represented in a biplot as a star of long arrows pointing out many directions. In this kind of context, variables 'compete' with each other to order the points according to their criterion. This is the case in protocol 2 (Fig. 3), where the orientation of inclusions (I2) has a clear readability while interpreting, for instance, the presence-abundance of chert (L33) can be misleading. The Appendix section C.8 explains this more thoroughly.

With this paper we hope to provide general archaeologists with a tool for accessing a straightforward image of the variability of their ceramic materials, thus assisting archaeological classification. However, this is an exploratory tool, and it is not designed to replace finer analyses of geological provenance and material science. Nor do we suggest dismissing other classical multivariate approaches, which are also readily available in R (Baxter, 2016). In this sense, the end products of the protocols (i.e., an R list object) contain a distance matrix that can be further used in other multivariate methods, such as discriminant and cluster analysis. We do not discard the possibility of applying this type of methodology in other archaeological materials and we encourage future development in this direction.

Funding

This work was supported by the R&D&I projects CAMOTECCER (HAR2012-32653) and CERAC (HAR2016-75133-C3-1-P) led by V. Martínez and J.M. Gurt, and funded by the Spanish Ministry of Economy and Competitiveness (MINECO). A. Angourakis worked on this paper through the FPI contract (BES-2013-062691), and V. Martínez through the post-doctoral research contract Ramón y Cajal (RYC-2014-15789), all funded by MINECO.

Acknowledgements

We would like to thank Dr J. Buxeda i Garrigós and Dr Ll. Vila Socias for providing us with chemical results from several workshops, as well as Dr. Patrick Quinn for several suggestions concerning the display and evaluation of protocols results. We also are very grateful for the corrections, comments, and suggestions of the anonymous reviewers, which have greatly improved this paper.

Appendix. Supplementary data

Appendices and supplementary data related to this article can be found at http://dx.doi.org/10.1016/j.jas.2018.03.007.

References

Aitchison, J., 1982. The statistical analysis of compositional data. J. R. Stat. Soc. Ser. B 44, 139–177.
Anderson, M.J., Walsh, D.C.I., 2013. PERMANOVA, ANOSIM, and the Mantel test in the face of heterogeneous dispersions: what null hypothesis are you testing? Ecol. Monogr. 83, 557–574. http://dx.doi.org/10.1890/12-2010.1.
Angourakis, A., 2017. biplot2d3d - an R Package for Generating Highly-customizable Biplots. Zenodohttp://dx.doi.org/10.5281/zenodo.889704.
Angourakis, A., Martinez, V., 2018. cerUB Tutorial. https://andros-spica.github.io/cerUB_tutorial/.
Angourakis, A., Martínez Ferreras, V., 2017. cerUB - Protocols for Exploring Archaeometric Data (R Package). Zenodohttp://dx.doi.org/10.5281/zenodo.975450.
Baxter, M.J., 2016. Multivariate Analysis of Archaeometric Data: an Introduction. Academia.edu. https://www.academia.edu/24456912/Multivariate_Analysis_of_Archaeometric_Data_An_Introduction.
Baxter, M.J., 2008. Mathematics, statistics and archaeometry: The past 50 years or so. Archaeometry 50, 968–982. http://dx.doi.org/10.1111/j.1475-4754.2008.00427.x.
Baxter, M.J., Beardah, C.C., Papageorgiou, I., Cau Ontiveros, M.-Á., Day, P.M., Kilikoglou, V., 2008. On statistical approaches to the study of ceramic artefacts using geochemical and petrographic data. Archaeometry 50, 142–157. http://dx.doi.org/10.1111/j.1475-4754.2007.00359.x.
Buxeda i Garrigós, J., 1999. Alteration and Contamination of Archaeological Ceramics: The Perturbation Problem. J. Archaeol. Sci. 26, 295–313. http://dx.doi.org/10.1006/jasc.1998.0390.
Buxeda i Garrigós, J., Comas i Solà, M., Gurt Esparraguera, J.M., 2002. Roman amphorae production in Baetulo (Badalona, Catalonia). Evidence of Pascual 1. In: Kilikoglou, V., Hein, A., Maniatis, Y. (Eds.), Modern Trends in Scientific Studies on Ancient Ceramics. BAR International Series 1011, Oxford, pp. 277–285.
Cau Ontiveros, M.-Á., Day, P.M., Baxter, M.J., Papageorgiou, I., Iliopoulos, I., Montana, G., 2004. Exploring automatic grouping procedures in ceramic petrology. J. Archaeol. Sci. 31, 1325–1338. http://dx.doi.org/10.1016/j.jas.2004.03.006.
Cressell, R., 1990. 'A New Technology' Revisited. Archaeol. Rev. Camb. 9, 39–54.
Dixon, P., 2003. VEGAN, a package of R functions for community ecology. J. Veg. Sci. 14, 927–930. http://dx.doi.org/10.1111/j.1654-1103.2003.tb02228.x.
Filzmoser, P., Hron, K., Reimann, C., 2009. Principal component analysis for compositional data with outliers. Environmetrics 20, 621–632. http://dx.doi.org/10.1002/env.966.
Gabriel, K.R., 1971. The biplot graphic display of matrices with application to principal component analysis. Biometrika 58, 453–467. http://dx.doi.org/10.1093/biomet/58.3.453.
Gandrud, C., 2016. Reproducible Research with R and RStudio. Chapman and Hall/CRC Press.
Gosselain, O.P., 1995. Identités techniques. Le travail de la poterie au Cameroun méridional. Ph.D. dissertation. University of Brussels.
Gower, J.C., 1971. A general coefficient of similarity and some of its properties. Biometrics 27, 857–871. http://dx.doi.org/10.2307/2528823.
Jari Oksanen, Blanchet, F.G., Kindt, R., Legendre, P., Minchin, P.R., O'Hara, R.B., Simpson, G.L., Solymos, P., Stevens, M.H.H., Wagner, H., 2016. Vegan: Community Ecology Package.
Lemonnier, P., 1976. La description des chaînes opératoires: contribution à l'analyze des systèmes techniques. Tech. Cult. 1, 100–151.
Maritan, L., Angelini, I., Artioli, G., Mazzoli, C., Saracino, M., 2009. Secondary phosphates in the ceramic materials from Frattesina (Rovigo, North-Eastern Italy). J. Cult. Herit. 10, 144–151. http://dx.doi.org/10.1016/J.CULHER.2008.01.008.
Maritan, L., Mazzoli, C., 2004. Phosphates in archaeological finds: implications for environmental conditions of burial. Archaeometry 46, 673–683. http://dx.doi.org/10.1111/j.1475-4754.2004.00182.x.
Martín-Fernández, J.A., Buxeda i Garrigós, J., Pawlowsky-Glahn, V., 2015. Logratio analysis in archeometry: principles and methods. In: Barceló, J.A., Bogdanovic, I. (Eds.), Mathematics and Archaeology. CRC press, Boca Raton FL, pp. 178–189.
Martínez Ferreras, V., 2015. La difusión comercial de las ánforas vinarias de Hispania Citerior-Tarraconensis (s. I a.C. - I d.C.). Roman Archaeology 4. Archaeopress, Oxford.
Martínez Ferreras, V., 2014. Ánforas vinarias de Hispania Citerior-Tarraconensis (s. I a.C. - I d.C.). Caracterización arqueométrica. Roman and Late Antique Mediterranean Pottery 4. Archaeopress, Oxford.
Martínez Ferreras, V., Capelli, C., Cabella, R., Nieto Prieto, X., 2013. From Hispania Tarraconensis (NE Spain) to Gallia Narbonensis (S France). New data on Pascual 1 amphora trade in the Augustan period. Appl. Clay Sci. 82, 70–78. http://dx.doi.org/10.1016/j.clay.2013.06.021.
Martínez Ferreras, V., Capelli, C., Jézégou, M.-P., Salvat, M., Castellvi, G., Cabella, R., 2015. The Port-Vendres 4 Shipwreck Cargo: evidence of the Roman wine trade in the western Mediterranean. Int. J. Naut. Archaeol. 44, 277–299. http://dx.doi.org/10.1111/1095-9270.12109.
Marwick, B., 2017. Computational reproducibility in archaeological research: basic principles and a case study of their implementation. J. Archaeol. Meth. Theor 24, 424–450. http://dx.doi.org/10.1007/s10816-015-9272-9.
Matthew, A.J., Woods, A.J., Oliver, C., 1991. Spots before the eyes: New comparison charts for visual percentage estimation in archaeological material. In: Middleton, A., Freestone, I. (Eds.), Recent Developments in Ceramic Petrology. British Museum, London, pp. 245–259.
Miró, J., 1988. La producción de ánforas romanas en Catalunya. Un estudio sobre el comercio del vino de la Tarraconense (siglos I aC.-I dC.). BAR International Series 473, Oxford.
Ownby, M.F., Huntley, D.L., Peeples, M.A., 2014. A combined approach: using NAA and petrography to examine ceramic production and exchange in the American southwest. J. Archaeol. Sci. 52, 152–162. http://dx.doi.org/10.1016/j.jas.2014.08.018.
Palarea-Albaladejo, J., Martín-Fernández, J.A., 2015. zCompositions – R package for multivariate imputation of left-censored data under a compositional approach. Chemometr. Intell. Lab. Syst. 143, 85–96.
Pavoine, S., Vallet, J., Dufour, A.-B., Gachet, S., Daniel, H., 2009. On the challenge of treating various types of variables: application for improving the measurement of functional diversity. Oikos 118, 391–402. http://dx.doi.org/10.1111/j.1600-0706.2008.16668.x.
Pawlowsky-Glahn, V., Buccianti, A., 2011. Compositional Data Analysis;: Theory and Applications. Wiley.
Perlman, I., Asaro, F., 1969. Pottery Analysis by Neutron Activation. Archaeometry 11, 21–38. http://dx.doi.org/10.1111/j.1475-4754.1969.tb00627.x.
Podani, J., 1999. Extending Gower's General Coefficient of Similarity to Ordinal Characters on JSTOR. Taxon 48, 331–340. http://dx.doi.org/10.2307/1224438.
Quinn, P.S., 2013. Ceramic Petrography: the Interpretation of Archaeological Pottery and Related Artefacts in Thin Section. Archaeopress, Oxford.
R Core Team, 2015. R: a Language and Environment for Statistical Computing.
Rice, P.M., 1987. Pottery Analysis: a Sourcebook, second ed. The University of Chicago Presshttp://dx.doi.org/10.7208/chicago/9780226923222.001.0001.
Rice, P.M., Saffer, M.E., 1982. Cluster analysis of mixed-level data: Pottery provenience as an example. J. Archaeol. Sci. 9, 395–409. http://dx.doi.org/10.1016/0305-4403(82)90045-0.
Sayre, E.V., 1976. Brookhaven procedures for statistical analyses of multivariate archaeometric data. In: Conference on Applications of Physical Sciences to Medieval Archaeology, Berkeley and Los Angeles, CA, USA, 18 Mar 1975.
Schiffer, M.B., Skibo, J.M., 1997. The explanation of artifact variability. Am. Antiq. 62,

27–50. http://dx.doi.org/10.2307/282378.
Schiffer, M.B., Skibo, J.M., 1987. Theory and Experiment in the Study of Technological Change. Curr. Anthropol. 28, 595–622. http://dx.doi.org/10.1086/203601.
Schwedt, A., Mommsen, H., Zacharias, N., Buxeda i Garrigós, J., 2006. Analcime crystallization and compositional profiles-comparing approaches to detect post-depositional alterations in archaeological pottery. Archaeometry 48, 237–251. http://dx.doi.org/10.1111/j.1475-4754.2006.00254.x.
Shepard, A.O., 1965. Rio Grande glaze-paint pottery: A test of petrographic analysis. In: Matson, F.R. (Ed.), Ceramics and Man. Aldine Publishing Company, Chicago, pp. 62–87.
Shepard, A.O., 1956. Ceramics for the Archaeologist. Carnegie Institution of Washington, Washington.
Sillar, B., Tite, M.S., 2000. The challenge of 'technological choices' for materials science approaches in archaeology. Archaeometry 42, 2–20. http://dx.doi.org/10.1111/j.1475-4754.2000.tb00863.x.
Stoltman, J.B., 1989. a quantitative approach to the petrographic analysis of ceramic thin sections. Am. Antiq. 54, 147–160. http://dx.doi.org/10.2307/281336.
Templ, M., Hron, K., Filzmoser, P., 2011. robCompositions: an R-package for robust statistical analysis of compositional data. In: Pawlowsky-Glahn, V. (Ed.), Compositional Data Analysis: Theory and Applications. John Wiley and Sons, pp. 341–355.
Tite, M.S., 2008. Ceramic production, provenance and Use—a review. Archaeometry 50, 216–231. http://dx.doi.org/10.1111/j.1475-4754.2008.00391.x.
van den Boogaart, K.G., Tolosana, R., Bren, M., 2014. Compositions: Compositional Data Analysis.
Vila Socias, L., 2011. Una Arqueometria del Canvi Tecnològic: producció i consum d'àmfores durant el canvi d'Era en la zona nord de la costa catalana. Universitat de Barcelona.
Vila Socias, L., Martínez Ferreras, V., 2015. Caracterización arqueométrica de las ánforas romanas del Collet de Sant Antoni de Calonge, in: La Alfarería Romana Del Collet Est (Calonge, Girona). BAR International Series 2770, Oxford, pp. 211–224.
Vila Socias, L., Martínez Ferreras, V., Buxeda i Garrigós, J., Kilikoglou, V., 2009. Differences in technological and functional models of contemporary amphorae production in neighbouring areas. In: Proceedings of the 36th Internatuional Symposium of Archeometrie (ISA 2006). Québec, pp. 253–259.
Whitbread, I.K., 1995. Greek transport Amphorae: a Petrological and Archaeological Study. Fitch Labo. ed. British School at Athens, Athens.